

## Reduction of Substrates by Nitrogenases

Lance C. Seefeldt,\* Zhi-Yong Yang,\* Dmitriy A. Lukyanov,\* Derek F. Harris, Dennis R. Dean, Simone Raugei, and Brian M. Hoffman\*



Cite This: <https://dx.doi.org/10.1021/acs.chemrev.9b00556>



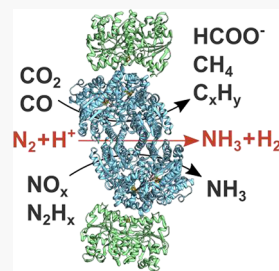
Read Online

ACCESS |

Metrics & More

Article Recommendations

**ABSTRACT:** Nitrogenase is the enzyme that catalyzes biological N<sub>2</sub> reduction to NH<sub>3</sub>. This enzyme achieves an impressive rate enhancement over the uncatalyzed reaction. Given the high demand for N<sub>2</sub> fixation to support food and chemical production and the heavy reliance of the industrial Haber–Bosch nitrogen fixation reaction on fossil fuels, there is a strong need to elucidate how nitrogenase achieves this difficult reaction under benign conditions as a means of informing the design of next generation synthetic catalysts. This Review summarizes recent progress in addressing how nitrogenase catalyzes the reduction of an array of substrates. New insights into the mechanism of N<sub>2</sub> and proton reduction are first considered. This is followed by a summary of recent gains in understanding the reduction of a number of other nitrogenous compounds not considered to be physiological substrates. Progress in understanding the reduction of a wide range of C-based substrates, including CO and CO<sub>2</sub>, is also discussed, and remaining challenges in understanding nitrogenase substrate reduction are considered.



### CONTENTS

- 1. Introduction
- 2. Nitrogenases
  - 2.1. Enzymes
  - 2.2. Cofactors
- 3. Mechanism of Nitrogenase Reduction of Protons and N<sub>2</sub>
  - 3.1. Reductive Elimination/Oxidative Addition (*re/oa*) Mechanism: As Proposed
  - 3.2. Demonstration that Nitrogenase Functions Through the *re/oa* Equilibrium
    - 3.2.1. *re/oa* Mechanism Generates the Key Constraints Revealed by Experiment
    - 3.2.2. There Are No Reductive Activation Steps Prior to Catalysis
  - 3.3. Exploring the *re/oa* Mechanism
    - 3.3.1. Reductive Elimination Involves an H<sub>2</sub>-Bound Intermediate
    - 3.3.2. E<sub>2</sub>(2H) States 1b and 1c Are Hydride Isomers
    - 3.3.3. Density Functional Studies of the *re/oa* Equilibrium
    - 3.3.4. High-Resolution ENDOR Spectroscopy Coupled with Quantum Chemical Calculations Reveals the Structure of Janus Intermediate E<sub>4</sub>(4H)
    - 3.3.5. E<sub>1</sub> Forms by Reduction of Fe, Not Mo
  - 3.4. Kinetic Description of the Competing Reactions at E<sub>4</sub>(4H)
    - 3.4.1. All Three Nitrogenases Employ the *re/oa* Mechanism

### 3.5. Structure–Function Relationship During Nitrogenase Catalysis

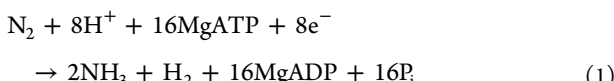
- A 4. Nonphysiological N-Based Substrates
- B 4.1. Range of N-Based Substrates
- B 4.2. N<sub>2</sub>H<sub>x</sub> Substrates
- C 4.3. NO<sub>x</sub> Substrates
- C 4.4. Mechanisms and Insights
- C 5. C-Based Substrates
- D 5.1. Alkyne Substrates
- D 5.2. CO as Inhibitor and Substrate
- D 5.3. CO<sub>2</sub> as Substrate
- D 5.4. Other C Substrates
- E 6. Concluding Remarks
- E Author Information
- F Corresponding Authors
- F Authors
- F Notes
- F Biographies
- F Acknowledgments
- F References

**Special Issue:** Reactivity of Nitrogen from the Ground to the Atmosphere

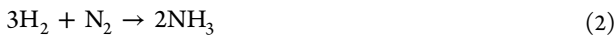
**Received:** September 5, 2019

## 1. INTRODUCTION

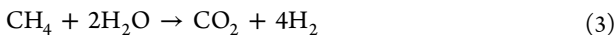
The element nitrogen (N) is a constituent of many industrially and biologically important molecules, and thus there is a high worldwide demand for usable forms of N.<sup>1–4</sup> The major simple molecular states of N constitute the global biogeochemical nitrogen cycle, with dinitrogen (N<sub>2</sub>) being the most abundant form constituting 78% of the Earth's atmosphere.<sup>5–10</sup> While abundant, N<sub>2</sub> is not generally useable directly but instead must first be “fixed” into a form that is useful for industrial or biological processes.<sup>1,2,11,12</sup> The reduction of N<sub>2</sub> to NH<sub>3</sub>, called nitrogen fixation, is the largest contributor of fixed nitrogen into the global N cycle. This reduction reaction occurs at scale in comparable amounts through two processes, the Haber–Bosch industrial reaction<sup>13–15</sup> and by the action of the enzyme nitrogenase operating inside specialized microorganisms, called diazotrophs, found throughout the biosphere.<sup>11,16–18</sup> Nitrogenase catalyzes the N<sub>2</sub> reduction reaction having the following optimal (limiting) stoichiometry:<sup>19–23</sup>



As indicated by eq 1, N<sub>2</sub> reduction by nitrogenase is fundamentally an electrochemical process, employing electrons and protons. In that sense, it differs qualitatively from the chemical industrial Haber–Bosch process, which employs H<sub>2</sub> as the source of reducing equivalents and H (eq 2):<sup>3</sup>



The nitrogenase catalyzed reaction requires energy input in the form of hydrolysis of ATP, whereas 90% of the energy input for the Haber–Bosch process is used to make the H<sub>2</sub> reactant from methane<sup>24</sup> (eq 3):



Finally, the nitrogenase stoichiometry (eq 1) incorporates the obligatory production of one H<sub>2</sub> per N<sub>2</sub> reduced, a long-debated idea that has been established only recently.<sup>21,23</sup>

Enzyme-catalyzed reactions, like all catalyzed reactions, are often measured by the rate enhancement achieved over the uncatalyzed reaction.<sup>25–27</sup> Although nitrogenase catalyzes the reduction of N<sub>2</sub> to 2 NH<sub>3</sub> with a seemingly low rate constant of  $\sim 1 \text{ s}^{-1}$ ,<sup>19,20,28,29</sup> this corresponds to a large enhancement over the uncatalyzed reaction that places it as one of the most impressive known catalysts.

Research on nitrogenase over decades has endeavored to understand this complex enzyme and elucidate the mechanism by which this remarkable catalyst achieves its rate enhancement.<sup>20,21,23,30–37</sup> Other reviews in this volume detail diverse aspects of how nitrogenase works, including how electron transfer occurs and the roles of ATP hydrolysis, how spectroscopy provides insights into the properties of the active site metal clusters, and how metal site cofactors are biosynthesized. In this Review, we detail how the field has advanced over the last  $\sim 6$  years, with an emphasis on the recent breakthroughs in our understanding of how the active site metal cluster achieves substrate reduction.

Although the physiological substrates are protons and N<sub>2</sub>, nitrogenases can also reduce a number of other substrates, such as acetylene (C<sub>2</sub>H<sub>2</sub>), carbon dioxide (CO<sub>2</sub>), diazene (HN=NH), and hydrazine (H<sub>2</sub>N–NH<sub>2</sub>).<sup>20,39,40</sup> We also review the current understanding of the mechanism of reduction of these alternative substrates, which not only

providing new insights into the mechanism of nitrogenase, but also provides insights into possible ways nitrogenase might be used to carry out useful reductions other than N<sub>2</sub> fixation.

## 2. NITROGENASES

### 2.1. Enzymes

There are three known isozymes of nitrogenase: the molybdenum-dependent Mo-nitrogenase, vanadium-dependent V-nitrogenase, and iron-only Fe-nitrogenase.<sup>20,41–49</sup> The nitrogenases are broadly distributed throughout nature with corresponding genes necessary to produce nitrogenases predicted in 13 phyla of bacteria and one phylum of archaea.<sup>18,50</sup> Mo-nitrogenase is the predominant isozyme,<sup>51</sup> but many diazotrophs carry genes for at least one, if not both, of the other isozymes.<sup>44</sup> Because of this distribution, the V-nitrogenase and Fe-nitrogenase are often called “alternative” nitrogenases.<sup>41,44,52</sup> Expression of the isozymes appears to be primarily regulated by metal availability, wherein the absence of Mo or the inability to transport Mo efficiently, one of the alternative systems is expressed.<sup>43,44,46,49,53</sup>

Structures of the Mo- and V-nitrogenase, reviewed elsewhere in this issue, show them to have similar quaternary structures.<sup>54–60</sup> The structure of Fe-nitrogenase has not been solved, but available genetic and spectroscopic evidence indicates it is similar to the other two,<sup>43,45</sup> as depicted in Figure 1. All three isozymes are two-component protein

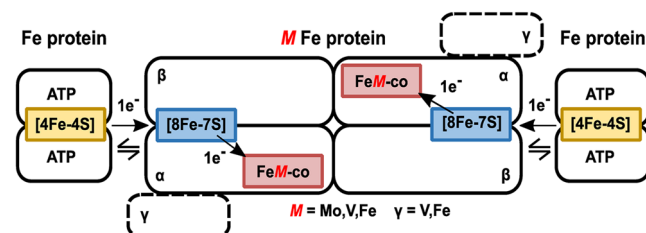


**Figure 1.** General nitrogenase architecture. Schematic of nitrogenase structures showing the electron delivery Fe protein component and the catalytic MFe protein component (M = Mo, V, Fe). MoFe protein is an  $\alpha_2\beta_2$ , and VFe and FeFe proteins are  $\alpha_2\beta_2\gamma_2$  heterohexamers. Adapted with permission from ref 38. Copyright 2018 American Chemical Society.

systems<sup>61,62</sup> with the catalytic components for each being encoded by unique gene clusters. Mo-nitrogenase is encoded by *nif* genes,<sup>50,63</sup> V-nitrogenase by *vnf* genes,<sup>64–66</sup> and Fe-nitrogenase by *anf* genes.<sup>66,67</sup> The two component proteins are a catalytic component, or MFe protein (M = Mo, V, Fe) (NifDK, VnfDGK, AnfDGK), which receives electrons from the electron delivery component, or Fe protein (NifH, VnfH, AnfH).<sup>20,31,41,43,44</sup> The MFe proteins form as two identical catalytic halves; MoFe protein is an  $\alpha_2\beta_2$  heterotetramer and VFe and FeFe proteins are  $\alpha_2\beta_2\gamma_2$  heterohexamers.<sup>41,43,68</sup> Each catalytic half houses an [8Fe-7S] P-cluster and an active site cofactor called FeMo-co,<sup>55–57,69–71</sup> FeV-co,<sup>58,72,73</sup> or FeFe-co<sup>38</sup> as the site of substrate binding and reduction. Fe protein for all three isozymes is a homodimer, which houses a single [4Fe-4S] cluster and two nucleotide-binding sites for ATP (Figure 1).<sup>54,60</sup>

In all three isozymes, electron flow originates from the [4Fe-4S] cluster of the Fe protein, and proceeds through the P-cluster, eventually ending on the active site cofactor FeM-co

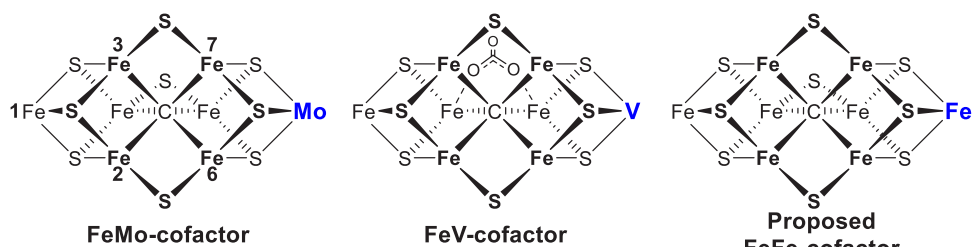


**Figure 2.** Structures of the FeMo-cofactor of Mo-nitrogenase,<sup>56,57,69,79</sup> FeV-cofactor of V-nitrogenase,<sup>58,72</sup> and proposed structure of the FeFe-cofactor of Fe-nitrogenase.<sup>80</sup> View is looking down on the Fe2, 3, 6, 7 face as indicated by the Fe atom numbering on FeMo-cofactor. Not shown are the cysteine coordinating Fe1, and the histidine and the R-homocitrate tail that ligate the Mo, V, or Fe are shown in blue.

(Figure 2).<sup>74–77</sup> The process of electron flow is complex and is covered in detail in other chapters of this Review.

## 2.2. Cofactors

Electrons and protons are accumulated, and substrates are reduced on the active site cofactor (FeMo-co, FeV-co, and FeFe-co, Figure 2). FeMo-co has the chemical composition [7Fe-9S-Mo-C-(R)-homocitrate] and is often referred to as the M-cluster.<sup>56,57,69,70,78,79</sup> FeV-co has a chemical composition of [7Fe-8S-V-C-(R)-homocitrate], with a carbonate ligand bound in place of the ninth sulfur and is sometimes referred to as V-cluster.<sup>58,59,72</sup> The FeFe-co is less well studied, but from spectroscopic studies is inferred to have a chemical composition of [8Fe-9S-C-(R)-homocitrate].<sup>80</sup>

## 3. MECHANISM OF NITROGENASE REDUCTION OF PROTONS AND N<sub>2</sub>

Extensive studies in the 1970s and 1980s<sup>20,31,81</sup> led to the development of the Lowe–Thorneley kinetic scheme for catalysis by the Mo-dependent nitrogenase, Figure 3.<sup>20,31,81</sup>

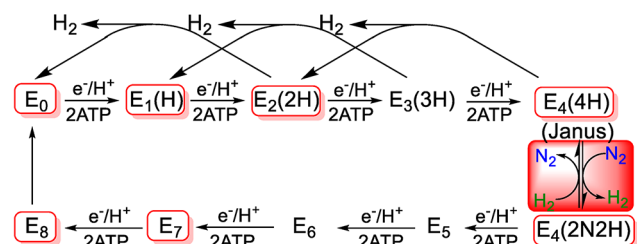


**Figure 3.** Simplified 8[e<sup>−</sup>/H<sup>+</sup>] kinetic scheme for nitrogen reduction. In the Lowe–Thorneley E<sub>n</sub> notation, n = number of [e<sup>−</sup>/H<sup>+</sup>] added to FeMo-co; in parentheses, the stoichiometry of H/N bound to FeMo-co. The re/oa equilibrium is highlighted in red, and the intermediates in red boxes have been freeze trapped for spectroscopic study.

This describes the transformations among catalytic intermediates, denoted E<sub>n</sub> where n is the number of steps of electron/proton delivery from the nitrogenase Fe protein to the active-site iron–molybdenum cofactor ([7Fe-9S-Mo-C-R-homocitrate]; FeMo-co) Figure 2.<sup>23,82</sup> This scheme's central feature was the mysterious proposal of obligatory formation of one mole of H<sub>2</sub> per mole of N<sub>2</sub> reduced, with the attendant limiting stoichiometric requirement of 8[e<sup>−</sup>/H<sup>+</sup>] per reduction of one N<sub>2</sub> to 2NH<sub>3</sub>, as given by eq 1, in agreement with stoichiometric measurements by Simpson and Burris,<sup>19</sup> but in contrast to the six reducing equivalents from 3H<sub>2</sub> used in the Haber–Bosch reaction.<sup>14</sup>

Some early reports presented possible explanations for the proposed connection between H<sub>2</sub> evolution and N<sub>2</sub> reduction, including models that involve metal-bound hydrides.<sup>20,31,83–92</sup> These speculations invoked multiple forms of hydride intermediates,<sup>31,88,90</sup> as they sought to explain three important observations of nitrogenase catalysis: (i) obligatory H<sub>2</sub> evolution during N<sub>2</sub> reduction by Mo-nitrogenase (eq 1),<sup>19,93</sup> (ii) H<sub>2</sub> (D<sub>2</sub>) as competitive inhibitors of N<sub>2</sub> reduction,<sup>88,90,94,95</sup> and (iii) N<sub>2</sub>-dependent HD formation by Mo-nitrogenase during N<sub>2</sub> reduction in the presence of D<sub>2</sub>.<sup>85,88–90,96–100</sup> One report suggested a dihydride intermediate after accumulation of three or four reducing equivalents (E<sub>3</sub> or E<sub>4</sub> in Figure 3) on the active site, and even suggested that N<sub>2</sub> somehow binds by displacing one H<sub>2</sub>.<sup>31,87</sup> Metal-hydride intermediates were also proposed to be involved in the reduction of C-based substrates (e.g., C<sub>2</sub>H<sub>2</sub> and cyclopropene).<sup>101–103</sup> In parallel, progress in understanding binding and activation of small molecules, such as N<sub>2</sub> and NO<sub>3</sub><sup>−</sup>, by metal-hydride and metal-dihydrogen inorganic compounds suggested possible N<sub>2</sub> reduction mechanisms that involved hydrides.<sup>83,84,104–108</sup> Such mechanistic speculations included that N<sub>2</sub> binds to Mo-nitrogenase by displacing H<sub>2</sub> through a Mo-dihydride or trihydride intermediate,<sup>83,104</sup> that an H<sub>2</sub> complex bound to Mo might play an important role for N<sub>2</sub> binding,<sup>105</sup> and that nitrogenase evolves H<sub>2</sub> through the reductive elimination of a dihydride species bound to either Mo or Fe, favoring the binding and reduction of N<sub>2</sub>.<sup>106</sup> Such multiple contradictory models, although insightful and provocative, were neither experimentally established nor excluded at the time they were suggested.

Despite the connection between N<sub>2</sub> reduction and H<sub>2</sub> release implied by the kinetic scheme of Figure 3, and the speculations it generated, in fact it had been neither confirmed nor universally accepted<sup>20,84</sup> that there is an obligatory, mechanistic requirement for formation of one H<sub>2</sub> per N<sub>2</sub> reduced to two NH<sub>3</sub>, with the apparent “waste” of 2[e<sup>−</sup>/H<sup>+</sup>] delivered at the cost of 4 ATP hydrolyzed. Beyond that, none of the intermediate states proposed in LT scheme (Figure 3) had been trapped for characterization: the “boxes” connected by the kinetic scheme were empty. Key breakthroughs came after the determination of the structure of the active site FeMo-cofactor<sup>55,56</sup> and the application of a combined strategy using genetic, biochemical, and biophysical methods characterize nitrogenase intermediates trapped during turnover with different substrates as previously reviewed<sup>21,23,33,36,82,110</sup> and further detailed in the following sections. As a result of these recent studies, seven of the ten states in the kinetic cycle have now been trapped for study (boxed in red in Figure 3).<sup>21,23,33,82</sup>

An important step in characterizing catalytic intermediates was the trapping and characterization of an organometallic intermediate allyl alcohol bound as a ferracycle to a single Fe of FeMo-co during turnover with the substrate propargyl alcohol (Figure 4).<sup>109</sup> This was followed by characterization of an

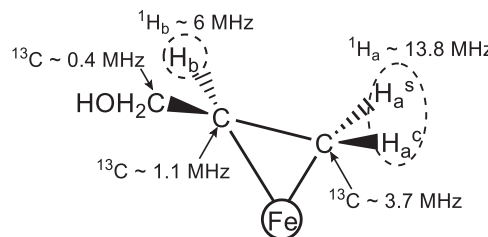


**Figure 4.** Propargyl alcohol reduction intermediate with hyperfine couplings indicated. Reproduced with permission from ref 109. Copyright 2004 American Chemical Society.

electron-accumulation intermediate (FeMo-co spin  $S = 1/2$ ) trapped during turnover of MoFe protein having the  $\alpha$ -70<sup>Val $\rightarrow$ Ile</sup> substitution,<sup>111</sup> which apparently prevents access by all substrates to the active site, other than protons.<sup>112</sup> Because electron delivery cannot be experimentally synchronized during turnover, the number of electrons accumulated by this intermediate ( $n$ ) was not evident. To determine this, the system was frozen to 77 K to prevent further electron delivery by reduced Fe protein, and then, it was warmed while frozen (cryoannealing) until relaxation toward  $E_0$  is enabled through a process involving 2-electron steps in which an  $H_2$  is released (see Figure 3). This cryoannealing electron-counting protocol showed this state relaxes in two steps with loss of  $H_2$  in each step, first to  $E_2(2H)$  and thence to  $E_0$ .<sup>113</sup> As shown in Figure 3, this identifies the intermediate as the key  $E_4(4H)$  “Janus” state (defined below),<sup>21</sup> which has accumulated four of the eight reducing equivalents required by eq 1. <sup>1,2</sup>H/<sup>95</sup>Mo ENDOR spectroscopy further showed that these equivalents are stored as two [Fe—H—Fe] bridging hydrides,<sup>111,114</sup> not as a previously imagined Mo—H species.<sup>83,104</sup> The  $E_4(4H)$  state of the native/wild-type (WT) enzyme itself<sup>115</sup> exhibits identical EPR/ENDOR and photophysical characteristics to this state when trapped in the  $\alpha$ -70<sup>Val $\rightarrow$ Ile</sup>/ $\alpha$ -195<sup>His $\rightarrow$ Gln</sup> altered protein.<sup>116</sup> As the WT intermediate accumulates in lower abundance, it has proven to be convenient to have these faithfully equivalent versions of the WT state.<sup>115,116</sup>

### 3.1. Reductive Elimination/Oxidative Addition (re/oa) Mechanism: As Proposed

The  $E_4(4H)$  intermediate represents a critical transition point in the  $N_2$  reduction pathway, Figure 3; as both the culmination of the catalytic phase of electron/proton accumulation by the enzyme and the initial step in the  $N_2$  reduction phase, it is poised to “fall back” to the  $E_0$  resting state by successive release of two  $H_2$ ,<sup>113</sup> but equally poised to eliminate  $H_2$  and proceed to reduce  $N_2$  to two  $NH_3$  through the accumulation of four more equivalents, hence the name, Janus, for the Roman god of transitions.<sup>21</sup> The trapping of this intermediate for study opened, for the first time, the possibility of directly testing for/characterizing the proposed equilibrium between two  $E_4$ -level states that interconvert through  $N_2$  binding/release coupled to  $H_2$  release/binding without additional  $[e^-/H^+]$  input, as visualized in Figure 3.

The experimental determination that  $E_4(4H)$  stored four reducing equivalents as bridging hydrides<sup>111,114</sup> offered

explanations of numerous features of nitrogenase mechanism that had defied explanation for decades,<sup>20,106</sup> while forging a connection between nitrogenase catalysis and the organometallic chemistry of metal hydrides.<sup>106,108,117–119</sup> See the earlier reviews for an account of early speculations about a possible role for hydrides in nitrogen fixation.<sup>20,84</sup>

The connection thus established to the chemistry of metal hydrides offered a potential explanation for and justification of the previously mysterious stoichiometry incorporated in eq 1. This explanation was proposed in a pair of “white papers” that showed how the obligatory  $H_2$  formation during nitrogenase  $N_2$  reduction might explain key experimental observations related to mechanism.<sup>21,23</sup> Once it was recognized that  $E_4(4H)$  contains two bridging hydrides, then the chemistry of metal-dihydride complexes<sup>117–119</sup> identifies the proposed  $[E_4(4H) + N_2] \leftrightarrow [E_4(2N2H) + H_2]$  equilibrium (Figure 3) as representing the reductive elimination (re) of  $H_2$  and its reverse, the oxidative addition (oa) of  $H_2$ : a mechanistically coupled re/oa equilibrium Figure 5. The re and release of  $H_2$

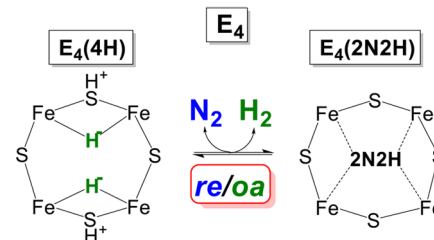


**Figure 5.** Schematic of re/oa equilibrium. In the indicated equilibrium, the binding and activation of  $N_2$  is mechanistically coupled to the re of  $H_2$ , as described in the text. Adapted with permission from ref 116. Copyright 2016 American Chemical Society.

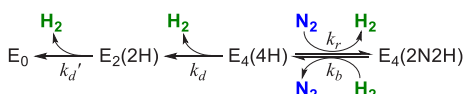
drives the most difficult (first) step of  $N_2$  cleavage: reduction of the  $N_2$  triple bond to a diazene level ( $2N2H$ ) intermediate through delivery to the substrate of the remaining two reducing equivalents.<sup>21</sup> As mentioned above and discussed in detail below, this proposal also offered an explanation of the key constraints on a mechanism for nitrogen fixation that had been developed over decades of study.<sup>20</sup>

### 3.2. Demonstration that Nitrogenase Functions Through the re/oa Equilibrium

The process of defining the mechanistic core of  $N_2$  activation, the re/oa equilibrium, as visualized in Figure 5, involved multiple steps over a number of years. It included the demonstration that high-spin ( $S = 3/2$ ) intermediates previously trapped during turnover under argon of wild type enzyme are  $E_2(2H)$  isomers,<sup>120–123</sup> and was completed by a capstone study of native nitrogenase that trapped and monitored both  $E_4(4H)$  and  $E_4(2N2H)$  as a function of turnover conditions.<sup>22,115,116,124,125</sup> In so doing, it completed the process of establishing that native nitrogenase is activated by the re/oa equilibrium, which mechanistically requires the loss of one  $H_2$  per  $N_2$  and results in the attendant  $8e^-$  stoichiometry shown in eq 1.<sup>19,23</sup>

Having identified the EPR spectra of all of the states involved in the relaxation of the  $E_4(4H)$  and  $E_4(2N2H)$  (Scheme 1), it was possible to monitor the kinetics of the relaxation of WT  $E_4(2N2H)$  to the resting-state  $E_0$ .<sup>115,124</sup> The progress curves for the relaxation of  $E_4(2N2H)$  and kinetically linked intermediates during cryoannealing of WT enzyme at  $-50^\circ C$  presented in Figure 6 are well described by the curves

**Scheme 1. Kinetic Scheme for the Decay of Freeze-Trapped  $E_4(2N2H)$  Derived from Figure 3<sup>a</sup>**



Reproduced with permission from ref 124. Copyright 2015 American Chemical Society. <sup>a</sup> $k_r$  and  $k_b$  are the second-order rate constants for *re* and its reverse;  $k_d$  and  $k_d'$  are the rate constants for the irreversible decay of  $E_4(4H)$  and  $E_2(2H)$ , respectively.

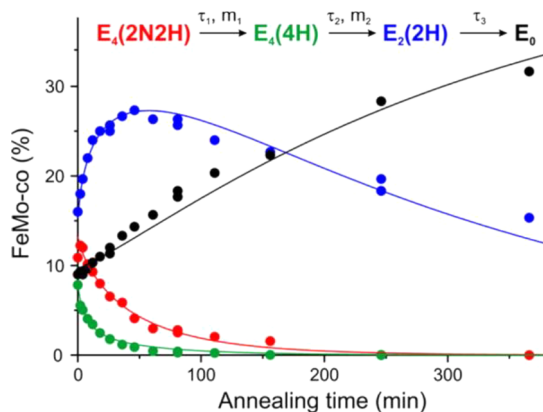


**Figure 6.** Time courses of four EPR detected states during  $-50\text{ }^\circ\text{C}$  cryoannealing of WT low  $P(\text{N}_2) \sim 0.05\text{ atm}$  turnover in  $\text{H}_2\text{O}$ . The data colors correspond to those in the kinetic scheme (top) and the lines correspond to fits to that scheme. Stretched exponential  $\exp(-(t/\tau)^m)$  parameters of the first two fast steps are  $\tau_1 = 43\text{ min}$ ,  $m_1 = 0.79$  and  $\tau_2 = 6\text{ min}$ ,  $m_2 = 0.8$ , and the third slow step fitted as exponential with  $\tau_3 = 330\text{ min}$ . Reproduced with permission from 115. Copyright 2016 American Chemical Society.

calculated from fits to the sequential kinetic scheme involving the *re/oa* equilibrium of Scheme 1.<sup>115,124</sup> Not only does  $E_4(2\text{N}2\text{H})$  relax to  $E_4(4\text{H})$ , but the amount of trapped  $E_4(2\text{N}2\text{H})$  increases with increasing  $[\text{N}_2]$ , while the amount of  $E_4(4\text{H})$  decreases (Figure 7).<sup>115,124</sup>

Correspondingly, the rate of relaxation increases with increasing  $[\text{H}_2]$ , and decreases with increasing  $[\text{N}_2]$ .<sup>115,124</sup> This kinetic coupling of the loss of  $E_4(2\text{N}2\text{H})$  to the formation of  $E_4(4\text{H})$  through *oa* of  $\text{H}_2$ , directly establishes the operation of the *re/oa* equilibrium and its kinetic reversibility.

The observation of both  $E_4(4\text{H})$  and  $E_4(2\text{N}2\text{H})$  in samples freeze-quenched during  $\text{N}_2$  fixation allowed measurement of the equilibrium constant for *re/oa*,  $K_{\text{re}} = k_r/k_b$  (Figure 5; Scheme 1).<sup>115</sup> This was done by estimating the relative amounts of  $E_4(4\text{H})$  and  $E_4(2\text{N}2\text{H})$  freeze-trapped under experimentally varied partial pressures of  $\text{N}_2$  and  $\text{H}_2$ , yielding the *re/oa* equilibrium constant,  $K_{\text{re}}$  and the free energy for the equilibrium, eqs 4 and 5

$$K_{\text{re}} = \frac{E_4(2\text{N}2\text{H})}{E_4(4\text{H})} \cdot \frac{P(\text{H}_2)}{P(\text{N}_2)} \quad (4)$$

$$\Delta_{\text{re}}G^\circ = -RT \ln(K_{\text{re}}) \sim -2\text{ kcal/mol} \quad (5)$$

Thus, this first step in the reduction of  $\text{N}_2$  by nitrogenase is essentially thermoneutral,  $\Delta_{\text{re}}G^\circ \sim -2\text{ kcal/mol}$ , whereas direct hydrogenation of gas-phase  $\text{N}_2$  is endergonic by more than 50 kcal/mol.<sup>115</sup>

### 3.2.1. *re/oa* Mechanism Generates the Key Constraints Revealed by Experiment.

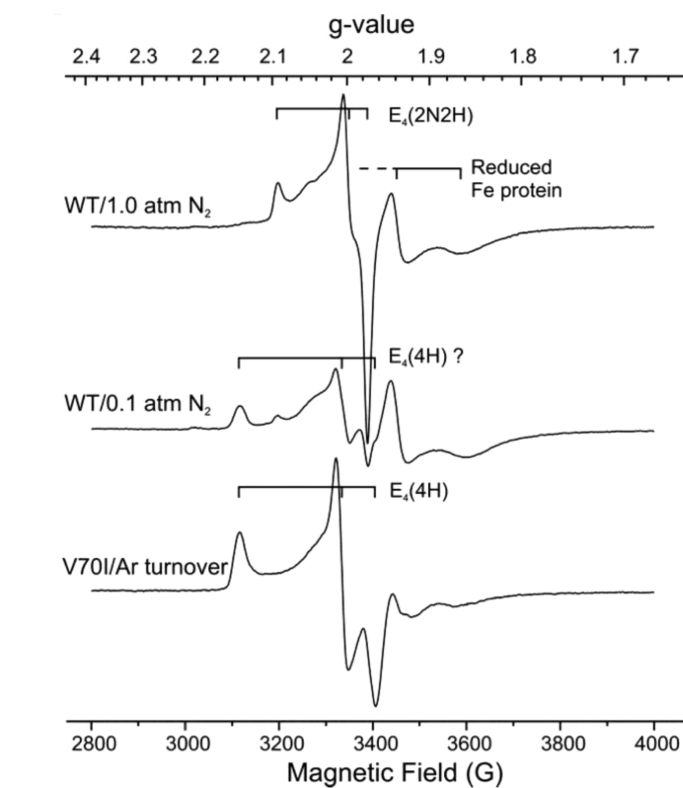


**Figure 7.** X-band EPR spectra of WT nitrogenase turnover samples trapped under 1 atm of  $\text{N}_2$  (with stirring to facilitate transfer of  $\text{H}_2$  formed during turnover into the headspace<sup>124</sup>), and under low  $P(\text{N}_2)$  in  $\text{H}_2\text{O}$  buffer (without stirring) shown in comparison with spectrum of  $E_4(4\text{H})$  state trapped during turnover of  $\alpha$ -70<sup>Val→Ile</sup> MoFe protein of the same concentration. Reproduced with permission from ref 115. Copyright 2016 American Chemical Society.

revealed several puzzling features of nitrogen fixation by nitrogenase whose mechanistic origins were not understood, but ultimately served as *key constraints* on any proposed mechanism, Chart 1.<sup>20,21,23</sup> A series of experiments has shown that all of these constraints are generated by the functioning of the *re/oa* mechanism.

### Chart 1. Key Constraints on the Nitrogenase Mechanism<sup>20</sup>

*D<sub>2</sub> or T<sub>2</sub> only react during N<sub>2</sub> Turnover, during which:*

- (a) 2HD form stoichiometrically:*  
 $\text{M-N}_2 + \text{D}_2 + 2\text{H}^+ + 2\text{e}^- \rightarrow 2\text{HD} + \text{M} + \text{N}_2$
- (b) No Scrambling with solvent:*  
No  $\text{T}^+$  released to solvent under  $T_2$
- (c) Reduction Level of this reaction:*  
 $\text{D}_2/T_2$  reacts at  $E_4(2\text{N}2\text{H})$  level

These constraints arise from previously confusing results from turnover in the presence of  $\text{D}_2$  or  $\text{T}_2$ . It was found that  $\text{D}_2$  and  $\text{T}_2$  only react with nitrogenase during turnover under an  $\text{N}_2/\text{D}_2$  or  $\text{N}_2/\text{T}_2$  atmosphere<sup>90,98</sup> at the  $E_4(2\text{N}2\text{H})$  reduction level (c); in this reaction  $\text{D}_2$  is stoichiometrically reduced to two HD (with  $\text{H}_2\text{O}$  buffer) (a);<sup>88,89,98</sup> corresponding turnover with  $\text{T}_2$  does not lead to exchange of  $\text{T}^+$  into  $\text{H}_2\text{O}$  solvent (b).<sup>90</sup> It has now been shown that all these  $\text{D}_2/\text{T}_2$  constraints arise through the reverse of the *re* process, Figure 5, namely, the oxidative addition (*oa*) of  $\text{H}_2$  with loss of  $\text{N}_2$ .<sup>21,23</sup> According to the mechanism, during turnover under  $\text{D}_2/\text{N}_2$ , reaction with  $\text{D}_2$  generates

dideutero- $E_4$  with two  $[\text{Fe}-\text{D}-\text{Fe}]$  bridging deuterides that do not exchange with solvent,<sup>22</sup> and the same is true for  $T_2$ . These  $E_4(4\text{H})$  isotopologues, which are denoted  $E_4(2\text{L}^-; 2\text{H}^+)$ ,  $\text{L} = \text{D}$  or  $\text{T}$ , would relax through  $E_2(\text{L}^-; \text{H}^+)$  to  $E_0$  with successive loss of two  $\text{HL}$ .<sup>21,113</sup>

The proposed formation of the  $E_4(2\text{D}^-; 2\text{H}^+)$  and  $E_2(\text{D}^-; \text{H}^+)$  states through the thermodynamically allowed reverse of *re*, the *oa* of  $\text{D}_2$  with accompanying release of  $\text{N}_2$ , in fact was the first successful test of the *re/oa* mechanism. When these states were formed during turnover under  $\text{N}_2/\text{D}_2$ , the nonphysiological substrate acetylene ( $\text{C}_2\text{H}_2$ ) intercepted them to generate deuterated ethylenes ( $\text{C}_2\text{H}_3\text{D}$  and  $\text{C}_2\text{H}_2\text{D}_2$ ).<sup>22</sup> More recently the  $E_4(2\text{D}^-; 2\text{H}^+)$  and  $E_4(2\text{H}^-; 2\text{D}^+)$  states were observed and characterized by EPR spectroscopy and by studies of isotope effects on the photophysical properties of these isotopologues.<sup>115</sup>

**3.2.2. There Are No Reductive Activation Steps Prior to Catalysis.** In recent years, mechanistic proposals have posited that multiple  $[\text{e}^-/\text{H}^+]$  must be delivered to the true resting-state FeMo-co to activate it to a state that acts as the  $E_0$  in an  $8[\text{e}^-/\text{H}^+]$  catalytic cycle equivalent to the scheme of Figure 3.<sup>126</sup> First, of course, no such preactivation process was observed in the many presteady state measurements carried out on as-isolated nitrogenase over decades.<sup>20,31</sup> But most importantly the measurements of the relaxation of the odd-electron  $S = 1/2$   $E_4(4\text{H})$  with release of  $2\text{H}_2$  (Figure 6)<sup>113</sup> unambiguously show that it relaxes directly to the same EPR-active odd-electron  $E_0$  ( $S = 3/2$ ) resting state that has been isolated and characterized crystallographically, not to a different state, which at least in one model, would not even be odd-electron.<sup>126</sup> And there is no doubt that  $E_4(4\text{H})$  indeed relaxes to the crystallographically characterized  $E_0$  state. The identity of the crystalline  $E_0$  and the putative  $E_0$  formed by  $E_4(4\text{H})$  relaxation is established by the identity of the EPR spectra of the solution  $E_0$  formed by relaxation and that of the crystalline  $E_0$ ,<sup>57,127</sup> both of which precisely match the long-established EPR spectrum of as-isolated Mo-nitrogenase in solution.

### 3.3. Exploring the *re/oa* Mechanism

Upon establishing that nitrogen fixation by nitrogenase operates through the *re/oa* mechanism with its  $8[\text{e}^-/\text{H}^+]$  stoichiometry, further experiments and computation have been used to explore the microscopic details.

**3.3.1. Reductive Elimination Involves an  $\text{H}_2$ -Bound Intermediate.** The demonstration that the  $E_4(4\text{H})$  Janus intermediate has accumulated four reducing equivalents as two  $[\text{Fe}-\text{H}-\text{Fe}]$  bridging hydrides, and the resulting link thus forged between nitrogenase catalysis and the organometallic chemistry of metal hydrides, inspired examination of the behavior of  $E_4(4\text{H})$  under photolysis as a test of this linkage and as a means of obtaining atomic-level details of the *re* activation process. The photolysis of transition metal dihydride complexes typically results in the release of  $\text{H}_2$ ,<sup>108,128–135</sup> and it was found that  $\text{H}_2$  release in fact occurred during *in situ* 450 nm photolysis of  $E_4(4\text{H})$  in an EPR cavity at temperatures below 20 K.<sup>116,125</sup> These studies, as supported by density functional theory (DFT) calculations,<sup>136</sup> showed that an  $\text{H}_2$  complex on the ground adiabatic potential energy surface  $E_4(\text{H}_2; 2\text{H})$  becomes populated during catalysis, but this state cannot lose  $\text{H}_2$  because the resultant, denoted  $[\text{E}_4(2\text{H})^* + \text{H}_2]$ , is at inaccessibly high energy.<sup>125</sup> However,  $\text{N}_2$  can bind and displace the  $\text{H}_2$  of  $E_4(\text{H}_2; 2\text{H})$  to complete the conversion

of  $[\text{E}_4(4\text{H}) + \text{N}_2]$  into  $[\text{E}_4(2\text{N}2\text{H}) + \text{H}_2]$ , as represented in Figure 8.<sup>136</sup>

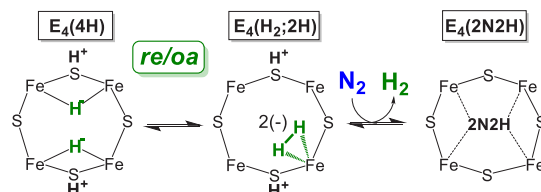


**Figure 8.** Cartoon version of suggested catalytic pathway for *re/oa* activation of FeMo-co for  $\text{N}_2$  reduction. Reproduced with permission from ref 125. Copyright 2017 American Chemical Society.

### 3.3.2. $E_2(2\text{H})$ States 1b and 1c Are Hydride Isomers.

As a further use of hydride photolysis to explore nitrogenase function, it was shown that  $E_2(2\text{H})/1\text{b}$  stores the two reducing equivalents as a hydride, almost surely with the  $[\text{Fe}-\text{H}-\text{Fe}]$  bridging mode of binding, and that 1c is a *hydride isomer* of  $E_2(2\text{H})/1\text{b}$ , either with the hydride bridging a different pair of Fe or having converted to a terminal hydride, as visualized in Figure 9.<sup>123</sup> Relatively modest differences in the occupancy

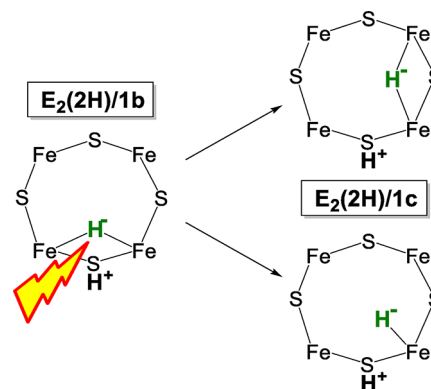


**Figure 9.** Schematic representation of photolysis conversion of  $[\text{Fe}-\text{H}-\text{Fe}]$  hydride bridge of  $E_2(2\text{H})/1\text{b}$  into isomer  $E_2(2\text{H})/1\text{c}$  with either a hydride bridge between a different pair of Fe ions or an Fe–H terminal hydride. Adapted with permission from ref 123. Copyright 2018 American Chemical Society

ratio of the two  $E_2(2\text{H})$  hydride conformers during turnover,  $1\text{b}/1\text{c} \sim (2-3)/1$ , suggested that the two are able to readily interconvert during fluid-solution turnover.<sup>123</sup>

**3.3.3. Density Functional Studies of the *re/oa* Equilibrium.** The structure and energetics of possible nitrogenase intermediates were recently explored by DFT calculations on a broad range of structural models for the active site and a variety of DFT exchange and correlation functionals.<sup>136–139</sup> These computations<sup>136</sup> showed that it is necessary to include all residues (and water molecules) interacting directly with FeMo-co via specific H-bonds interactions, nonspecific local electrostatic interactions, and steric confinement to prevent spurious disruption of FeMo-co<sup>126,140–142</sup> upon accumulation of  $4[\text{e}^-/\text{H}^+]$ . These calculations indicated an important role of sulfide hemilability in the overall conversion of  $E_0$  to a diazene-level intermediate, as suggested by X-ray crystallographic studies.<sup>58,59,143,144</sup> Perhaps most importantly, they explained *how* the enzyme *mechanistically* couples exothermic  $\text{H}_2$  formation to endothermic cleavage of the  $\text{N}\equiv\text{N}$  triple bond in the nearly thermoneutral

(a)

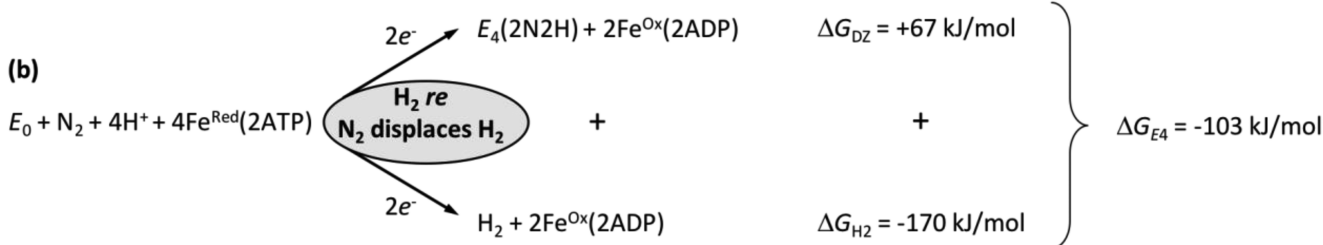
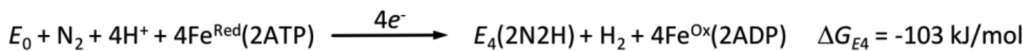


**Figure 10.** Energetics of formation of  $E_4(2N2H)$  from the enzymatic reactants and its decomposition into two individual two-electron, two-proton processes, each involving the hydrolysis of 2ATP per electron: the formation of  $E_4(2N2H)$  and of  $H_2$ , which are coupled through displaces and releases  $H_2$  formed by *re* from  $E_4(4H)$ . Adapted with permission from 136. Copyright 2018 National Academy of Sciences.

*re/oa* equilibrium discovered experimentally (Figure 10), while preventing the futile generation of two  $H_2$  without  $N_2$  reduction: hydride *re* generates an  $H_2$  complex, again in agreement with experiment, and  $H_2$  is only lost when displaced by  $N_2$ , to form an end-on  $N_2$  complex, which then proceeds to a diazene-level intermediate.<sup>136</sup>

**3.3.4. High-Resolution ENDOR Spectroscopy Coupled with Quantum Chemical Calculations Reveals the Structure of Janus Intermediate  $E_4(4H)$ .** Because of the central role of  $E_4(4H)$  in the *re/oa* mechanism, it was essential to characterize its structure. The original  $^1H$  ENDOR study of  $E_4(4H)$ ,<sup>111</sup> and subsequent  $^{95}Mo$  and  $^{57}Fe$  ENDOR study<sup>114,145</sup> demonstrated that FeMo-co in  $E_4(4H)$  contains two  $[Fe-H-Fe]$  bridging hydrides but were unable to provide a satisfactory picture of the relative spatial relationships of the two hydrides. The nature of  $E_4(4H)$  has been the subject of numerous recent computational studies based on DFT.<sup>136–139</sup>

The lowest-free-energy  $E_4$  isomers obtained from the DFT studies reported so far have two of the four hydrogens located on  $\mu_2$ -S atoms, while the other two hydrogens are either present as hydrides in bridging positions between two Fe atoms, or in mixed bridging/terminal position on the  $Fe_{2,3,6,7}$  face of FeMo-co,<sup>136,137,146,147</sup> or as a dihydrogen ( $n^2-H_2$ ) adduct bound to either  $Fe_2$ <sup>136,137,147</sup> or  $Fe_6$ .<sup>147</sup>

As we pointed out, limitations in DFT-based schemes—the only ones computationally feasible for a systematic study of complex systems, such as FeMo-co—make it difficult to determine the ground-state structure of  $E_4(4H)$  based on DFT-derived relative energies alone. To emphasize this issue, careful computational analyses carried out by the research groups of Ryde<sup>137,146,148,149</sup> and Bjornsson<sup>139,147</sup> have clearly shown that the exchange and correlation functional adopted in the DFT calculations largely affect the ordering of possible  $E_4$  isomers, which differ on the location of the hydrides. This uncertainty is further aggravated by intrinsic deficiency of broken symmetry DFT calculations which are simply unable to capture the multideterminant character of the electronic structure of FeMo-co. A detailed discussion of all of these issues has been presented by Cao and Ryde.<sup>146</sup>

To determine how the Janus intermediate binds its two hydrides, exhaustive, high-resolution CW-stochastic  $^1H$ -ENDOR experiments were performed using improved ENDOR methodologies and updated equipment.<sup>150</sup> Figure 11 illustrates the remarkable spectroscopic resolution and strong orientation selection that enabled the previously

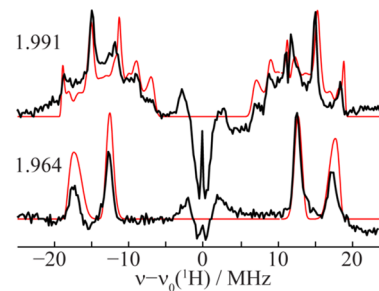


**Figure 11.** 35 GHz  $^1H$  stochastic-field modulation detected (stochastic CW) ENDOR spectra of  $E_4(4H)$  in  $70^{Val \rightarrow Ile}/\alpha-195^{His \rightarrow Gln}$  MoFe protein, acquired at  $g = 1.991$  and  $1.964$  (black) and summed simulations (red). The signal with  $v_0(^1H) \pm \sim 3$  MHz, with both positive and negative features, represents transient responses from weakly coupled, more distant protons. Reproduced with permission ref 150. Copyright 2019 American Chemical Society.

unattainable determination of absolute hyperfine-interaction signs. The important results for structural assessments were the findings that (i) the dipolar–electron–nuclear hyperfine coupling tensors for the two hydrides were coaxial, (ii) each had “rhombic symmetry” (two components with equal and opposite signs; one null component), and (iii) the *signed* tensor components for the two hydrides were permuted relative to each other.

These findings provided critical constraints on the structure of  $E_4(4H)$ , but did not by themselves implicate a particular structure, and so experiment was coupled to the DFT computations. Just as the DFT computations could not discriminate among candidates for the  $E_4(4H)$  ground state, neither could they discriminate through computations of the dipolar hyperfine couplings. However, the DFT structures are robust and so the ENDOR measurements were coupled to DFT structural models through an analytical point-dipole Hamiltonian for the hydride electron–nuclear dipolar coupling to its “anchoring” Fe ions, an approach that overcomes limitations inherent in both experimental interpretation and computational accuracy. The simple point-dipole approximation was not expected to provide quantitatively accurate results for the magnitudes of the hyperfine tensor components because of the delocalized nature of the electron density in the FeMo-co.<sup>147</sup> Instead, for each of the DFT-derived candidate structures for  $E_4(4H)$  ground state the dipole approach was simply used to assess the relative orientation of

the dipolar interaction tensors for the two hydrides of a structural model when each had a rhombic tensor, and this was compared to the experimentally determined relative tensor orientation.<sup>146,147,150</sup>

This comparison alone enabled discrimination among possible  $E_4(4H)$  isomers.<sup>23,111</sup> The result: the freeze-trapped, lowest-energy Janus intermediate structure is  $E_4(4H)^{(a)}$ , Figure 12. As the calculations indicated the presence of a number of

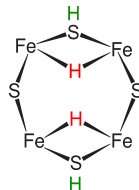


**Figure 12.** Cartoon of the 2,3,6,7 face of the ground state isomer of  $E_4(4H)$ , denoted  $E_4(4H)^{(a)}$  as found by BS-DFT computation. Reproduced with permission from ref 150. Copyright 2019 American Chemical Society.

isomers close in energy,<sup>137,139,146,147,150</sup> it was envisioned that at ambient temperatures the  $E_4(4H)$  hydrides become fluxional, with a dynamic population of multiple isomers.

As additional DFT computations are carried out, suggesting variations on the  $E_4(4H)$  structure, the results of this ENDOR study, in conjunction with the analytical point-dipole Hamiltonian, will continue to provide the benchmark against which those structures can be tested.

**3.3.5.  $E_1$  Forms by Reduction of Fe, Not Mo.** The  $E_1(H)$  state as prepared both by low-flux turnover and by radiolytic cryoreduction were investigated using a combination of Mo K $\alpha$ -HERFD (high energy resolution fluorescence detection) and Fe K-edge PFY (partial-fluorescence yield) X-ray absorption spectroscopy techniques.<sup>151</sup> The results demonstrate that this state is formed by an Fe-centered reduction and that Mo does not change redox state, a further indication that Mo is only indirectly involved in substrate reduction, which occurs at Fe. This conclusion is further supported by a recent Mo and Fe K-edge EXAFS (extended X-ray absorption fine structure) characterization of  $E_0$  and  $E_1$  states in combination with QM/MM calculations that supported protonation of a belt sulfide (S2B or SSA) in  $E_1$ .<sup>152</sup>

### 3.4. Kinetic Description of the Competing Reactions at $E_4(4H)$

As can be seen in Figure 13, the reactions of  $E_4(4H)$  can be viewed as a competition: the forward direction of the *re/oa* equilibrium, involving binding of  $N_2$  and displacement of  $H_2$ , competes with the relaxation of  $E_4(4H)$  through hydride

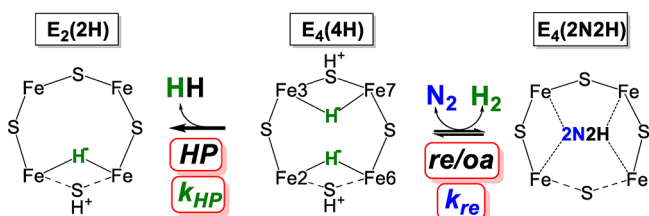


**Figure 13.** Reactions of the  $E_4$  state.  $N_2$  binds through *re* with rate constant  $k_{re}$  to the right.  $H_2$  evolves through HP with rate constant  $k_{HP}$  to the left. Reproduced with permission 153. Copyright 2018 American Chemical Society.

protonolysis (HP), which releases  $H_2$  without  $N_2$  binding.<sup>153,154</sup> The competition between these two reactions is defined by the ratio of their rate constants  $k_{re}$  for the forward reaction and  $k_{HP}$  for the relaxation reaction and modulated by the ratio of the partial pressures of  $N_2$  and  $H_2$ . A kinetic model was developed that yields, under high electron flux conditions (high Fe protein to MoFe protein molar ratio), the values of these two rate constants from the fitting of the ratio,  $H_2$  formed divided by  $N_2$  reduced, as a function of the partial pressure of  $N_2$ . As can be seen in Figure 14<sup>154</sup> and from

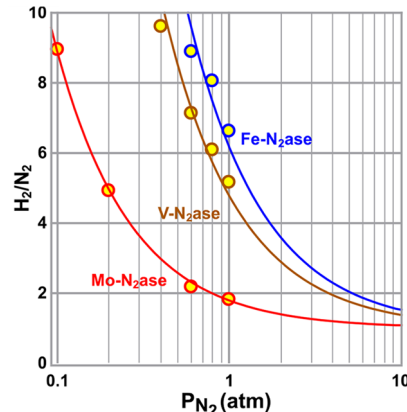


**Figure 14.** Ratio of  $H_2$  evolved to  $N_2$  reduced as a function of partial pressure  $N_2$  for all three nitrogenase isozymes. The fits to this data for each enzyme produce the value of its parameter  $\rho = k_{re}/k_{HP}$ . Reproduced with permission from ref 154. Copyright 2019 American Chemical Society.

measurements by many groups, at 1 atm of  $N_2$ , Mo-nitrogenase shows  $H_2/N_2 < 2$  and the ratio asymptotically approaches unity with increasing  $N_2$  partial pressure. The fit to the data of Figure 14 yielded  $k_{re}/k_{HP} = 5.1 \text{ atm}^{-1}$ . This considerable preference for the forward reaction is truly remarkable when considering the expected reactivity of a metal hydride toward protonolysis as observed in many reductive catalysts. Corresponding suppression of the formation of  $H_2$  by an HP reaction in synthetic catalysts for  $N_2$  reduction is one of the grand challenges in catalyst design.

The two other isozyme of Mo-nitrogenase, the V- and Fe-nitrogenases, share similar architecture to the Mo-enzyme, but as noted above, have different polypeptides that present different active site environments and different active site metal clusters.<sup>43,58</sup> At 1 atm of  $N_2$ , it can be seen that the V- and Fe-nitrogenase show much higher ratios of  $H_2$  formed per  $N_2$  reduced (Figure 14). Application of the high-flux kinetic model to the V- and Fe-nitrogenases, revealed reduced values of the rate-constant ratio compared to Mo-nitrogenase,  $k_{re}/k_{HP} = 1.1$  and  $0.78 \text{ atm}^{-1}$ , respectively.<sup>154</sup> Further analysis pinpointed that whereas the values for  $k_{re}$  for the V- and Fe-nitrogenases are as much as 10-fold smaller than  $k_{re}$  for the Mo enzyme, the values of  $k_{HP}$  differ by less than 2-fold. In short, the V- and Fe-nitrogenases are not better at the HP side-reaction, but rather are poorer at the productive *re* reaction. The source of these differences among the three nitrogenase isozyme remains to be deduced.<sup>153,154</sup>

**3.4.1. All Three Nitrogenases Employ the *re/oa* Mechanism.** The differences in rate constants among the three isozymes might suggest a different mechanism for  $N_2$  binding and activation. However, this is not so. The *re/oa*

mechanism involves an equilibrium between the  $E_4(4H)$  state and the  $E_4(2N2H)$  state. This predicts  $H_2$  inhibition of  $N_2$  reduction and the formation of HD during turnover under mixed  $D_2$  and  $N_2$ , both of which were found for all three isozymes. These observations establish that all three nitrogenase isoforms follow the same *re/oa* mechanism.<sup>38,153,154</sup>

### 3.5. Structure–Function Relationship During Nitrogenase Catalysis

One of the persistent challenges in nitrogenase research is to understand how protein and cluster dynamics might participate in the mechanism.<sup>32,33,35–37,68,75,156–168</sup> Many structural and spectroscopic studies have shown that the resting state of nitrogenase is largely unreactive, suggesting that motion of the surrounding protein or changes in ligation of FeMo-co might be essential in catalysis.<sup>32,33,82,158</sup> A number of calculations have suggested changes in FeMo-co that could be occurring during catalysis, including breaking of one or more the Fe–C bonds<sup>126,140,141,169–171</sup> or breaking one or more Fe–S bonds.<sup>136,172–177</sup> Recent structural studies have observed significant changes in the FeMo-co and FeV-co structures that might point to dynamics relevant to catalysis.<sup>58,59,143,144,178</sup> In one such study, it was observed that MoFe protein under turnover with CO shows the substitution of one of the belt sulfide ligand S2B by a bridging CO ligand<sup>143</sup> (see section 5.2 for more details). These studies point to lability in one or more of the Fe–S bonds during turnover.<sup>178,179</sup> This lability was seen in the computational study of the *re/oa* equilibrium described in sections 3.3.3 and 3.3.4.<sup>136</sup> Recently, a structure of the V-nitrogenase by Einsle et al. showed FeV-cofactor with two belt sulfide ligands substituted by a proposed carbonate and a light atom (N(H) or O(H), Figure 15).<sup>59,155</sup> Even though the identity of the light atom

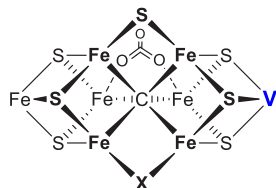


Figure 15. FeV-cofactor structure proposed by X-ray structure ( $X = NH$ )<sup>59</sup> and theoretical calculations ( $X = OH$ ).<sup>155</sup>

ligand is under debate, the plausible implication and relevance to the  $N_2$  reduction mechanism by nitrogenase have initiated vigorous discussion.<sup>156,180,181</sup> The recent progress in spectroscopic studies on nitrogenase intermediates<sup>162</sup> and the X-ray structures of nitrogenase from turnover mixtures promises further progress in understanding the dynamics of the metalloclusters, especially the active site FeM-cofactor during substrate/inhibitor interaction.

## 4. NONPHYSIOLOGICAL N-BASED SUBSTRATES

### 4.1. Range of N-Based Substrates

An important property of nitrogenases is the ability to bind and reduce a number of nonphysiological substrates.<sup>20,39,40</sup> A common, but not universal, property of nitrogenase substrates is that they are small and contain double or triple bonds. The study of how these alternative substrates interact with nitrogenase has provided important mechanistic insights.<sup>20,23,33,41,82</sup> In this section, recent work on a number of alternative substrates that contain N is reviewed.

### 4.2. $N_2H_x$ Substrates

As shown in the *re/oa* kinetic scheme of Figure 3, following the formation of  $E_4(2N2H)$ , the catalytic cycle traverses four states that contain partially reduced species of  $N_2$ .<sup>21,23</sup> Researchers have long considered two competing proposals for this “second half” of the kinetic scheme, which invoke distinctly different intermediates, Figure 16. In the “distal” (D) pathway, utilized

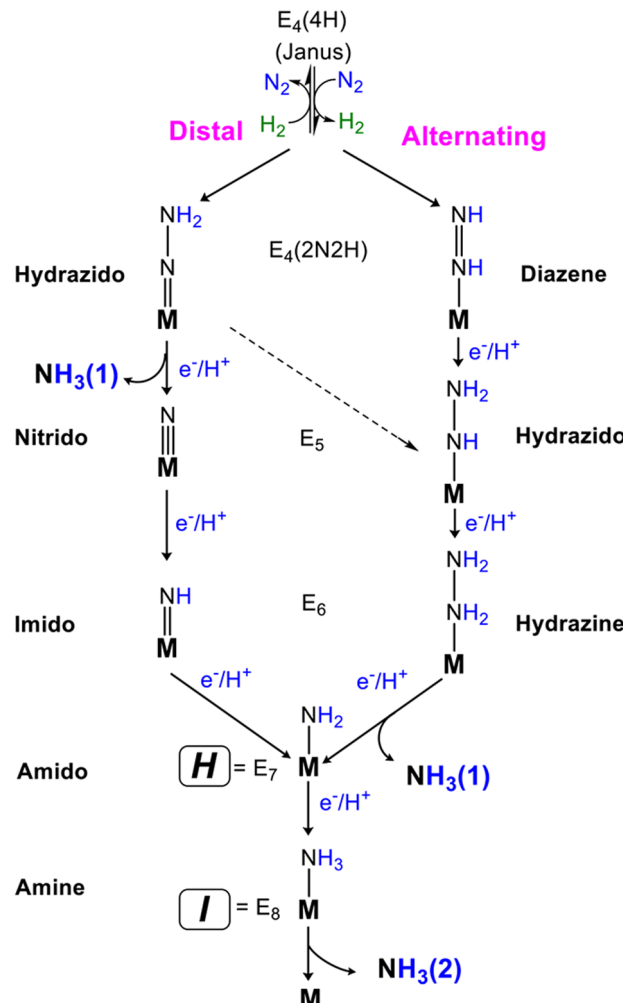


Figure 16. Proposed  $N_2$  reduction pathways with M representing the active site FeMo-cofactor. A distal reduction pathway (D) and an alternating reduction pathway (A) are displayed with plausible key intermediates. The hybrid-A pathway is indicated by a dashed arrow.<sup>182</sup>

by  $N_2$ -fixing inorganic Mo complexes,<sup>83,183–185</sup> the distal N of Fe-bound  $N_2$  is hydrogenated in three steps. The first  $NH_3$  is then liberated with the addition of the fifth  $[e^-/H^+]$  overall, to generate the nitrido species,  $E_5$ . This nitrido-N is then hydrogenated three times to yield the second  $NH_3$ . In the “alternating” (A) pathway that has been suggested to apply to reaction at Fe of FeMo-co,<sup>175,186</sup> the two N’s instead are hydrogenated alternately, with a four-electron and proton reduced species equivalent to hydrazine ( $N_2H_4$ ) formed as the  $E_6$  intermediate. In this case, the first  $NH_3$  is only liberated during the next hydrogenation step, the formation of  $E_7$  (Figure 16).<sup>33,82</sup> Peters et al. has proposed what might be called a hybrid-A pathway,<sup>182</sup> in which  $E_4$  on the D pathway is converted to  $E_5$  on the A pathway. Consequently, as with the

limiting A pathway, the first  $\text{NH}_3$  also is released with formation of  $\text{E}_7$ , as shown.

Previous studies demonstrated that the diazene analogs methyldiazene ( $\text{CH}_3\text{—N}=\text{NH}$ ), dimethyldiazene ( $\text{CH}_3\text{—N}=\text{NH—CH}_3$ ) and diazirine ( $\text{CH}_2\text{N}_2$ ) are substrates for nitrogenase, all being reduced to  $\text{NH}_3$ , and  $\text{CH}_x$  species.<sup>187,188</sup> The early studies on these substrates have been reviewed.<sup>93</sup> In 2007, the study of diazene ( $\text{HN}=\text{NH}$ ) as a substrate for Mo-dependent nitrogenase was expanded through the use of in situ generation from azodiformate.<sup>189</sup> The 4  $[\text{e}^-/\text{H}^+]$  reduction of diazene produced two equivalents of  $\text{NH}_3$ . The reduction of diazene was found to be inhibited by  $\text{H}_2$ , which is also an inhibitor of  $\text{N}_2$  reduction.<sup>189</sup> As can now be understood, in both cases the inhibition is a consequence of the *re/oa* mechanism as described in section 3. This result implies that diazene *must* enter the reaction pathway by forming the same diazene-level intermediate,  $\text{E}_4(2\text{N}_2\text{H})$ , as forms when  $\text{N}_2$  reacts with  $\text{E}_4(4\text{H})$ .<sup>23</sup> The addition of  $\text{H}_2$  then reverses the *re/oa* equilibrium, with the  $\text{E}_4(2\text{N}_2\text{H})$  undergoing *oa* with loss of  $\text{N}_2$  to generate  $\text{E}_4(4\text{H})$ . The  $\text{E}_4(2\text{N}_2\text{H})$  could form in one of two ways: direct reaction with  $\text{E}_0$  or, as proposed in 2012,<sup>190</sup> reaction with  $\text{E}_2(2\text{H})$  with loss of  $\text{H}_2$  through hydride protonation.

Recently it has also been shown that the 2  $[\text{e}^-/\text{H}^+]$  reduction of hydrazine to produce two equivalents of  $\text{NH}_3$ <sup>191</sup> is efficiently achieved by remodeling of the  $\alpha\text{-70}^{\text{Val}}$  residue around FeMo-cofactor of Mo-nitrogenase with a smaller side-chain amino acid (Ala).<sup>192</sup> In contrast to the  $\text{H}_2$  inhibition of diazene and  $\text{N}_2$  reduction, hydrazine reduction was not inhibited by  $\text{H}_2$ . This again is consistent with the scheme of Figure 3. Once the delivery of  $[\text{e}^-/\text{H}^+]$  to  $\text{E}_4(2\text{N}_2\text{H})$  has generated  $\text{E}_5$ , the enzyme has passed the *re/oa* equilibrium stage and is no longer susceptible to inhibition by  $\text{H}_2$ , while hydrazine appears on the A  $\text{N}_2$  reduction pathway at  $\text{E}_6$ .<sup>190</sup>

Two common intermediates have been freeze-trapped using MoFe protein variants with both diazene substrates ( $\text{CH}_3\text{—N}=\text{NH}$  and  $\text{HN}=\text{NH}$ ) and hydrazine  $\text{N}_2\text{H}_4$  (Figure 17):<sup>188,189,192,194</sup> a broad, low-field resonance  $\text{H}$  (non-Kramers

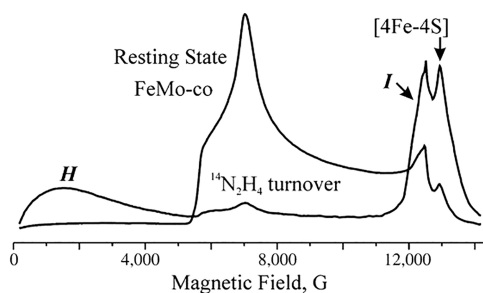


**Figure 17.** Q-band CW EPR spectrum of  $\alpha\text{-70}^{\text{Val}\rightarrow\text{Ala}}/\alpha\text{-195}^{\text{His}\rightarrow\text{Gln}}$  MoFe protein in the resting state and trapped during turnover with  $^{14}\text{N}_2\text{H}_4$  as substrate. Kramers intermediate I and non-Kramers intermediate, H, are noted in the turnover spectrum. Reproduced with permission from ref 190. Copyright 2012 Authors. Published by PNAS.

state,  $S \geq 2$ ) EPR-detectable in Q-band at 2 K; a Kramers state,  $S = 1/2$ , with  $\text{g} = [2.09, 2.01, 1.98]$ , denoted, I.<sup>190</sup> These intermediates have been fully characterized by X/Q-band EPR and  $^{15}\text{N}$ ,  $^{12}\text{H}$ -ENDOR, HYSCORE, and ESEEM spectroscopic studies. Their enzymatic and chemical assignments are  $\text{E}_7(\text{NH}_2) = \text{H}$  with  $\text{NH}_2$  bound to FeMo-cofactor and  $\text{E}_8(\text{NH}_3) = \text{I}$ , with a bound  $\text{NH}_3$ .<sup>190</sup>

### 4.3. $\text{NO}_x$ Substrates

Nitrite ( $\text{NO}_2^-$ ), nitrous oxide ( $\text{N}_2\text{O}$ ), and hydroxylamine ( $\text{NH}_2\text{OH}$ ) all are reduced by nitrogenase.<sup>20</sup> The recent characterization of nitrite as a nitrogenase substrate established that six-electron reduction of  $\text{NO}_2^-$  to  $\text{NH}_3$  by nitrogenase proceeds without the obligatory  $\text{H}_2$  evolution that is required for the reduction of  $\text{N}_2$ .<sup>193</sup> The kinetic observations and mechanistic implications of the first three of these substrates have been summarized in detail in an earlier review.<sup>20</sup> Hydroxylamine was recently reported as a nitrogenase substrate, being reduced by two electrons to  $\text{NH}_3$  and  $\text{H}_2\text{O}$ .<sup>193</sup> The reduction of each of these substrates is not inhibited by  $\text{H}_2$ , as in the case in the reduction of hydrazine. As with hydrazine, these results are as expected for reactions that involve intermediates that correspond to  $\text{E}_n$ ,  $n > 4$  (see above).

Freeze-trapping  $\alpha\text{-70}^{\text{Val}\rightarrow\text{Ala}}/\alpha\text{-195}^{\text{His}\rightarrow\text{Gln}}$  MoFe protein under turnover conditions with  $\text{NO}_2^-$  or  $\text{NH}_2\text{OH}$  as substrate resulted in the same two EPR-active species ( $S = 1/2$  and  $S \geq 2$ ) trapped with diazenes or hydrazine as substrate (Figure 18).

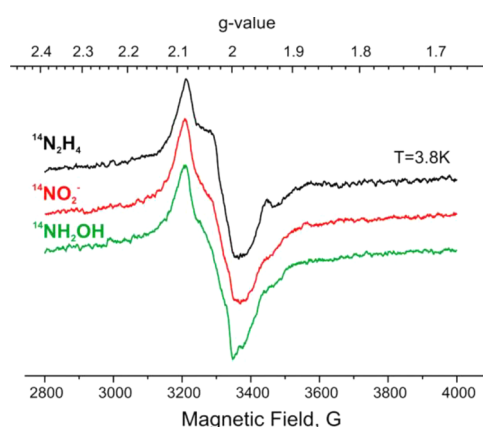


**Figure 18.** X-band EPR spectra of  $\alpha\text{-70}^{\text{Ala}}/\alpha\text{-195}^{\text{Gln}}$  MoFe protein turnover samples prepared with  $\text{N}_2\text{H}_4$  (black),  $\text{NO}_2^-$  (red), and  $\text{NH}_2\text{OH}$  (green) substrates. Reproduced with permission 193. Copyright 2014 American Chemical Society.

As confirmed by  $^1\text{H}$  and  $^{15}\text{N}$  pulsed ENDOR study, the  $S = 1/2$  intermediate of  $\text{NO}_2^-$  or  $\text{NH}_2\text{OH}$  are  $\text{E}_8(\text{NH}_3) = \text{I}$ ;  $^{14/15}\text{N}$  ESEEM studies confirmed the identity of the non-Kramers intermediates as  $\text{E}_7(\text{NH}_2) = \text{H}$  ( $S \geq 2$ ) for  $\text{NO}_2^-$  or  $\text{NH}_2\text{OH}$ .<sup>193</sup>

### 4.4. Mechanisms and Insights

The study of these N-based alternative substrates has provided evidence regarding the nature of the reaction pathway for  $\text{N}_2$  reduction: D or A (Figure 16). An alternating pathway for  $\text{N}_2$  hydrogenation is supported by the observation that (i) hydrazine is a product of  $\text{N}_2$  reduction by V-nitrogenase, which also functions through the *re/oa* mechanism,<sup>195</sup> and (ii) hydrazine was detected as a product by acid or base quenching of Mo-nitrogenase during  $\text{N}_2$  reduction.<sup>86,87</sup> Of course, as seen in Figure 16, in the D pathway the N—N bond is cleaved before hydrazine can be formed and so could not be formed during catalysis, thus indicating that the A pathway is followed by nitrogenase.

The kinetic and spectroscopic observations of nitrite and hydroxylamine reduction by nitrogenase led to the proposal of a  $[6\text{e}^-/7\text{H}^+]$  reduction mechanism of nitrite by nitrogenase (eq 6) as shown in the right panel of Figure 19.<sup>193</sup> In this

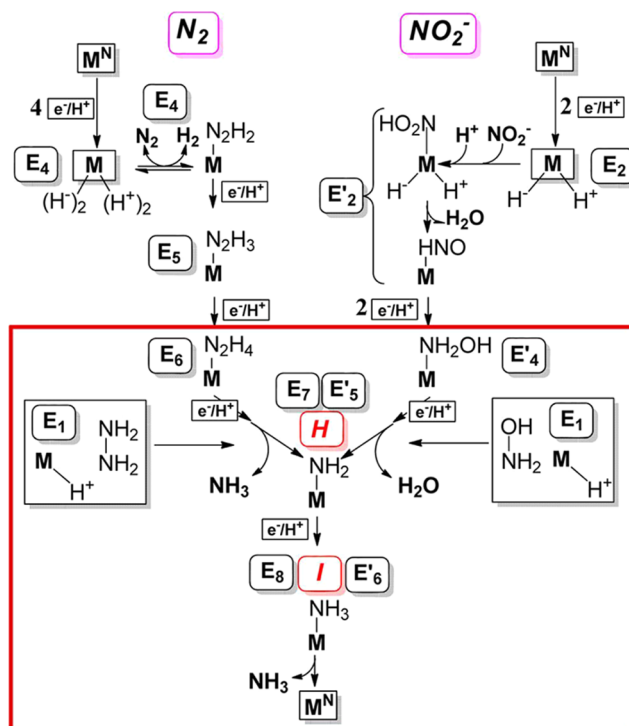
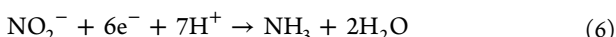


**Figure 19.** Comparison of the proposed reduction pathways of  $\text{N}_2$  (left) and nitrite (right) by nitrogenase ( $\text{M}$  represents FeMo-cofactor). An intermediate, labeled  $\text{E}_n$  on  $\text{N}_2$  pathway and  $\text{E}'_m$  on nitrite pathway, has accumulated  $n$  or  $m$   $[\text{e}^-/\text{H}^+]$ . (Boxed Region) Convergence of pathways for nitrite and  $\text{N}_2$  reduction by nitrogenase, as discussed in the text. Within this region, boxed reactions of  $\text{E}_1$  show the most direct routes by which  $\text{N}_2\text{H}_4$  and  $\text{NH}_2\text{OH}$  join their respective pathways. Reproduced with permission from ref 193. Copyright 2014 American Chemical Society.

mechanism,  $\text{NO}_2^-$  and one proton bind to FeMo-cofactor at the  $\text{E}_2$  state. After one water molecule was released, the resulting  $\text{M}-[\text{NO}^+]$  species reacts with the hydride on the same cofactor to avoid the formation of an  $\text{M}-[\text{NO}]$  “thermodynamic sink”.<sup>196</sup> The formation of an  $\text{M}-\text{HNO}$  species is similar to the reduction of heme-bound NO to bound HNO through hydride transfer from NADH by P450 NO reductase.<sup>197</sup> The  $\text{M}-\text{HNO}$  intermediate is then converted to further reduced species through a pathway analogous to the nitrite reduction by cytochrome c nitrite reductase (ccNIR),<sup>198–201</sup> including intermediates  $\text{H}$  ( $\text{M}-\text{NH}_2$ ) and  $\text{I}$  ( $\text{M}-\text{NH}_3$ ).<sup>190</sup>



Even though the binding and reduction mechanism of  $\text{N}_2$  and  $\text{NO}_2^-$  are totally different, the generation of common intermediates  $\text{H}$  and  $\text{I}$  from both the di-N substrates ( $\text{N}_2\text{H}_2$  and  $\text{N}_2\text{H}_4$ ) and mono-N substrates ( $\text{NO}_2^-$  and  $\text{NH}_2\text{OH}$ ) further confirmed the previous assignments of intermediate  $\text{H}$  to  $\text{M}-\text{NH}_2$  and  $\text{I}$  to  $\text{M}-\text{NH}_3$ , and their assignment to  $\text{E}_7$  and  $\text{E}_8$ , respectively.<sup>190,193</sup> These results are understood as arising from a convergence of the reduction pathways of  $\text{N}_2$  and  $\text{NO}_2^-$  in the late stage of the corresponding catalytic cycles as highlighted in the red box in Figure 19.<sup>193</sup>

Hydrazine and hydroxylamine were proposed to bind to  $\text{E}_1$  and undergo bond cleavage, forming the intermediate  $\text{H}$ , and  $\text{NH}_3$  and  $\text{H}_2\text{O}$ , respectively.<sup>190,193</sup> These results are consistent with the proposed alternating  $\text{N}_2$  reduction pathway by nitrogenase in which the first  $\text{NH}_3$  is released after delivery

of the seventh  $[\text{e}^-/\text{H}^+]$  to the  $\text{N}_2\text{H}_4$ -bound  $\text{E}_6$  state to form intermediate  $\text{H}$ . The intermediate  $\text{H}$  accepts one last pair of  $[\text{e}^-/\text{H}^+]$  to form intermediate  $\text{I}$ , which regenerates the  $\text{E}_0$  state to finish one catalytic cycle by releasing the second  $\text{NH}_3$ .<sup>21,23,190</sup>

## 5. C-BASED SUBSTRATES

In addition to the nonphysiological N-based substrates, nitrogenase interacts with a broad range of carbon (C)-based substrates/inhibitors. The utilization of these C-based substrates/inhibitors has greatly expanded the ability to probe nitrogenase mechanism, and their reduction has been reviewed.<sup>20,39,40,203</sup> In this section, we will focus on the progress in studying C-based substrates/inhibitors of nitrogenase since 2013,<sup>40</sup> referring to earlier work when necessary for clarity.

### 5.1. Alkyne Substrates

Alkynes were widely used as substrates and inhibitor in probing the substrate-binding sites and reduction mechanism of nitrogenase over the last half-century.<sup>20,39,40,179</sup> Acetylene was the first alkyne discovered early as an alternative substrate of nitrogenase,<sup>204</sup> with pioneering works studying the steady-state EPR of wild type<sup>205</sup> and  $\alpha$ -195<sup>His</sup>→<sup>Gln</sup>-substituted MoFe protein<sup>206</sup> with acetylene as substrate. The X- and Q-band EPR spectra of the freeze-trapped species exhibited three simultaneously generated  $S = 1/2$  signals: a rhombic  $S_{\text{EPR}1}$  signal with  $g = 2.12, 1.98, 1.95$ , a rhombic  $S_{\text{EPR}2}$  signal with  $g = 2.007, 2.000, 1.992$ , and a minor isotropic  $S_{\text{EPR}3}$  signal with  $g \approx 1.97$ .<sup>206,207</sup> Initial  $^{13}\text{C}$  and  $^1\text{H}$  ENDOR measurements on the  $S_{\text{EPR}1}$  signal suggested that it arises from a *substrate* complex, with two  $\text{C}_2\text{H}_2$ -derived species bound to the cofactor, one of them being a  $\text{C}_2\text{H}_2$  bound to the FeMo-cofactor by bridging two Fe ions of the  $\text{Fe}2,3,6,7$  face.<sup>207</sup> However, results described directly below, which were obtained for an intermediate trapped during turnover of the alkyne propargyl alcohol with the  $\alpha$ -70  $\text{Val} \rightarrow \text{Ala}$ -substituted MoFe protein suggested that this interpretation be reexamined. Subsequent, improved ENDOR measurements on  $S_{\text{EPR}1}$ , which included  $^{57}\text{Fe}$  ENDOR measurements, revealed interactions with three distinct carbon nuclei, again indicating that at least two  $\text{C}_2\text{H}_2$ -derived species are bound to the cofactor, but they suggested that this intermediate in fact contains an ethylene product bound as a ferracycle to a single Fe of a two-electron reduced ( $\text{E}_2$ ) FeMo-cofactor (Figure 20).<sup>202</sup>

It was long held that FeMo-cofactor contained within the MoFe protein required the accumulation of one or more electrons before any substrate or inhibitor could interact.<sup>20,209</sup> This conclusion was drawn from the lack of significant perturbations of the resting state ( $\text{E}_0$ ) FeMo-cofactor EPR

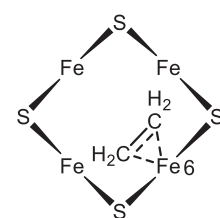


**Figure 20.** Schematic representation of chemical structure of  $S_{\text{EPR}1}$  species at  $\text{E}_2$  state, highlighting the ferracycle formed by  $\text{C}_2\text{H}_4$  binding to  $\text{Fe}_6$  as proposed in literature.<sup>202</sup> The 4Fe4S face represents the same orientation as in Figure 2.

signal line shape upon the addition of any inhibitors or substrates.<sup>20</sup> This situation changed with the report that when the  $\alpha$ -96<sup>Arg</sup>, located on one FeS face of FeMo-cofactor within the MoFe protein, was substituted by a series of other amino acids, the resulting MoFe protein variants showed perturbations of the FeMo-cofactor EPR signal ( $S = 3/2$ ,  $g = 4.26, 3.67, 2.00$ ) upon incubation of the resting state enzyme with the substrate acetylene or the inhibitor cyanide ( $\text{CN}^-$ ).<sup>208</sup> Both acetylene<sup>204,210,211</sup> and cyanide<sup>212–214</sup> were long ago reported as substrates for nitrogenase under turnover conditions, being reduced to ethylene ( $\text{C}_2\text{H}_4$ ) and methane ( $\text{CH}_4$ ) and ammonia ( $\text{NH}_3$ ), respectively. Incubation of resting-state  $\alpha$ -96<sup>Arg</sup>→Leu-substituted MoFe protein with acetylene or cyanide was found to decrease the normal FeMo-cofactor signal with appearance of new EPR signals having  $g = 4.50$  and  $3.50$  (Figure 21), and  $g$

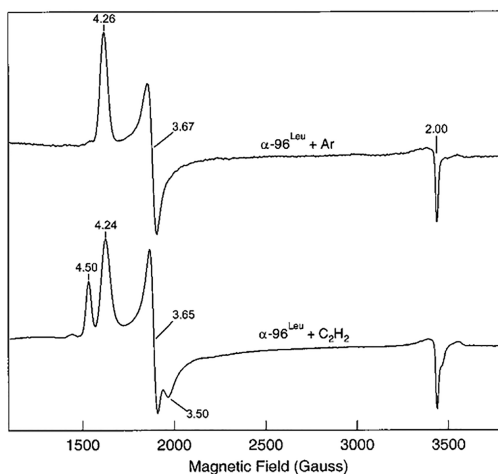


**Figure 21.** X-band EPR spectra of  $\alpha$ -96<sup>Leu</sup> MoFe protein under nonturnover conditions in the absence (top trace) and presence (bottom trace) of acetylene. Reproduced with permission from ref 208. Copyright 2001 American Chemical Society.

$= 4.06$ , respectively. Subsequent  $^{13}\text{C}$  ENDOR studies revealed direct, but weak, interactions between acetylene or  $\text{CN}^-$  and the resting-state FeMo-cofactor.<sup>208</sup> These observations were the first to show that substrates/inhibitors can interact with the resting state FeMo-cofactor contained within the MoFe protein.

Capitalizing on this finding, a recent X-ray crystallographic study of  $\alpha$ -96<sup>Arg</sup>→Gln-substituted MoFe protein in the presence of acetylene resulted in the first crystal structure with a substrate molecule, acetylene, captured near the active site FeMo-cofactor.<sup>215</sup> In the 1.70 Å crystal structure, the acetylene is located 4–5 Å away from Fe6 atom, which was supported by DFT calculations (Figure 22).<sup>215</sup> These results are consistent with the previous findings that nitrogenase binds some substrates at the 4Fe4S face of FeMo-co approached by the side chains of  $\alpha$ -70<sup>Val</sup> and  $\alpha$ -96<sup>Arg</sup>.<sup>33,36</sup> An  $^1\text{H}$  and  $^{57}\text{Fe}$  ENDOR study using wild-type and *NifV*<sup>–</sup> MoFe proteins from *Klebsiella pneumoniae* also revealed that acetylene binding to the resting-state MoFe protein can perturb the FeMo-cofactor environment.<sup>216</sup>

The first detailed characterization of alkyne-reduction intermediates, alluded to above, was carried out on states freeze-trapped during the turnover of nitrogenase modified by substitution of the valine at  $\alpha$ -70 position in MoFe protein by alanine.<sup>109,217,218</sup> This substitution allows the reduction of

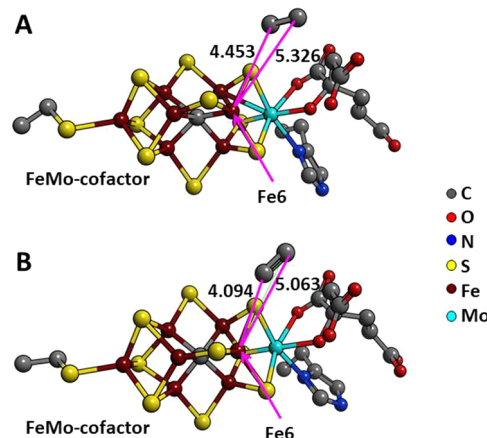


**Figure 22.** Comparison of the acetylene location at the FeMo-cofactor. The acetylene location at the FeMo-cofactor is compared between X-ray (A) and DFT optimized structures (B). The interatomic distances are shown with red lines. Reproduced with permission 215. Copyright 2017 Elsevier, Ltd.

longer-chain alkyne substrates,<sup>219,220</sup> such as propargyl alcohol ( $\text{HC}\equiv\text{CCH}_2-\text{OH}$ ).<sup>217</sup> When the  $\alpha$ -70<sup>Val</sup>→<sup>Ala</sup>-substituted MoFe protein was frozen in liquid nitrogen during steady-state turnover with propargyl alcohol as substrate, the  $S = 3/2$  EPR spectrum of the FeMo-cofactor was changed to a new  $S = 1/2$  signal.<sup>217,218</sup> Using  $^{1}\text{H}$ - and  $^{13}\text{C}$ -ENDOR spectroscopies, it was demonstrated that this  $S = 1/2$  signal originates from the FeMo-cofactor having the alkene allyl alcohol ( $\text{H}_2\text{C}=\text{CHCH}_2-\text{OH}$ ) reduction product bound as a ferracycle to a single Fe as shown in section 3 (Figure 4).<sup>109</sup>

This structural assignment was later supported by the EXAFS and NRVS examination of the same intermediate.<sup>162</sup> A similar  $S = 1/2$  signal was also observed when propargyl alcohol was replaced by propargyl amine ( $\text{HC}\equiv\text{CCH}_2-\text{NH}_2$ ) as substrate. Trapping of these two intermediates was shown to be dependent on pH and the presence of histidine at  $\alpha$ -195 position.<sup>218</sup> These results suggested that these intermediates are stabilized, and thereby trapped, by H-bonding interactions between either the  $-\text{OH}$  group or the  $-\text{NH}_3^+$  group and the imidazole of  $\alpha$ -195<sup>His</sup>. Theoretical calculations refining the binding mode and site pointed to  $\eta^2$  coordination at Fe6 of the FeMo-cofactor, as visualized in Figures 4 and 21.<sup>218</sup>

## 5.2. CO as Inhibitor and Substrate

CO was described as an inhibitor of wild-type Mo-nitrogenase in early studies, being shown to inhibit the reduction of all substrates except protons to make  $\text{H}_2$ .<sup>20,93,221</sup> CO inhibition of proton reduction was observed when the first sphere (substitution of homocitrate by citrate as in the *NifV*<sup>–</sup> mutant)<sup>222,223</sup> or secondary sphere environment of the FeMo-cofactor<sup>222,224,225</sup> was changed. Similar CO inhibition of proton reduction was also seen for Mo-nitrogenase under high pH conditions<sup>226</sup> and for V-nitrogenase.<sup>227,228</sup> Recently, CO was reported to stimulate the  $\text{H}_2$  production catalyzed by three MoFe protein variants,  $\alpha$ -277<sup>Cys</sup>,  $\alpha$ -192<sup>Asp</sup>, and  $\alpha$ -192<sup>Glu</sup> under high-electron flux conditions but not under low-electron flux conditions. These intriguing observations are apparently at odds with the observation that CO displays either no inhibitory or inhibitory effect on proton reduction catalyzed by Mo- and V-nitrogenases, as noted above.<sup>229</sup>

Trapping of nitrogenase by freezing during turnover under CO revealed a loss of the EPR spectrum of the resting state

FeMo-cofactor and appearance of two major different EPR signals.<sup>205,230–234</sup> In the presence of low concentrations of CO ( $[\text{CO}]:[\text{FeMo-cofactor}] \leq 1:1$ ), the  $S = 3/2$  spectrum of FeMo-cofactor changed to an  $S = 1/2$  spin state giving rise to a new rhombic EPR signal (denoted lo-CO) with  $g = 2.09, 1.97, 1.93$ . At higher concentrations of CO ( $\geq 0.5$  atm), an axial EPR signal ( $S = 1/2$ , called hi-CO) was observed with  $g = 2.17, 2.06, 2.06$ .<sup>205,231–234</sup> In addition to these trapped CO complexes, a small population of species at  $S = 3/2$  spin state, so-called hi(5)-CO, has been observed under high CO concentrations and higher electron flux in wild-type<sup>233</sup> and variant MoFe proteins.<sup>222,234</sup>

These trapped CO complexes of FeMo-cofactor have been well studied by advanced spectroscopic methods. ENDOR studies of lo-CO and hi-CO complexes using different isotopologues of CO and FeMo-cofactor characterized the two CO complexes.<sup>202,230,235–238</sup> Key conclusions from these studies were that in lo-CO the C of a single CO bridges two Fe ions (end-on mode) and in hi-CO, two CO terminally bind to two Fe ions in the “waist” of the FeMo-cofactor (Figure 23A). The hi(5)-CO complex has been suggested to contain two bridging CO molecules on the FeMo-cofactor.<sup>222</sup> Finally, EPR-monitored photolysis experiments revealed that a terminal CO

of hi-CO complex is photolabile, causing the state to reversibly convert to lo-CO. In contrast, both lo-CO and hi(5)-CO complexes are photostable.<sup>239</sup>

The  $E_n$  level of lo-CO and hi-CO remain a matter of considerable interest. It has been reported that lo-CO and hi-CO can be interconverted by adding CO to the former or pumping CO off of the latter, without redox or catalytic processes, thus demonstrating that they are at the same  $E_n$  level.<sup>233</sup> In addition, lo-CO can be converted to  $E_0$  by extensive pumping, which suggests that all three states are at the same,  $M^N (E_0)$ , redox level,<sup>233</sup> an idea consistent with  $^{57}\text{Fe}$  ENDOR measurements.<sup>145,237</sup> However, CO cannot bind to FeMo-cofactor in the resting state, and can only bind to the cofactor in a state formed during turnover under CO.<sup>233</sup> One possibility is that lo-CO is indeed an  $E_2$  state, and we have discussed this possibility.<sup>202</sup> However, such a state should have the two reducing equivalents stored as a hydride, and no such  $^1\text{H}$  ENDOR signal is observed.<sup>150,236</sup> Thus, it appears unlikely that lo-CO is an  $E_2$  state. To explain the combined observations one might imagine that CO binds to FeMo-cofactor in an  $E_2$  state, or in an  $E_1$  state that then receives a second electron, and that the resulting CO-bound  $E_2$  state loses  $\text{H}_2$  to form the observed lo-CO, which indeed is at an  $E_0$  redox level. The differing net spins,  $S = 3/2$  for resting state,  $S = 1/2$  for CO-bound states, would then merely reflect the influence of the CO binding. Clearly, a reexamination of the lo-CO state, including  $^{95}\text{Mo}$  ENDOR and DFT computations, would seem to be in order.

Although EPR and ENDOR give the optimal insights into properties of intermediates with half-integer spin states ( $S = 1/2, 3/2, 5/2, \dots$ ), rarely (intermediate H, section 4.2) can it probe intermediates with integer spin ( $S = 0, 1, 2, \dots$ ).<sup>190,193</sup> Stopped-flow FTIR studies are equally effective for all spin states.<sup>244–246</sup> Recently, IR-monitored photolysis studies of complexes of wild-type and two MoFe protein variants trapped during turnover with low electron flux under hi-CO conditions displayed a more complex landscape of hi-CO complexes.<sup>240–242</sup> Three different hi-CO complexes (designated as Hi-1, Hi-2 or hi(5)-CO, and Hi-3) were observed with absorptions at different energy levels. All hi-CO complexes have two CO bound to FeMo-cofactor and can reversibly release one CO to generate lo-CO complexes with one terminal, bridging, or protonated CO species. The three hi-CO complexes all have one CO terminally bound to FeMo-cofactor with the other ligand as a terminal, semibridging, or bridging/protonated CO ligand (Figure 23B).<sup>240–242</sup> Further photolysis and DFT study of Hi-3 with C–O stretching frequencies at 1938 and 1911  $\text{cm}^{-1}$  revealed that it has two terminal CO ligands bound to two adjacent Fe atoms in the FeMo-cofactor with an EPR silent  $S = 0$  spin state.<sup>241,242</sup> DFT calculations of the C–O stretching frequencies of hi-CO complexes also suggested that C–O frequencies at 1973 and 1680  $\text{cm}^{-1}$  in IR of Hi-1 species originated from a terminal  $-\text{CO}$  and a partially reduced  $-\text{CHO}$  ligands bound to two adjacent Fe sites as well, consistent with the EXAFS and NRVS observations for the wild-type enzyme.<sup>242</sup> Recent NRVS studies of nitrogenase under high CO conditions revealed that the FeMo-cofactor undergoes significant structural perturbation upon  $-\text{CO}/-\text{CHO}$  binding.<sup>242</sup> The identification of Fe–CO stretching and Fe–C–O bending modes in the range of 470–560  $\text{cm}^{-1}$  in NRVS provided the first confirmation that binding is indeed at Fe sites,<sup>23,110</sup> extending the many studies noted above that showed the heterometal,

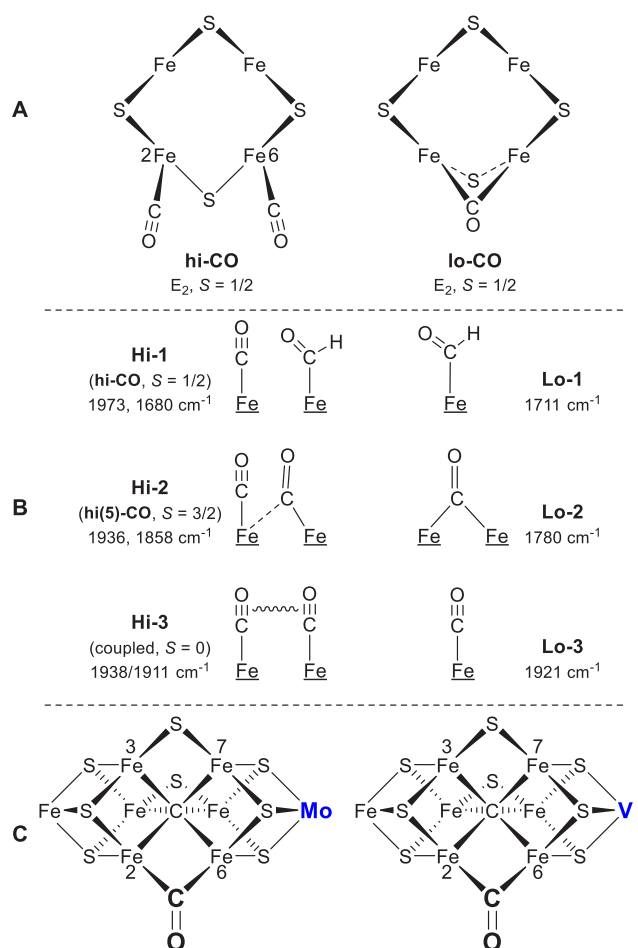


**Figure 23.** Schematic structures of CO complexes as proposed based on (A) EPR/ENDOR,<sup>202,230,235–238</sup> (B) IR-monitored photolysis,<sup>240–242</sup> and (C) X-ray crystallography of Mo-nitrogenase<sup>143</sup> and EPR comparison of Mo- and V-nitrogenases.<sup>243</sup> The presence of a bound carbonate in the VFe-co was revealed later by X-ray crystallography.

Mo in FeMo-cofactor, may tune the properties of the cofactor, but is not directly involved in valence changes or substrate reduction.<sup>114,151</sup>

As described above, structures of the FeMo-cofactors with CO or CO-derived ligands have been proposed based on the different spectroscopic studies (Figure 23). In 2014, Rees et al.<sup>143</sup> reported the first X-ray crystal structure of a CO-bound state of the MoFe protein with 1.5 Å resolution, using crystals obtained from a solution, following turnover in the presence of CO and C<sub>2</sub>H<sub>2</sub>. Surprisingly, the structure showed the bridging CO proposed for lo-CO, but it was found to bind to the FeMo-cofactor by replacing one of the belt sulfide ligands, S2B (Figure 23C). Correspondingly, a recent EPR study of the CO-modified MoFe protein generated under the same conditions that yielded the CO-modified crystals yielded a spectrum that almost exactly matches that reported for lo-CO.<sup>243</sup> The dissociation of a belt sulfide is a central factor in the developing view, noted above, that FeMo-cofactor is not structurally rigid<sup>71,143</sup> during turnover.

The exchange of CO for S<sup>2-</sup> on the FeMo-cofactor is reversible under turnover conditions.<sup>143</sup> Thus, CO inhibition of acetylene reduction could be recovered when the CO-bound MoFe protein crystals were dissolved and incubated in an assay mixture, and the structure of MoFe protein crystals obtained from this mixture revealed the loss of the bridging CO ligand and the reinstallation of the belt sulfide, thus restoring the resting state FeMo-cofactor structure. Even though a plausible sulfide binding site (SBS) was proposed, the origin and mechanism of insertion of the belt sulfide ligand are still not clear.

About a decade ago, CO was discovered to be a substrate of V- and Mo-nitrogenases producing both CH<sub>4</sub> and short-chain hydrocarbons as products.<sup>227,228,247</sup> Two or more CO could be reduced and coupled to make multi-C hydrocarbons at low rates when turned over with Fe protein and MgATP. The reactivity of FeMo-co- and FeV-co-reconstituted apo-MoFe protein (apo-NifDK) toward CO reduction has also recently been explored.<sup>248</sup> It was found that both FeMo-co- and FeV-co-reconstituted NifDK protein showed similar hydrocarbon product profiles from CO to that of wild-type Mo-nitrogenases, with much lower rates compared to that by V-nitrogenase.<sup>227,228</sup> However, a ~100 times increase of hydrocarbon formation from CO reduction was observed when FeMo-cofactor was housed in a VFe protein scaffold compared to that housed in its native MoFe protein scaffold.<sup>249</sup> These results highlighted a combined contribution from the protein environment and cofactor properties toward CO reduction.

It has also been reported that CO can bind to the V-nitrogenase in the absence of Fe protein/MgATP (nonturnover) as electron-delivery agent, but instead in the presence of the reductants dithionite ( $E^0 = -0.66$  V), Eu<sup>II</sup>-EGTA ( $E^0 = -0.88$  V), and Eu<sup>II</sup>-DTPA ( $E^0 = -1.14$  V).<sup>243</sup> The comparison of the EPR spectrum of the CO-bound VFe protein to that of the CO-modified MoFe protein led the authors to propose replacement of a belt-sulfide by a bridging CO ligand (Figure 23C).<sup>143,243</sup> They reported that the CO of this CO-bound VFe protein could be further reduced to methane when subjected to turnover condition with Fe protein (VnfH)/MgATP and dithionite, revealing the relevance of this CO-bound state to the catalytic turnover of CO as substrate.<sup>243</sup>

It has been long believed that CO does not bind to FeMo-cofactor of Mo-nitrogenase in the resting state ( $E_0$ ), which is

further supported by a recent electrochemical study of CO interaction with FeMo-cofactor in MoFe protein with Eu<sup>III/II</sup>-L (L = BAPTA, EGTA, DTPA) as electron mediators.<sup>250</sup> However, the binding of CO to FeV-cofactor in the absence of Fe protein/MgATP (resting-state VFe protein as suggested)<sup>243</sup> indicates that it might be risky to simply expand the concept of resting-state  $E_0$  of Mo-nitrogenase to V- and Fe-nitrogenases without careful consideration of the fine-tuning effect of heterometals (Mo, V, and Fe) and secondary environments on the electronic structure of FeM-cofactor. For example, to date, the FeV-cofactor in as-isolated VFe protein always has a CO<sub>3</sub><sup>2-</sup> ligand that does not exist in any MoFe protein crystal structures observed.<sup>58,59</sup> Clearly, CO interacts with nitrogenases in complex ways, with some aspects still needing resolution.

In 2013, the possible connection between CO reduction and the interstitial carbide in the active site FeMo-cofactor was explored.<sup>251</sup> It was found that reconstitution of apo-MoFe protein with <sup>14</sup>C-labeled FeMo-cofactor in the resting state and upon turnover with acetylene and N<sub>2</sub> did not show any dilution of the <sup>14</sup>C-label in the active site, indicating that the interstitial carbide cannot be exchanged during turnover. Moreover, the GC-MS characterization of the hydrocarbon products from reaction mixtures with the combined use of <sup>12/13</sup>C-enriched CO substrate and the carbide in the active site revealed that the interstitial carbide could not be used as a substrate and incorporated into the hydrocarbon products.<sup>251</sup> These results are consistent with a role for carbide in stabilizing the structural integrity of FeMo-cofactor<sup>71</sup> as it proceeds through different conformational states during catalysis.

### 5.3. CO<sub>2</sub> as Substrate

CO<sub>2</sub> was reported as a substrate for nitrogenase in 1995, being reduced by two electrons to CO.<sup>252</sup> The form of CO<sub>2</sub> (CO<sub>3</sub><sup>2-</sup>, HCO<sub>3</sub><sup>-</sup>, and CO<sub>2</sub>) that is the substrate remains unclear. Recently, it was reported that in the crystal structures of V-nitrogenase a CO<sub>3</sub><sup>2-</sup> ligand replaced one of the belt-sulfide ligands of the active site FeV-cofactor (Figure 2).<sup>58</sup> This proposed CO<sub>3</sub><sup>2-</sup> ligand is also present in a plausible turnover-relevant structure of the FeV-cofactor,<sup>59</sup> further complicating the origin of this CO<sub>3</sub><sup>2-</sup> ligand and the relevance to the CO<sub>2</sub> reducing ability of nitrogenases.

Later studies reported that CO<sub>2</sub> could be reduced by eight electrons/protons to methane (CH<sub>4</sub>) by a remodeled Mo-nitrogenase having amino acid substitutions  $\alpha$ -70<sup>Val→Ala</sup>/ $\alpha$ -195<sup>His→Gln</sup>.<sup>254</sup> In 2016, light-driven *in vivo* CO<sub>2</sub> reduction to CH<sub>4</sub> by an anoxygenic phototroph, *Rhodopseudomonas palustris* (*R. palustris*), which expressed the same remodeled Mo-nitrogenase, was reported.<sup>255</sup> This catalytic ability was conferred upon *R. palustris* by use of a variant of the transcription factor NifA that can activate expression of nitrogenase under all growth conditions.<sup>256–259</sup> More recently, the *in vivo* CH<sub>4</sub> production from CO<sub>2</sub> reduction has been confirmed to be catalyzed by the wild-type Fe-only nitrogenase from *R. palustris* and several other nitrogen-fixing bacteria.<sup>260</sup> The CH<sub>4</sub> production by the Fe-only nitrogenase in *R. palustris* was found sufficient to support the growth of an obligate CH<sub>4</sub>-utilizing *Methylomonas* strain. These results suggest that active Fe-only nitrogenase, present in diverse organisms, contributes CH<sub>4</sub> that could shape microbial community interactions.<sup>260</sup>

Recently, it was discovered that Mo-nitrogenase catalytically reduces carbon dioxide (CO<sub>2</sub>) to formate (HCOO<sup>-</sup>) at rates

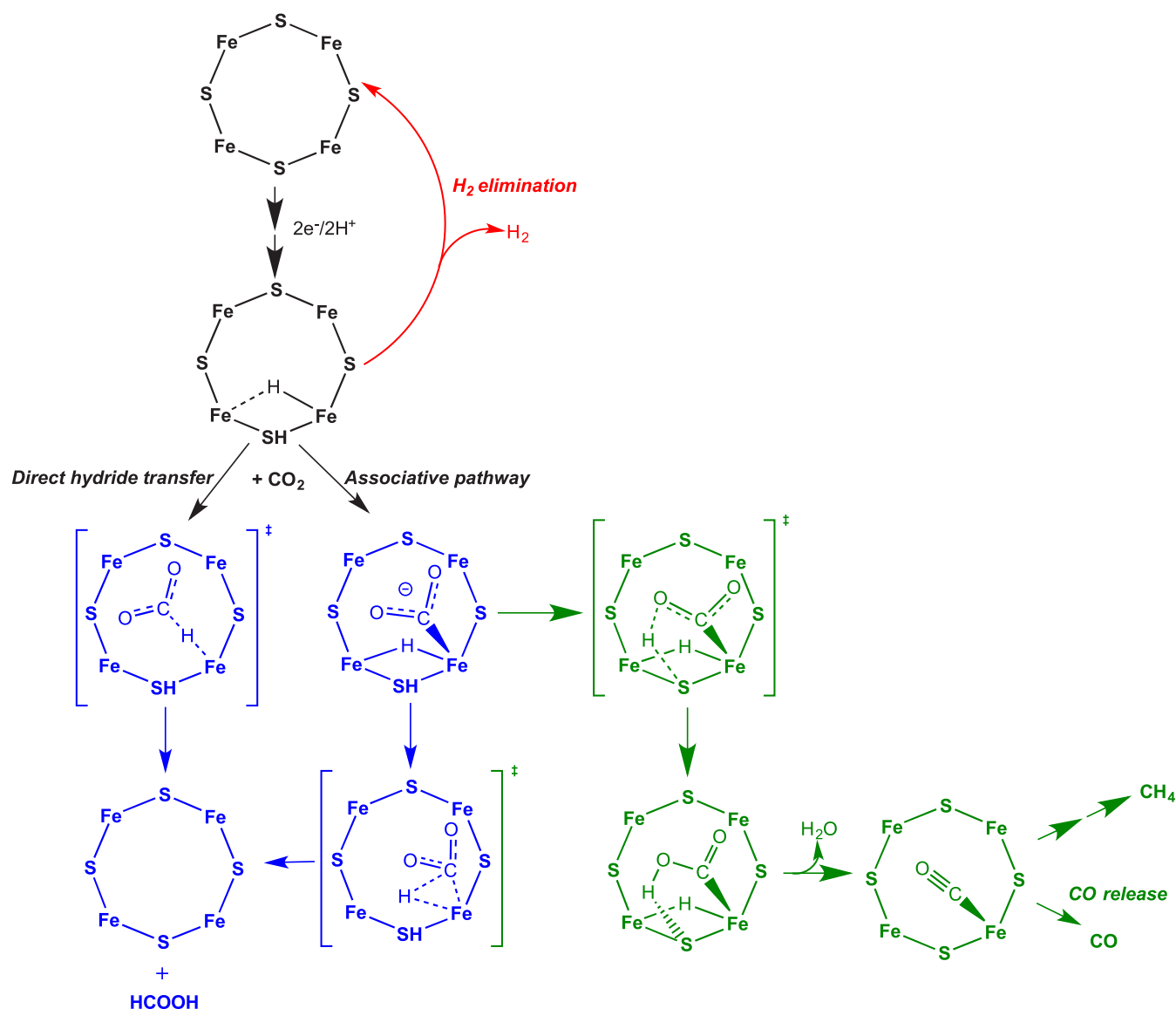


**Figure 24.** Possible  $\text{CO}_2$  reduction pathways.  $\text{CO}_2$  activation at one  $\text{FeS}$  face of the  $\text{E}_2$  state of  $\text{FeMo-co}$  is shown. The  $\text{E}_2$  state is proposed to contain a single  $\text{Fe}$ -hydride and a proton bound to a sulfide shown bound to one face of  $\text{FeMo-co}$ . Reduction to formate (blue pathways) can go by either direct hydride transfer or an associative pathway. A pathway to formation of  $\text{CO}$  and  $\text{CH}_4$  is shown in the green. Adapted with permission from ref 253. Copyright 2016 American Chemical Society.

>10 times faster than that of  $\text{CO}_2$  reduction to  $\text{CO}$  and  $\text{CH}_4$ .<sup>253</sup> This reaction was not inhibited by  $\text{H}_2$ , indicating that  $\text{CO}_2$  reduction does not involve the *re/oa* equilibrium central to  $\text{N}_2$  binding/activation, as expected if the reduction occurs a  $\text{E}_n$  states with  $n < 4$ .<sup>253</sup> In fact, DFT calculations<sup>136</sup> on the doubly reduced  $\text{FeMo}$ -cofactor ( $\text{E}_2$  state) with a  $\text{Fe}$ -bound hydride and  $\text{S}$ -bound proton favor a direct reaction of  $\text{CO}_2$  with the hydride (direct hydride transfer reaction pathway, see Figure 24 and 25, lower blue pathway), with facile hydride transfer to  $\text{CO}_2$  yielding formate. In contrast, a significant barrier is observed for reaction of  $\text{Fe}$ -bound  $\text{CO}_2$  with the hydride (associative reaction pathway, Figure 25, upper blue pathway), which leads to  $\text{CO}$  and  $\text{CH}_4$ . Importantly, computations revealed that protein residues above the reactive face of the  $\text{FeMo}$ -cofactor hamper the  $\text{CO}_2$  access to the hydridic hydrogen. In particular, steric hindrance from the side chain of  $\alpha$ -70<sup>Val</sup> or  $\alpha$ -96<sup>Arg</sup> introduces a barrier for the direct hydride transfer favoring the competitive elimination of  $\text{H}_2$

over  $\text{HCOO}^-$  formation. Consistent with this finding,  $\text{MoFe}$  proteins with amino acid substitutions near  $\text{FeMo}$ -cofactor ( $\alpha$ -70<sup>Val</sup> $\rightarrow$ <sup>Ala</sup>/ $\alpha$ -195<sup>His</sup> $\rightarrow$ <sup>Gln</sup>) are found to significantly alter the distribution of products between formate and  $\text{CO}/\text{CH}_4$ .<sup>253</sup> The formate formation by  $\text{Fe}$ -nitrogenase reduction of  $\text{CO}_2$  was also reported to have a higher efficiency than that of  $\text{Mo}$ -nitrogenase.<sup>261</sup>

The analysis of the electronic properties of  $\text{FeMo}$ -cofactor during the hydride transfer revealed a strong charge transfer from the  $\sigma(\text{Fe}-\text{H})$  bonding orbital to the  $\pi^*(\text{C}=\text{O})$  antibonding orbital, which results in the heterolytic  $\text{Fe}-\text{H} \rightarrow \text{Fe}^+ + \text{H}^-$  bond cleavage and the transfer of the hydride to  $\text{CO}_2$ . The exergonic nature of the direct hydride transfer ( $\Delta G^0 = -26$  kcal/mol) suggests that the hydricity of the  $\text{E}_2$  state,  $\Delta G_{\text{H}^-}$ , is sufficient to transfer a hydride to  $\text{CO}_2$  to generate formate, that is, the hydricity is below that of formate ( $\text{HCOO}^- \rightarrow \text{CO}_2 + \text{H}^-$ ,  $\Delta G_{\text{H}^-} = +24.1$  kcal/mol).<sup>262</sup>

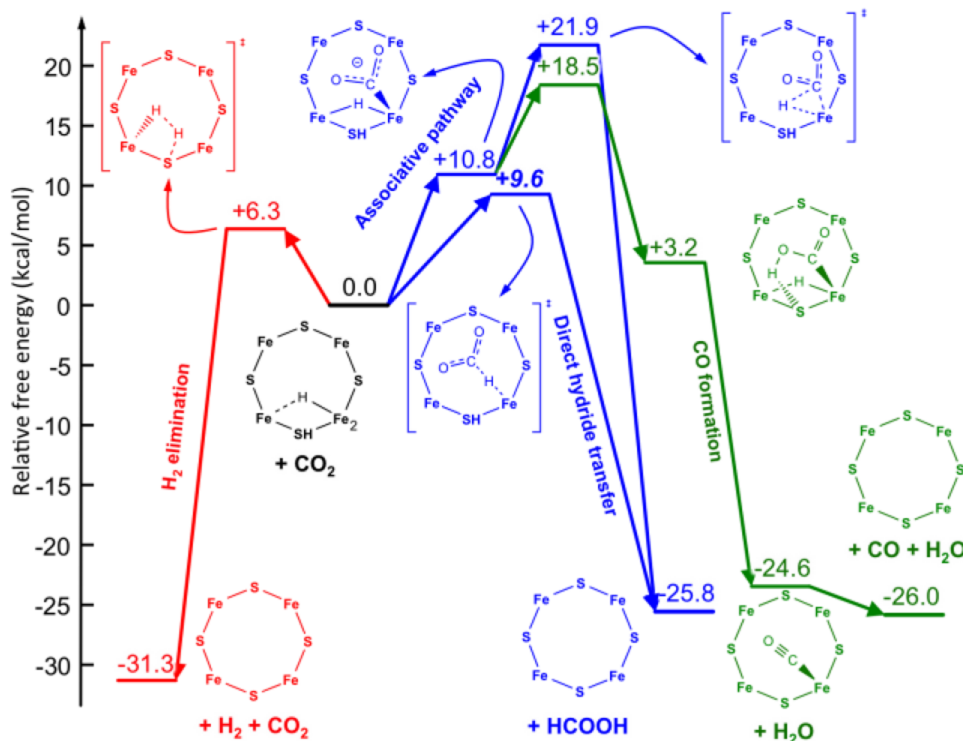


**Figure 25.** Computed free energy diagram for  $\text{CO}_2$  reduction and  $\text{H}_2$  formation occurring at the  $\text{E}_2$  state of FeMo-cofactor. Reproduced with permission <sup>253</sup>. Copyright 2016 American Chemical Society.

The same computational investigation revealed a pathway leading to the formation of CO from  $\text{E}_2(2\text{H})\text{-CO}_2$ , which starts with the exergonic transfer of the protic S–H hydrogen to one of the oxygen atoms of  $\text{CO}_2$  (Figure 25, green pathway).<sup>253</sup> Although the small size of the adopted computational models introduces a rather large uncertainty, initial protonation of  $\text{CO}_2$  by other ionizable residues, such as  $\alpha\text{-96}^{\text{Arg}}$ , was found very unlikely. The formation of CO proceeds with the transfer of the Fe–H hydrogen (as a proton rather than a hydride) to that oxygen, which results in the exoergic dissociation of a water molecule.<sup>253</sup>

The competitive formation of  $\text{H}_2$  from the  $\text{E}_2(2\text{H})$  state was also investigated computationally (Figure 25, red pathway). It was found that the release of  $\text{H}_2$  is a facile and exergonic process ( $\Delta G^0 = -31.3$  kcal/mol). The exergonic nature of the formation of  $\text{H}_2$  is consistent with the observation that  $\text{H}_2$  cannot reduce FeMo-cofactor. It is of interest to point out that, as with the direct hydride pathway for the  $\text{CO}_2$  reduction, the Fe–H behaves as a hydride that is protonated by S–H, with the overall  $\text{H}_2$  elimination driven by a  $\sigma(\text{Fe–H})$  to  $\sigma^*(\text{S–H})$  charge transfer.<sup>253</sup>

In a separate study of  $\text{CO}_2$  reduction by nitrogenases, it was found that both Mo- and V-nitrogenases can reduce  $\text{CO}_2$  to CO yielding substoichiometric amounts of product compared to the amount of the proteins used.<sup>263,264</sup> Different from its Mo-counterpart, the V-nitrogenase can further reduce  $\text{CO}_2$  to  $\text{CD}_4$ ,  $\text{C}_2\text{D}_4$ , and  $\text{C}_2\text{D}_6$  in  $\text{D}_2\text{O}$  buffer with substoichiometric amounts of products after 3 h incubation. The product profile of  $\text{CO}_2$  reduction was further expanded to  $\leq \text{C}_4$  hydrocarbons in an ATP-independent study of V-nitrogenase with  $\text{Eu}^{\text{II}}\text{-DTPA}$  as reductant, with all products showing a turnover number (TON)  $< 1$ .<sup>264,265</sup>

#### 5.4. Other C Substrates

As analogs of carbon dioxide, isocyanic acid/cyanate ( $\text{HNCO}/\text{OCN}^-$ ), thiocyanate ( $\text{SCN}^-$ ), and carbon disulfide ( $\text{CS}_2$ ) are substrates of wild-type Mo-nitrogenase.<sup>252,266</sup> The slow turnover rates for the reduction of these substrates allowed trapping intermediates by rapid freeze-quench. Dependent on pH and isocyanic acid concentration, the EPR spectra of nitrogenase during turnover in the presence of  $\text{HNCO}$  displayed signals with  $g$ -values corresponding to lo-CO and hi-CO complexes indicating the production of CO.<sup>266</sup> The initial EPR study of trapped intermediates from thiocyanate and carbon disulfide reduction by nitrogenase revealed a similar  $S = 1/2$  spin state signal (denoted “c”), indicating a sulfur-containing intermediate bound to FeMo-cofactor.<sup>266</sup> Further detailed EPR and  $^{13}\text{C}$ -ENDOR study<sup>267</sup> revealed the presence of three sequentially formed intermediates trapped during  $\text{CS}_2$  reduction: “a” with  $g = 2.035, 1.982, 1.973$ ; “b” with  $g = 2.111, 2.002, 1.956$ ; and a previously observed “c” with  $g = 2.211, 1.996, 1.978$ . All three intermediates were suggested to have  $\text{CS}_2$ -derived fragments bound to one or two Fe atoms on FeMo-cofactor. The first formed intermediate “a” might contain an activated  $\text{CS}_2$  bound to FeMo-cofactor in side-on mode, and the third intermediate “c” was suggested to contain a “ $\text{C}\equiv\text{S}$ ” species terminally bound to the cofactor through C atom.<sup>267</sup>

Recently, the potential of selenocyanate ( $\text{SeCN}^-$ ) as nitrogenase substrate and inhibitor was evaluated.<sup>144</sup> Compared to  $\text{SCN}^-$  and cyanide ( $\text{CN}^-$ ), it was found that  $\text{SeCN}^-$  is a poor substrate in terms of methane production. In addition,  $\text{SeCN}^-$  is a potent, yet reversible inhibitor of acetylene reduction by nitrogenase with an inhibition constant ( $K_i(\text{SeCN}^-) = 410 \pm 30 \mu\text{M}$ )<sup>144</sup> 30 times lower than that observed for  $\text{SCN}^-$  ( $K_i(\text{SCN}^-) = 12.7 \pm 1.2 \text{ mM}$ ).<sup>266</sup> In

contrast to full inhibition of acetylene reduction by  $\text{SeCN}^-$ , the proton reduction was inhibited to a lesser extent.<sup>144</sup>

Rees et al. resolved a MoFe protein crystal structure at 1.6 Å resolution isolated from an assay mixture that included 25 mM  $\text{SeCN}^-$ , revealing a quantitative substitution of the belt sulfide S2B by a selenide ligand.<sup>144</sup> A time course series of crystallographic structures demonstrated the migration of the selenide ligand from the original Se2B position to the other two belt sulfide positions (SSA and S3A) during acetylene reduction, as opposed to little or no migration of Se2B during proton reduction. The Se was completely lost and replaced by S after a sufficient number of catalytic turnovers of acetylene. Turning over of the Se-incorporated MoFe protein in the presence of CO and  $\text{C}_2\text{H}_2$  resulted in the migration of Se from 2B position to the other two belt positions and high occupancy of bridging CO ligand in the Se2B position (Figure 26).<sup>144</sup>

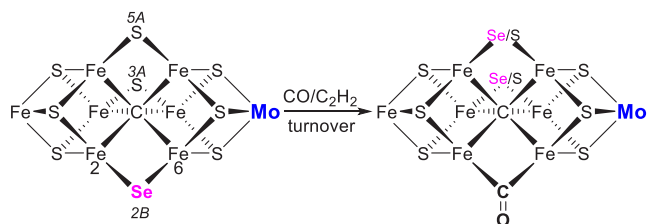


**Figure 26.** Simplified schematic representation of conversion of Se-modified FeMo-cofactor by CO, highlighting the migration of  $\text{Se}^{2-}$  to S3A and SSA position from the Se2B position.<sup>144</sup>

The lability of the S2B position toward ligand exchange during substrate reduction confirms the long-proposed Fe2–Fe6 edge as a primary interaction site for substrates and inhibitors.<sup>23,33,36,40,59,110,144,156</sup> Application of advanced X-ray absorption spectroscopies to these Se- and CO-substituted FeMo-cofactors revealed a significant asymmetry with regard to the electronic distribution about the cluster, and a redox reorganization mechanism within the cluster has been postulated.<sup>268</sup>

As discussed above, the migration of Se2B into the other two belt positions displayed a reversible and substrate-dependent pattern.<sup>144</sup> This apparent “ratcheting” motion of the selenide in three belt positions on the FeMo-co suggests a dynamic structural change (e.g., the interchange of the belt sulfides through swapping Fe–S partners in the prismatic 6Fe core) of the cluster, while still bound in the protein upon turnover.<sup>144,269</sup> The mechanism of this apparent “ratcheting” motion is not yet clear. On basis of the DFT calculations,<sup>179</sup> the rotation of the prismatic part of the FeMo-co as a whole is less possible. Other pathways involving small molecules, such as S and Se atom carriers, has been suggested and is worth considering.<sup>179</sup> The motion might be substrate specific.<sup>269</sup> These studies open the door to further exploration of structure–function relationships of the active site of nitrogenase during nitrogen fixation. Moreover, the mutual substitution reactions between different small molecule ligands,  $\text{S}^{2-}$ ,  $\text{Se}^{2-}$ , CO, and possibly acetylene, should be considered in light of the relative bond dissociation energy between different Fe–L bonds, where L = S, Se, or C.

## 6. CONCLUDING REMARKS

Remarkable progress has been achieved in understanding aspects of the mechanism of nitrogenase reduction of a wide range of substrates, including protons and  $\text{N}_2$ , nonphysiological

N substrates, and C substrates. For  $\text{N}_2$  and proton reduction, studies over the last 10 years have provided an understanding of the critical  $\text{E}_4$  step where  $\text{N}_2$  binds, and  $\text{H}_2$  is released. Many lines of evidence have revealed the enzyme functions with the limiting  $8\text{e}^-$  stoichiometry of eq 1 and Figure 3 because the *re* and release of  $\text{H}_2$  is required to drive one of the most challenging reactions in biology, cleavage of the  $\text{N}\equiv\text{N}$  triple bond. This exoergic loss of  $\text{H}_2$  from  $\text{E}_4(4\text{H})$ , the Janus intermediate drives  $\text{N}_2$  binding and formation of the first stage in actual  $\text{N}_2$  reduction, the  $\text{E}_4(2\text{N}2\text{H})$  state. The enzyme *mechanistically* couples exothermic  $\text{H}_2$  formation to endothermic cleavage of the  $\text{N}\equiv\text{N}$  triple bond in the nearly thermoneutral *re/oa* equilibrium.

One of the tasks remaining is to determine whether there is an alternative pathway, with  $\text{H}_2$  *re* and release at  $\text{E}_3(3\text{H})$ , as also proposed by Lowe and Thorneley. The evidence for this process is not strong, and the question must be re-examined. In the future, it would be useful to develop direct spectroscopic probes of the  $\text{E}_n$  FeMo-cofactor intermediates with odd-*n* (even-electron) that could give the types of insight that have been gained using EPR on even-*n* (odd-electron) species.

The additional questions about the mechanism of nitrogenase reduction of N-substrates include the following. Foremost is unambiguously distinguishing between alternating (A) and distal (D) pathways for  $\text{N}_2$  reduction. The fundamental difference between these two pathways is the stage at which the N–N bond is cleaved and the first  $\text{NH}_3$  formed:  $\text{E}_5$  for D versus  $\text{E}_7$  for A. The two trapped reduction intermediates, H and I, do not directly distinguish, as they are respectively  $\text{E}_7$  and  $\text{E}_8$ , stages past N–N cleavage. However, the weight of the evidence provided by studies of the non-native N-substrates points to the A pathway, as described above. Nonetheless, more studies are needed, in particular, trapping and characterization of the odd-electron  $\text{E}_6$  state. An initial step in this direction is studies of  $\text{E}_1$ , and it has been suggested, but not confirmed, that a recent crystal structure of VFe represents  $\text{E}_6$  or  $\text{E}_7$ .<sup>59</sup>

In delivering each  $[\text{e}^-/\text{H}^+]$  to FeMo-cofactor, the critical step is the  $\text{P} \rightarrow \text{M}$  electron transfer that must be accompanied by  $\text{H}^+$  delivery. One might well ask whether this occurs through proton coupled electron transfer (PCET) or coupled electron–proton transfer (CEPT). The ability to observe by EPR both  $\text{E}_7$  and  $\text{E}_8$  (H and I) provides a chance to study the conversion of H to I by cryoreduction/annealing, as has been done for the  $\text{E}_0$  to  $\text{E}_1$  conversion.

For nonphysiological N substrates, an important question is understanding how the N species is hydrogenated. Is this through migratory insertion of FeMo-cofactor bound hydride species? Is there any significant structural rearrangement/change that plays important roles during binding/activation/hydrogenation? Answers to such questions will take our understanding of the mechanism to the next level.

Progress in understanding nitrogenase reduction of C-based substrates spans decades, with the most recent advances coming for acetylene, CO, and  $\text{CO}_2$ . A clearer picture of the mechanism for  $\text{CO}_2$  and CO reduction is emerging, with the Fe-hydrides again at the center of the chemistry. Clearly understanding how nitrogenase reduces these C-bound substrates is important in gaining insights into the chemistry that can be achieved at the active site metal clusters. These reactions have also been suggested as a possible avenue for advancing biotechnology for hydrocarbon production. However, the direct use of nitrogenase or its cofactors to contribute

to the production of feedstocks or CO<sub>2</sub> sequestration at a useful scale is likely to be an insurmountable challenge given the lack of robustness of the enzymes and their associated cofactors.

Nitrogenase first became available for critical studies in its purified form more than half a century ago.<sup>61,62,270</sup> This was followed by steady progress in understanding the catalytic function of this complex enzyme, with rapid recent progress in determining the enzyme mechanism as described in this Review. Similar progress in addressing the many remaining issues, including those just mentioned, is expected.

## AUTHOR INFORMATION

### Corresponding Authors

**Lance C. Seefeldt** — *Department of Chemistry and Biochemistry, Utah State University, Logan, Utah 84322, United States;*  [orcid.org/0000-0002-6457-9504](https://orcid.org/0000-0002-6457-9504);

Phone: +1.435.797.3964; Email: [lance.seefeldt@usu.edu](mailto:lance.seefeldt@usu.edu)

**Zhi-Yong Yang** — *Department of Chemistry and Biochemistry, Utah State University, Logan, Utah 84322, United States;*  [orcid.org/0000-0001-8186-9450](https://orcid.org/0000-0001-8186-9450); Email: [nkyzy@hotmail.com](mailto:nkyzy@hotmail.com)

**Dmitriy A. Lukyanov** — *Department of Chemistry, Northwestern University, Evanston, Illinois 60208, United States;*  [orcid.org/0000-0002-4542-1648](https://orcid.org/0000-0002-4542-1648); Email: [d-lukyanov@northwestern.edu](mailto:d-lukyanov@northwestern.edu)

**Brian M. Hoffman** — *Department of Chemistry, Northwestern University, Evanston, Illinois 60208, United States;*  [orcid.org/0000-0002-3100-0746](https://orcid.org/0000-0002-3100-0746); Phone: +1.847.491.3104; Email: [bmh@northwestern.edu](mailto:bmh@northwestern.edu)

### Authors

**Derek F. Harris** — *Department of Chemistry and Biochemistry, Utah State University, Logan, Utah 84322, United States;*  [orcid.org/0000-0003-4277-2976](https://orcid.org/0000-0003-4277-2976)

**Dennis R. Dean** — *Biochemistry Department, Virginia Tech, Blacksburg, Virginia 24061, United States;*  [orcid.org/0001-8960-6196](https://orcid.org/0001-8960-6196)

**Simone Raugei** — *Physical and Computational Sciences Directorate, Pacific Northwest National Laboratory, Richland, Washington 99352, United States;*  [orcid.org/0000-0001-9118-8480](https://orcid.org/0000-0001-9118-8480)

Complete contact information is available at:

<https://pubs.acs.org/10.1021/acs.chemrev.9b00556>

### Notes

The authors declare no competing financial interest.

### Biographies

Lance C. Seefeldt received a B.S. degree in chemistry from the University of Redlands in California and a Ph.D. in biochemistry from the University of California at Riverside. He was a postdoctoral fellow at the Center for Metalloenzyme Studies at the University of Georgia before joining the faculty of the Chemistry and Biochemistry Department at Utah State University, where he is now Professor and Department Head. He was recently awarded the D. Wynne Thorne Career Research Award and was elected a Fellow of the American Association for the Advancement of Science. Over the past 30 years, his research has focused on elucidating the mechanism of nitrogenase.

Zhi-Yong Yang received a B.S. degree in chemistry in 2001 and a Ph.D. degree in organic chemistry in 2006 from Nankai University in

Tianjin, China. Following a position at Shanghai ChemPartner as an organic chemist, he joined Prof. Lance Seefeldt's lab at Utah State University and was awarded with a Ph.D. degree in biochemistry in 2013. After a postdoctoral training in the same group, he was promoted to Researcher in 2017. During the past 19 years, his research has covered biomimetic chemistry of hydrogenases and the mechanism of nitrogenase. His research interest is in understanding the mechanism of small molecule activation catalyzed by biological and synthetic catalysts, including kinetics, thermodynamics, electron transfer, and energy transduction.

Dmitriy A. Lukyanov received a M.S. degree and a Ph.D. from Kazan State University. He is a Research Associate at Northwestern University. During the last 14 years, his research work has focused on investigation of nitrogenase catalysis with application of various Electron Paramagnetic Resonance (EPR) techniques.

Derek F. Harris received a B.S. in biology from Dixie State University and a M.S. and Ph.D. in biochemistry from Utah State University. He continues to study nitrogenase enzymes as a postdoctoral fellow at Utah State University.

Dennis R. Dean received a B.A. from Wabash College and a Ph.D. from Purdue University. He is currently a University Distinguished Professor at Virginia Tech, where he has also served as the Director of the Fralin Life Sciences Institute, the Virginia Bioinformatics Institute and Vice President for Research. He is a Fellow of the American Association for the Advancement of Science and a Fellow of the American Academy of Microbiology.

Simone Raugei obtained a Ph.D. in theoretical chemistry from the University of Florence (Italy) in 2000 with Prof. Vincenzo Schettino. In 1997–1998, he studied at the Max Planck Institute for Solid State Physics in Stuttgart (Germany) under the supervision of Prof. Michele Parrinello. From 2000 to 2002, he joined the University of Pennsylvania (USA) as a postdoctoral fellow in the group of Prof. Michael L. Klein. From 2002 to 2009, he was an Assistant Professor at the School for Advanced Studies in Trieste (Italy). Since 2010, he has been a senior Scientist at the Pacific Northwest National Laboratory. His current scientific activity focuses on the computational and theoretical modeling of chemical and biochemical processes for energy storage and energy delivery.

Brian M. Hoffman is the Charles E. and Emma H. Morrison Professor of Chemistry and Professor of Molecular Biosciences at Northwestern University. His undergraduate studies were at the University of Chicago, PhD with Harden McConnell at the California Institute of Technology, and Postdoctoral work at the Massachusetts Institute of Technology with Alex Rich. His research in Bioinorganic Chemistry has included measurements of long-range electron transfer between proteins, in addition to determinations of metalloenzyme mechanisms through development and implementation of electron–nuclear double resonance (ENDOR) techniques. He is a member of the National Academy of Sciences and the American Academy of Arts and Sciences.

### ACKNOWLEDGMENTS

The work in the Seefeldt and Dean groups was supported by grants from the US Department of Energy (DOE), Office of Science, Basic Energy Sciences (BES) (Grants DESC0010687 and DESC0010834). The work of Raugei was supported by the US DOE, Office of Science, BES, Division of Chemical Sciences, Geosciences, and Biosciences. Work in the Hoffman Laboratory was supported by the National Science Foundation (Grant) and the National Institutes of Health (Grant GM111097) and the US Department of Energy (DOE),

Office of Science, Basic Energy Sciences (BES) (Grant DE-SC0019342).

## REFERENCES

- (1) Smil, V. *Enriching the Earth: Fritz Haber, Carl Bosch, and the Transformation of World Food Production*; MIT Press: Cambridge, MA, 2004.
- (2) Erisman, J. W.; Galloway, J. N.; Dise, N. B.; Sutton, M. A.; Bleeker, A.; Grizzetti, B.; Leach, A. M.; de Vries, W. *Nitrogen: Too Much of a Vital Resource*; Science Brief; WWF Nederland, 2015.
- (3) Chen, J. G.; Crooks, R. M.; Seefeldt, L. C.; Bren, K. L.; Bullock, R. M.; Daresbourg, M. Y.; Holland, P. L.; Hoffman, B.; Janik, M. J.; Jones, A. K.; et al. Beyond Fossil Fuel–Driven Nitrogen Transformations. *Science* **2018**, *360*, No. eaar6611.
- (4) Dawson, C. J.; Hilton, J. Fertiliser Availability in a Resource-Limited World: Production and Recycling of Nitrogen and Phosphorus. *Food Policy* **2011**, *36*, S14–S22.
- (5) Erisman, J. W.; Galloway, J. N.; Seitzinger, S.; Bleeker, A.; Dise, N. B.; Petrescu, A. M. R.; Leach, A. M.; de Vries, W. Consequences of Human Modification of the Global Nitrogen Cycle. *Philos. Trans. R. Soc., B* **2013**, *368*, 20130116.
- (6) Galloway, J. N.; Townsend, A. R.; Erisman, J. W.; Bekunda, M.; Cai, Z.; Freney, J. R.; Martinelli, L. A.; Seitzinger, S. P.; Sutton, M. A. Transformation of the Nitrogen Cycle: Recent Trends, Questions, and Potential Solutions. *Science* **2008**, *320*, 889–892.
- (7) Erisman, J. W.; Sutton, M. A.; Galloway, J.; Klimont, Z.; Winiwarter, W. How a Century of Ammonia Synthesis Changed the World. *Nat. Geosci.* **2008**, *1*, 636–639.
- (8) Fowler, D.; Coyle, M.; Skiba, U.; Sutton, M. A.; Cape, J. N.; Reis, S.; Jenkins, A.; Grizzetti, B.; Galloway, J. N.; Vitousek, P.; et al. The Global Nitrogen Cycle in the Twenty-First Century. *Philos. Trans. R. Soc., B* **2013**, *368*, 20130164.
- (9) Gruber, N.; Galloway, J. N. An Earth-System Perspective of the Global Nitrogen Cycle. *Nature* **2008**, *451*, 293–296.
- (10) Thamdrup, B. New Pathways and Processes in the Global Nitrogen Cycle. *Annu. Rev. Ecol. Evol. Syst.* **2012**, *43*, 407–428.
- (11) Raymond, J.; Siefert, J. L.; Staples, C. R.; Blankenship, R. E. The Natural History of Nitrogen Fixation. *Mol. Biol. Evol.* **2004**, *21*, 541–554.
- (12) Zhang, X.; Davidson, E. A.; Mauzerall, D. L.; Searchinger, T. D.; Dumas, P.; Shen, Y. Managing Nitrogen for Sustainable Development. *Nature* **2015**, *528*, 51–59.
- (13) Haber, F. Über die Darstellung des Ammoniaks aus Stickstoff und Wasserstoff. *Naturwissenschaften* **1922**, *10*, 1041–1049.
- (14) Ertl, G. Reactions at Surfaces: From Atoms to Complexity. *Angew. Chem., Int. Ed.* **2008**, *47*, 3524–3535.
- (15) Haber, F. The History of the Ammonia Process. *Naturwissenschaften* **1923**, *11*, 339–340.
- (16) Burris, R. H.; Roberts, G. P. Biological Nitrogen Fixation. *Annu. Rev. Nutr.* **1993**, *13*, 317–335.
- (17) Cheng, Q. Perspectives in Biological Nitrogen Fixation Research. *J. Integr. Plant Biol.* **2008**, *50*, 786–798.
- (18) Boyd, E. S.; Hamilton, T. L.; Peters, J. W. An Alternative Path for the Evolution of Biological Nitrogen Fixation. *Front. Microbiol.* **2011**, *2*, 205.
- (19) Simpson, F. B.; Burris, R. H. A. Nitrogen Pressure of 50 atm Does Not Prevent Evolution of Hydrogen by Nitrogenase. *Science* **1984**, *224*, 1095–1097.
- (20) Burgess, B. K.; Lowe, D. J. Mechanism of Molybdenum Nitrogenase. *Chem. Rev.* **1996**, *96*, 2983–3012.
- (21) Hoffman, B. M.; Lukyanov, D.; Dean, D. R.; Seefeldt, L. C. Nitrogenase: A Draft Mechanism. *Acc. Chem. Res.* **2013**, *46*, 587–595.
- (22) Yang, Z.-Y.; Khadka, N.; Lukyanov, D.; Hoffman, B. M.; Dean, D. R.; Seefeldt, L. C. On Reversible H<sub>2</sub> Loss upon N<sub>2</sub> Binding to FeMo-cofactor of Nitrogenase. *Proc. Natl. Acad. Sci. U. S. A.* **2013**, *110*, 16327–16332.
- (23) Hoffman, B. M.; Lukyanov, D.; Yang, Z.-Y.; Dean, D. R.; Seefeldt, L. C. Mechanism of Nitrogen Fixation by Nitrogenase: The next Stage. *Chem. Rev.* **2014**, *114*, 4041–4062.
- (24) Rafiqul, I.; Weber, C.; Lehmann, B.; Voss, A. Energy Efficiency Improvements in Ammonia Production—Perspectives and Uncertainties. *Energy* **2005**, *30*, 2487–2504.
- (25) Neet, K. E. Enzyme Catalytic Power Minireview Series. *J. Biol. Chem.* **1998**, *273*, 25527–25528.
- (26) Knowles, J. R. Enzyme Catalysis: Not Different, Just Better. *Nature* **1991**, *350*, 121–124.
- (27) Benkovic, S. J.; Hammes-Schiffer, S. A Perspective on Enzyme Catalysis. *Science* **2003**, *301*, 1196–1202.
- (28) Yang, Z.-Y.; Ledbetter, R.; Shaw, S.; Pence, N.; Tokmin-Lukaszewska, M.; Eilers, B.; Guo, Q.; Pokhrel, N.; Cash, V. L.; Dean, D. R.; et al. Evidence That the Pi Release Event Is the Rate-Limiting Step in the Nitrogenase Catalytic Cycle. *Biochemistry* **2016**, *55*, 3625–3635.
- (29) Badalyan, A.; Yang, Z.-Y.; Seefeldt, L. C. A Voltammetric Study of Nitrogenase Catalysis Using Electron Transfer Mediators. *ACS Catal.* **2019**, *9*, 1366–1372.
- (30) Mortenson, L. E.; Thorneley, R. N. Structure and Function of Nitrogenase. *Annu. Rev. Biochem.* **1979**, *48*, 387–418.
- (31) Thorneley, R. N. F.; Lowe, D. J. Kinetics and Mechanism of the Nitrogenase Enzyme. In *Molybdenum Enzymes*; Spiro, T. G., Ed.; Metal Ions in Biology; Wiley-Interscience Publications: New York, 1985; Vol. 7, pp 221–284.
- (32) Howard, J. B.; Rees, D. C. How Many Metals Does It Take to Fix N<sub>2</sub>? A Mechanistic Overview of Biological Nitrogen Fixation. *Proc. Natl. Acad. Sci. U. S. A.* **2006**, *103*, 17088–17093.
- (33) Seefeldt, L. C.; Hoffman, B. M.; Dean, D. R. Mechanism of Mo-Dependent Nitrogenase. *Annu. Rev. Biochem.* **2009**, *78*, 701–722.
- (34) Seefeldt, L. C.; Dean, D. R. Role of Nucleotides in Nitrogenase Catalysis. *Acc. Chem. Res.* **1997**, *30*, 260–266.
- (35) Igarashi, R. Y.; Seefeldt, L. C. Nitrogen Fixation: The Mechanism of the Mo-Dependent Nitrogenase. *Crit. Rev. Biochem. Mol. Biol.* **2003**, *38*, 351–384.
- (36) Dos Santos, P. C.; Igarashi, R. Y.; Lee, H.-I.; Hoffman, B. M.; Seefeldt, L. C.; Dean, D. R. Substrate Interactions with the Nitrogenase Active Site. *Acc. Chem. Res.* **2005**, *38*, 208–214.
- (37) Tezcan, F. A.; Kaiser, J. T.; Mustafi, D.; Walton, M. Y.; Howard, J. B.; Rees, D. C. Nitrogenase Complexes: Multiple Docking Sites for a Nucleotide Switch Protein. *Science* **2005**, *309*, 1377–1380.
- (38) Harris, D. F.; Lukyanov, D. A.; Shaw, S.; Compton, P.; Tokmin-Lukaszewska, M.; Bothner, B.; Kelleher, N.; Dean, D. R.; Hoffman, B. M.; Seefeldt, L. C. Mechanism of N<sub>2</sub> Reduction Catalyzed by Fe-Nitrogenase Involves Reductive Elimination of H<sub>2</sub>. *Biochemistry* **2018**, *57*, 701–710.
- (39) Burgess, B. K. Substrate Reactions of Nitrogenase. In *Metal Ions in Biology: Molybdenum Enzymes*; Spiro, T. G., Ed.; John Wiley and Sons: New York, 1985; pp 161–220.
- (40) Seefeldt, L. C.; Yang, Z.-Y.; Duval, S.; Dean, D. R. Nitrogenase Reduction of Carbon-Containing Compounds. *Biochim. Biophys. Acta, Bioenerg.* **2013**, *1827*, 1102–1111.
- (41) Eady, R. R. Structure–Function Relationships of Alternative Nitrogenases. *Chem. Rev.* **1996**, *96*, 3013–3030.
- (42) Hu, Y.; Lee, C. C.; Ribbe, M. W. Vanadium Nitrogenase: A Two-Hit Wonder? *Dalton Trans.* **2012**, *41*, 1118–1127.
- (43) Schneider, K.; Müller, A. Iron-Only Nitrogenase: Exceptional Catalytic, Structural and Spectroscopic Features. In *Catalysts for Nitrogen Fixation: Origins, Applications, and Research Progress*; Springer: Dordrecht, 2004; pp 281–307.
- (44) Hales, B. J. Alternative Nitrogenase. *Adv. Inorg. Biochem.* **1990**, *8*, 165–198.
- (45) McGlynn, S. E.; Boyd, E. S.; Peters, J. W.; Orphan, V. J. Classifying the Metal Dependence of Uncharacterized Nitrogenases. *Front. Microbiol.* **2013**, *3*, 419.
- (46) Waugh, S. I.; Paulsen, D. M.; Mylona, P. V.; Maynard, R. H.; Premakumar, R.; Bishop, P. E. The Genes Encoding the Delta Subunits of Dinitrogenases 2 and 3 Are Required for Mo-Independent Diazotrophic Growth by *Azotobacter vinelandii*. *J. Bacteriol.* **1995**, *177*, 1505–1510.

(47) Bishop, P. E.; Hawkins, M. E.; Eady, R. R. Nitrogen Fixation in Molybdenum-Deficient Continuous Culture by a Strain of *Azotobacter vinelandii* Carrying a Deletion of the Structural Genes for Nitrogenase (*nifHDK*). *Biochem. J.* **1986**, *238*, 437–442.

(48) Bishop, P. E.; Premakumar, R.; Dean, D. R.; Jacobson, M. R.; Chisnell, J. R.; Rizzo, T. M.; Kopczynski, J. Nitrogen Fixation by *Azotobacter vinelandii* Strains Having Deletions in Structural Genes for Nitrogenase. *Science* **1986**, *232*, 92–94.

(49) Betancourt, D. A.; Loveless, T. M.; Brown, J. W.; Bishop, P. E. Characterization of Diazotrophs Containing Mo-Independent Nitrogenases, Isolated from Diverse Natural Environments. *Appl. Environ. Microbiol.* **2008**, *74*, 3471–3480.

(50) Dos Santos, P. C.; Fang, Z.; Mason, S. W.; Setubal, J. C.; Dixon, R. Distribution of Nitrogen Fixation and Nitrogenase-like Sequences amongst Microbial Genomes. *BMC Genomics* **2012**, *13*, 162.

(51) Boyd, E. S.; Costas, A. M. G.; Hamilton, T. L.; Mus, F.; Peters, J. W. Evolution of Molybdenum Nitrogenase during the Transition from Anaerobic to Aerobic Metabolism. *J. Bacteriol.* **2015**, *197*, 1690–1699.

(52) Bishop, P. E.; Jarlenski, D. M.; Hetherington, D. R. Evidence for an Alternative Nitrogen Fixation System in *Azotobacter vinelandii*. *Proc. Natl. Acad. Sci. U. S. A.* **1980**, *77*, 7342–7346.

(53) Sippel, D.; Schlesier, J.; Rohde, M.; Trncik, C.; Decamps, L.; Djurdjevic, I.; Spatzal, T.; Andrade, S. L. A.; Einsle, O. Production and Isolation of Vanadium Nitrogenase from *Azotobacter vinelandii* by Molybdenum Depletion. *JBIC, J. Biol. Inorg. Chem.* **2017**, *22*, 161–168.

(54) Georgiadis, M. M.; Komiya, H.; Chakrabarti, P.; Woo, D.; Kornuc, J. J.; Rees, D. C. Crystallographic Structure of the Nitrogenase Iron Protein from *Azotobacter vinelandii*. *Science* **1992**, *257*, 1653–1659.

(55) Kim, J.; Rees, D. C. Structural Models for the Metal Centers in the Nitrogenase Molybdenum-Iron Protein. *Science* **1992**, *257*, 1677–1682.

(56) Einsle, O.; Tezcan, F. A.; Andrade, S. L. A.; Schmid, B.; Yoshida, M.; Howard, J. B.; Rees, D. C. Nitrogenase MoFe-Protein at 1.16 Å Resolution: A Central Ligand in the FeMo-cofactor. *Science* **2002**, *297*, 1696–1700.

(57) Spatzal, T.; Aksoyoglu, M.; Zhang, L.; Andrade, S. L. A.; Schleicher, E.; Weber, S.; Rees, D. C.; Einsle, O. Evidence for Interstitial Carbon in Nitrogenase FeMo Cofactor. *Science* **2011**, *334*, 940–940.

(58) Sippel, D.; Einsle, O. The Structure of Vanadium Nitrogenase Reveals an Unusual Bridging Ligand. *Nat. Chem. Biol.* **2017**, *13*, 956–960.

(59) Sippel, D.; Rohde, M.; Netzer, J.; Trncik, C.; Gies, J.; Grunau, K.; Djurdjevic, I.; Decamps, L.; Andrade, S. L. A.; Einsle, O. A Bound Reaction Intermediate Sheds Light on the Mechanism of Nitrogenase. *Science* **2018**, *359*, 1484–1489.

(60) Rohde, M.; Trncik, C.; Sippel, D.; Gerhardt, S.; Einsle, O. Crystal Structure of VnfH, the Iron Protein Component of Vanadium Nitrogenase. *JBIC, J. Biol. Inorg. Chem.* **2018**, *23*, 1049–1056.

(61) Bulen, W. A.; LeComte, J. R. The Nitrogenase System from *Azotobacter*: Two-Enzyme Requirement for N<sub>2</sub> Reduction, ATP-Dependent H<sub>2</sub> Evolution, and ATP Hydrolysis. *Proc. Natl. Acad. Sci. U. S. A.* **1966**, *56*, 979–986.

(62) Mortenson, L. E. Components of Cell-Free Extracts of *Clostridium Pasteurianum* Required for ATP-Dependent H<sub>2</sub> Evolution from Dithionite and for N<sub>2</sub> Fixation. *Biochim. Biophys. Acta, Gen. Subj.* **1966**, *127*, 18–25.

(63) Roberts, G. P.; MacNeil, T.; MacNeil, D.; Brill, W. J. Regulation and Characterization of Protein Products Coded by the *nif* (Nitrogen Fixation) Genes of *Klebsiella pneumoniae*. *J. Bacteriol.* **1978**, *136*, 267–279.

(64) Robson, R.; Woodley, P.; Jones, R. Second Gene (*NifH*) Coding for a Nitrogenase Iron Protein in *Azotobacter chroococcum* Is Adjacent to a Gene Coding for a Ferredoxin-like Protein. *EMBO J.* **1986**, *5*, 1159–1163.

(65) Joerger, R. D.; Wolfinger, E. D.; Bishop, P. E. The Gene Encoding Dinitrogenase Reductase 2 Is Required for Expression of the Second Alternative Nitrogenase from *Azotobacter vinelandii*. *J. Bacteriol.* **1991**, *173*, 4440–4446.

(66) Joerger, R. D.; Bishop, P. E.; Evans, H. J. Bacterial Alternative Nitrogen Fixation Systems. *Crit. Rev. Microbiol.* **1988**, *16*, 1–14.

(67) Joerger, R. D.; Jacobson, M. R.; Premakumar, R.; Wolfinger, E. D.; Bishop, P. E. Nucleotide Sequence and Mutational Analysis of the Structural Genes (*anfHDK*) for the Second Alternative Nitrogenase from *Azotobacter vinelandii*. *J. Bacteriol.* **1989**, *171*, 1075–1086.

(68) Howard, J. B.; Rees, D. C. Structural Basis of Biological Nitrogen Fixation. *Chem. Rev.* **1996**, *96*, 2965–2982.

(69) Lancaster, K. M.; Roemelt, M.; Ettenhuber, P.; Hu, Y.; Ribbe, M. W.; Neese, F.; Bergmann, U.; DeBeer, S. X-Ray Emission Spectroscopy Evidences a Central Carbon in the Nitrogenase Iron-Molybdenum Cofactor. *Science* **2011**, *334*, 974–977.

(70) Shah, V. K.; Brill, W. J. Isolation of an Iron-Molybdenum Cofactor from Nitrogenase. *Proc. Natl. Acad. Sci. U. S. A.* **1977**, *74*, 3249–3253.

(71) Grunenberg, J. The Interstitial Carbon of the Nitrogenase FeMo Cofactor Is Far Better Stabilized than Previously Assumed. *Angew. Chem., Int. Ed.* **2017**, *56*, 7288–7291.

(72) Rees, J. A.; Bjornsson, R.; Schlesier, J.; Sippel, D.; Einsle, O.; DeBeer, S. The Fe–V Cofactor of Vanadium Nitrogenase Contains an Interstitial Carbon Atom. *Angew. Chem., Int. Ed.* **2015**, *54*, 13249–13252.

(73) Fay, A. W.; Blank, M. A.; Lee, C. C.; Hu, Y.; Hodgson, K. O.; Hedman, B.; Ribbe, M. W. Characterization of Isolated Nitrogenase FeVco. *J. Am. Chem. Soc.* **2010**, *132*, 12612–12618.

(74) Peters, J. W.; Fisher, K.; Newton, W. E.; Dean, D. R. Involvement of the P-Cluster in Intramolecular Electron Transfer within the Nitrogenase MoFe Protein. *J. Biol. Chem.* **1995**, *270*, 27007–27013.

(75) Seefeldt, L. C.; Hoffman, B. M.; Peters, J. W.; Raugei, S.; Beratan, D. N.; Antony, E.; Dean, D. R. Energy Transduction in Nitrogenase. *Acc. Chem. Res.* **2018**, *51*, 2179–2186.

(76) Poudel, S.; Colman, D. R.; Fixen, K. R.; Ledbetter, R. N.; Zheng, Y.; Pence, N.; Seefeldt, L. C.; Peters, J. W.; Harwood, C. S.; Boyd, E. S. Electron Transfer to Nitrogenase in Different Genomic and Metabolic Backgrounds. *J. Bacteriol.* **2018**, *200*, e00757-17.

(77) Katz, F. E. H.; Owens, C. P.; Tezcan, F. A. Electron Transfer Reactions in Biological Nitrogen Fixation. *Isr. J. Chem.* **2016**, *56*, 682–692.

(78) Münck, E.; Rhodes, H.; Orme-Johnson, W. H.; Davis, L. C.; Brill, W. J.; Shah, V. K. Nitrogenase. VIII. Mössbauer and EPR Spectroscopy. The MoFe Protein Component from *Azotobacter vinelandii* OP. *Biochim. Biophys. Acta, Protein Struct.* **1975**, *400*, 32–53.

(79) Harris, T. V.; Szilagyi, R. K. Comparative Assessment of the Composition and Charge State of Nitrogenase FeMo-cofactor. *Inorg. Chem.* **2011**, *50*, 4811–4824.

(80) Krahn, E.; Weiss, B.; Kröckel, M.; Groppe, J.; Henkel, G.; Cramer, S.; Trautwein, A.; Schneider, K.; Müller, A. The Fe-Only Nitrogenase from *Rhodobacter capsulatus*: Identification of the Cofactor, an Unusual, High-Nuclearity Iron-Sulfur Cluster, by Fe K-Edge EXAFS and <sup>57</sup>Fe Mössbauer Spectroscopy. *JBIC, J. Biol. Inorg. Chem.* **2002**, *7*, 37–45.

(81) Wilson, P. E.; Nyborg, A. C.; Watt, G. D. Duplication and Extension of the Thorneley and Lowe Kinetic Model for *Klebsiella pneumoniae* Nitrogenase Catalysis Using a MATHEMATICA Software Platform. *Biophys. Chem.* **2001**, *91*, 281–304.

(82) Hoffman, B. M.; Dean, D. R.; Seefeldt, L. C. Climbing Nitrogenase: Toward a Mechanism of Enzymatic Nitrogen Fixation. *Acc. Chem. Res.* **2009**, *42*, 609–619.

(83) Pickett, C. J. The Chatt Cycle and the Mechanism of Enzymic Reduction of Molecular Nitrogen. *JBIC, J. Biol. Inorg. Chem.* **1996**, *1*, 601–606.

(84) Henderson, R. A. Metal Hydride Intermediates in Hydrogenases and Nitrogenases: Enzymological and Model Studies. In

Recent Advances in Hydride Chemistry; Peruzzini, M., Poli, R., Eds.; Elsevier: Amsterdam, 2001; pp 463–505.

(85) Jackson, E. K.; Parshall, G. W.; Hardy, R. W. F. Hydrogen Reactions of Nitrogenase. Formation of the Molecule HD by Nitrogenase and by an Inorganic Model. *J. Biol. Chem.* **1968**, *243*, 4952–4958.

(86) Thorneley, R. N. F.; Eady, R. R.; Lowe, D. J. Biological Nitrogen Fixation by Way of an Enzyme-Bound Dinitrogen-Hydride Intermediate. *Nature* **1978**, *272*, 557–558.

(87) Thorneley, R. N.; Lowe, D. J. The Mechanism of *Klebsiella pneumoniae* Nitrogenase Action: Pre-Steady-State Kinetics of an Enzyme-Bound Intermediate in N<sub>2</sub> Reduction and of NH<sub>3</sub> Formation. *Biochem. J.* **1984**, *224*, 887–894.

(88) Guth, J. H.; Burris, R. H. Inhibition of Nitrogenase-Catalyzed Ammonia Formation by Hydrogen. *Biochemistry* **1983**, *22*, 5111–5122.

(89) Jensen, B. B.; Burris, R. H. Effect of High pN<sub>2</sub> and High pD<sub>2</sub> on Ammonia Production, Hydrogen Evolution, and Hydrogen Deuteride Formation by Nitrogenases. *Biochemistry* **1985**, *24*, 1141–1147.

(90) Burgess, B. K.; Wherland, S.; Newton, W. E.; Stiefel, E. I. Nitrogenase Reactivity: Insight into the Nitrogen-Fixing Process through Hydrogen-Inhibition and HD-Forming Reactions. *Biochemistry* **1981**, *20*, 5140–5146.

(91) Leigh, G. J. The Mechanism of Dinitrogen Reduction by Molybdenum Nitrogenases. *Eur. J. Biochem.* **1995**, *229*, 14–20.

(92) Thorneley, R. N. F.; Lowe, D. J. Nitrogenase: Substrate Binding and Activation. *JBIC, J. Biol. Inorg. Chem.* **1996**, *1*, 576–580.

(93) Rivera-Ortiz, J. M.; Burris, R. H. Interactions among Substrates and Inhibitors of Nitrogenase. *J. Bacteriol.* **1975**, *123*, 537–545.

(94) Strandberg, G. W.; Wilson, P. W. Formation of the Nitrogen-Fixing Enzyme System in *Azotobacter vinelandii*. *Can. J. Microbiol.* **1968**, *14*, 25–31.

(95) Hwang, J. C.; Chen, C. H.; Burris, R. H. Inhibition of Nitrogenase-Catalyzed Reductions. *Biochim. Biophys. Acta, Bioenerg.* **1973**, *292*, 256–270.

(96) Hoch, G. E.; Schneider, K. C.; Burris, R. H. Hydrogen Evolution and Exchange, and Conversion of N<sub>2</sub>O to N<sub>2</sub> by Soybean Root Nodules. *Biochim. Biophys. Acta* **1960**, *37*, 273–279.

(97) Wherland, S.; Burgess, B. K.; Stiefel, E. I.; Newton, W. E. Nitrogenase Reactivity: Effects of Component Ratio on Electron Flow and Distribution during Nitrogen Fixation. *Biochemistry* **1981**, *20*, 5132–5140.

(98) Li, J.-L.; Burris, R. H. Influence of pN<sub>2</sub> and pD<sub>2</sub> on HD Formation by Various Nitrogenases. *Biochemistry* **1983**, *22*, 4472–4480.

(99) Dilworth, M. J.; Fisher, K.; Kim, C.-H.; Newton, W. E. Effects on Substrate Reduction of Substitution of Histidine-195 by Glutamine in the  $\alpha$ -Subunit of the MoFe Protein of *Azotobacter vinelandii* Nitrogenase. *Biochemistry* **1998**, *37*, 17495–17505.

(100) Fisher, K.; Dilworth, M. J.; Newton, W. E. Differential Effects on N<sub>2</sub> Binding and Reduction, HD Formation, and Azide Reduction with  $\alpha$ -195<sup>His</sup>- and  $\alpha$ -191<sup>Gln</sup>-Substituted MoFe Proteins of *Azotobacter vinelandii* Nitrogenase. *Biochemistry* **2000**, *39*, 15570–15577.

(101) Ashby, G. A.; Dilworth, M. J.; Thorneley, R. N. F. *Klebsiella pneumoniae* Nitrogenase. Inhibition of Hydrogen Evolution by Ethylene and the Reduction of Ethylene to Ethane. *Biochem. J.* **1987**, *247*, 547–554.

(102) Lowe, D. J.; Fisher, K.; Thorneley, R. N. *Klebsiella pneumoniae* Nitrogenase: Mechanism of Acetylene Reduction and Its Inhibition by Carbon Monoxide. *Biochem. J.* **1990**, *272*, 621–625.

(103) Leigh, G. J.; McMahon, C. N. The Organometallic Chemistry of Nitrogenases. *J. Organomet. Chem.* **1995**, *500*, 219–225.

(104) Chatt, J.; Richards, R. L. The Reactions of Dinitrogen in Its Metal Complexes. *J. Organomet. Chem.* **1982**, *239*, 65–77.

(105) Crabtree, R. H. Dihydrogen Binding in Hydrogenase and Nitrogenase. *Inorg. Chim. Acta* **1986**, *125*, L7–L8.

(106) Ogo, S.; Kure, B.; Nakai, H.; Watanabe, Y.; Fukuzumi, S. Why Do Nitrogenases Waste Electrons by Evolving Dihydrogen? *Appl. Organomet. Chem.* **2004**, *18*, 589–594.

(107) MacKay, B. A.; Fryzuk, M. D. Dinitrogen Coordination Chemistry: On the Biomimetic Borderlands. *Chem. Rev.* **2004**, *104*, 385–402.

(108) Ballmann, J.; Munhá, R. F.; Fryzuk, M. D. The Hydride Route to the Preparation of Dinitrogen Complexes. *Chem. Commun.* **2010**, *46*, 1013–1025.

(109) Lee, H.-I.; Igarashi, R. Y.; Laryukhin, M.; Doan, P. E.; Dos Santos, P. C.; Dean, D. R.; Seefeldt, L. C.; Hoffman, B. M. An Organometallic Intermediate during Alkyne Reduction by Nitrogenase. *J. Am. Chem. Soc.* **2004**, *126*, 9563–9569.

(110) Seefeldt, L. C.; Dance, I. G.; Dean, D. R. Substrate Interactions with Nitrogenase: Fe versus Mo. *Biochemistry* **2004**, *43*, 1401–1409.

(111) Igarashi, R. Y.; Laryukhin, M.; Dos Santos, P. C.; Lee, H.-I.; Dean, D. R.; Seefeldt, L. C.; Hoffman, B. M. Trapping H<sup>+</sup> Bound to the Nitrogenase FeMo-cofactor Active Site during H<sub>2</sub> Evolution: Characterization by ENDOR Spectroscopy. *J. Am. Chem. Soc.* **2005**, *127*, 6231–6241.

(112) Barney, B. M.; Igarashi, R. Y.; Dos Santos, P. C.; Dean, D. R.; Seefeldt, L. C. Substrate Interaction at an Iron-Sulfur Face of the FeMo-cofactor during Nitrogenase Catalysis. *J. Biol. Chem.* **2004**, *279*, S3621–S3624.

(113) Lukyanov, D.; Barney, B. M.; Dean, D. R.; Seefeldt, L. C.; Hoffman, B. M. Connecting Nitrogenase Intermediates with the Kinetic Scheme for N<sub>2</sub> Reduction by a Relaxation Protocol and Identification of the N<sub>2</sub> Binding State. *Proc. Natl. Acad. Sci. U. S. A.* **2007**, *104*, 1451–1455.

(114) Lukyanov, D.; Yang, Z.-Y.; Dean, D. R.; Seefeldt, L. C.; Hoffman, B. M. Is Mo Involved in Hydride Binding by the Four-Electron Reduced (E<sub>4</sub>) Intermediate of the Nitrogenase MoFe Protein? *J. Am. Chem. Soc.* **2010**, *132*, 2526–2527.

(115) Lukyanov, D.; Khadka, N.; Yang, Z.-Y.; Dean, D. R.; Seefeldt, L. C.; Hoffman, B. M. Reductive Elimination of H<sub>2</sub> Activates Nitrogenase to Reduce the N≡N Triple Bond: Characterization of the E<sub>4</sub>(4H) Janus Intermediate in Wild-Type Enzyme. *J. Am. Chem. Soc.* **2016**, *138*, 10674–10683.

(116) Lukyanov, D.; Khadka, N.; Yang, Z.-Y.; Dean, D. R.; Seefeldt, L. C.; Hoffman, B. M. Reversible Photoinduced Reductive Elimination of H<sub>2</sub> from the Nitrogenase Dihydride State, the E<sub>4</sub>(4H) Janus Intermediate. *J. Am. Chem. Soc.* **2016**, *138*, 1320–1327.

(117) Hartwig, J. *Organotransition Metal Chemistry: From Bonding to Catalysis*; University Science Books: Sausalito, CA, 2010.

(118) Crabtree, R. H. *The Organometallic Chemistry of the Transition Metals*, 5th ed.; Wiley: Hoboken, NJ, 2009.

(119) Peruzzini, M.; Poli, R. *Recent Advances in Hydride Chemistry*; Elsevier Science B. V.: Amsterdam, The Netherlands, 2001.

(120) Fisher, K.; Newton, W. E.; Lowe, D. J. Electron Paramagnetic Resonance Analysis of Different *Azotobacter vinelandii* Nitrogenase MoFe-Protein Conformations Generated during Enzyme Turnover: Evidence for S = 3/2 Spin States from Reduced MoFe-Protein Intermediates. *Biochemistry* **2001**, *40*, 3333–3339.

(121) Fisher, K.; Lowe, D. J.; Tavares, P.; Pereira, A. S.; Huynh, B. H.; Edmondson, D.; Newton, W. E. Conformations Generated during Turnover of the *Azotobacter vinelandii* Nitrogenase MoFe Protein and Their Relationship to Physiological Function. *J. Inorg. Biochem.* **2007**, *101*, 1649–1656.

(122) Lukyanov, D.; Yang, Z.-Y.; Duval, S.; Danyal, K.; Dean, D. R.; Seefeldt, L. C.; Hoffman, B. M. A Confirmation of the Quench-Cryoannealing Relaxation Protocol for Identifying Reduction States of Freeze-Trapped Nitrogenase Intermediates. *Inorg. Chem.* **2014**, *53*, 3688–3693.

(123) Lukyanov, D. A.; Khadka, N.; Yang, Z.-Y.; Dean, D. R.; Seefeldt, L. C.; Hoffman, B. M. Hydride Conformers of the Nitrogenase FeMo-cofactor Two-Electron Reduced State E<sub>2</sub>(2H), Assigned Using Cryogenic Intra-Electron Paramagnetic Resonance Cavity Photolysis. *Inorg. Chem.* **2018**, *57*, 6847–6852.

(124) Lukyanov, D.; Yang, Z.-Y.; Khadka, N.; Dean, D. R.; Seefeldt, L. C.; Hoffman, B. M. Identification of a Key Catalytic Intermediate

Demonstrates That Nitrogenase Is Activated by the Reversible Exchange of  $N_2$  for  $H_2$ . *J. Am. Chem. Soc.* **2015**, *137*, 3610–3615.

(125) Lukyanov, D.; Khadka, N.; Dean, D. R.; Raugei, S.; Seefeldt, L. C.; Hoffman, B. M. Photoinduced Reductive Elimination of  $H_2$  from the Nitrogenase Dihydride (Janus) State Involves a FeMo-cofactor- $H_2$  Intermediate. *Inorg. Chem.* **2017**, *56*, 2233–2240.

(126) Siegbahn, P. E. M. Model Calculations Suggest That the Central Carbon in the FeMo-cofactor of Nitrogenase Becomes Protonated in the Process of Nitrogen Fixation. *J. Am. Chem. Soc.* **2016**, *138*, 10485–10495.

(127) Gurbel, R. J.; Bolin, J. T.; Ronco, A. E.; Mortenson, L.; Hoffman, B. M. Single-Crystal EPR and ENDOR Study of Nitrogenase from *Clostridium pasteurianum*. *J. Magn. Reson.* **1991**, *91*, 227–240.

(128) Yu, Y.; Sadique, A. R.; Smith, J. M.; Dugan, T. R.; Cowley, R. E.; Brennessel, W. W.; Flaschenriem, C. J.; Bill, E.; Cundari, T. R.; Holland, P. L. The Reactivity Patterns of Low-Coordinate Iron-Hydride Complexes. *J. Am. Chem. Soc.* **2008**, *130*, 6624–6638.

(129) Smith, J. M.; Sadique, A. R.; Cundari, T. R.; Rodgers, K. R.; Lukat-Rodgers, G.; Lachicotte, R. J.; Flaschenriem, C. J.; Vela, J.; Holland, P. L. Studies of Low-Coordinate Iron Dinitrogen Complexes. *J. Am. Chem. Soc.* **2006**, *128*, 756–769.

(130) Dugan, T. R.; Holland, P. L. New Routes to Low-Coordinate Iron Hydride Complexes: The Binuclear Oxidative Addition of  $H_2$ . *J. Organomet. Chem.* **2009**, *694*, 2825–2830.

(131) Colombo, M.; George, M. W.; Moore, J. N.; Pattison, D. I.; Perutz, R. N.; Virrels, I. G.; Ye, T.-Q. Ultrafast Reductive Elimination of Hydrogen from a Metal Carbonyl Dihydride Complex; a Study by Time-Resolved IR and Visible Spectroscopy. *J. Chem. Soc., Dalton Trans.* **1997**, *0*, 2857–2860.

(132) Perutz, R. N. Metal Dihydride Complexes: Photochemical Mechanisms for Reductive Elimination. *Pure Appl. Chem.* **1998**, *70*, 2211–2220.

(133) Perutz, R. N.; Procacci, B. Photochemistry of Transition Metal Hydrides. *Chem. Rev.* **2016**, *116*, 8506–8544.

(134) Ozin, G. A.; McCaffrey, J. G. The Photoreversible Oxidative-Addition, Reductive-Elimination Reactions  $Fe + H_2 \rightleftharpoons FeH_2$  in Low-Temperature Matrixes. *J. Phys. Chem.* **1984**, *88*, 645–648.

(135) Whittlesey, M. K.; Mawby, R. J.; Osman, R.; Perutz, R. N.; Field, L. D.; Wilkinson, M. P.; George, M. W. Transient and Matrix Photochemistry of  $Fe(Dmpe)_2H_2$  ( $Dmpe = Me_2PCH_2CH_2Me_2$ ): Dynamics of C-H and H-H Activation. *J. Am. Chem. Soc.* **1993**, *115*, 8627–8637.

(136) Raugei, S.; Seefeldt, L. C.; Hoffman, B. M. Critical Computational Analysis Illuminates the Reductive-Elimination Mechanism That Activates Nitrogenase for  $N_2$  Reduction. *Proc. Natl. Acad. Sci. U. S. A.* **2018**, *115*, E10521–E10530.

(137) Cao, L.; Ryde, U. Extremely Large Differences in DFT Energies for Nitrogenase Models. *Phys. Chem. Chem. Phys.* **2019**, *21*, 2480–2488.

(138) Siegbahn, P. E. M.; Blomberg, M. R. A. A Systematic DFT Approach for Studying Mechanisms of Redox Active Enzymes. *Front. Chem.* **2018**, *6*, 644.

(139) Benediksson, B.; Bjornsson, R. QM/MM Study of the Nitrogenase MoFe Protein Resting State: Broken-Symmetry States, Protonation States, and QM Region Convergence in the FeMoco Active Site. *Inorg. Chem.* **2017**, *56*, 13417–13429.

(140) Siegbahn, P. E. M. Is There Computational Support for an Unprotonated Carbon in the  $E_4$  State of Nitrogenase? *J. Comput. Chem.* **2018**, *39*, 743–747.

(141) Siegbahn, P. E. M. The Mechanism for Nitrogenase Including All Steps. *Phys. Chem. Chem. Phys.* **2019**, *21*, 15747–15759.

(142) McKee, M. L. A. New Nitrogenase Mechanism Using a  $CFe_8S_9$  Model: Does  $H_2$  Elimination Activate the Complex to  $N_2$  Addition to the Central Carbon Atom? *J. Phys. Chem. A* **2016**, *120*, 754–764.

(143) Spatzal, T.; Perez, K. A.; Einsle, O.; Howard, J. B.; Rees, D. C. Ligand Binding to the FeMo-cofactor: Structures of CO-Bound and Reactivated Nitrogenase. *Science* **2014**, *345*, 1620–1623.

(144) Spatzal, T.; Perez, K. A.; Howard, J. B.; Rees, D. C. Catalysis-Dependent Selenium Incorporation and Migration in the Nitrogenase Active Site Iron-Molybdenum Cofactor. *eLife* **2015**, *4*, No. e11620.

(145) Doan, P. E.; Telser, J.; Barney, B. M.; Igarashi, R. Y.; Dean, D. R.; Seefeldt, L. C.; Hoffman, B. M.  $^{57}Fe$  ENDOR Spectroscopy and ‘Electron Inventory’ Analysis of the Nitrogenase  $E_4$  Intermediate Suggest the Metal-Ion Core of FeMo-cofactor Cycles through Only One Redox Couple. *J. Am. Chem. Soc.* **2011**, *133*, 17329–17340.

(146) Cao, L.; Ryde, U. What Is the Structure of the  $E_4$  Intermediate in Nitrogenase? *J. Chem. Theory Comput.* **2020**, DOI: [10.1021/acs.jctc.9b01254](https://doi.org/10.1021/acs.jctc.9b01254).

(147) Thorhallsson, A. Th.; Benediksson, B.; Bjornsson, R. A Model for Dinitrogen Binding in the  $E_4$  State of Nitrogenase. *Chem. Sci.* **2019**, *10*, 11110–11124.

(148) Cao, L.; Calderaru, O.; Ryde, U. Protonation States of Homocitrate and Nearby Residues in Nitrogenase Studied by Computational Methods and Quantum Refinement. *J. Phys. Chem. B* **2017**, *121*, 8242–8262.

(149) Cao, L.; Calderaru, O.; Ryde, U. Protonation and Reduction of the FeMo Cluster in Nitrogenase Studied by Quantum Mechanics/Molecular Mechanics (QM/MM) Calculations. *J. Chem. Theory Comput.* **2018**, *14*, 6653–6678.

(150) Hoeke, V.; Tociu, L.; Case, D. A.; Seefeldt, L. C.; Raugei, S.; Hoffman, B. M. High-Resolution ENDOR Spectroscopy Combined with Quantum Chemical Calculations Reveals the Structure of Nitrogenase Janus Intermediate  $E_4(4H)$ . *J. Am. Chem. Soc.* **2019**, *141*, 11984–11996.

(151) Van Stappen, C.; Davydov, R.; Yang, Z.-Y.; Fan, R.; Guo, Y.; Bill, E.; Seefeldt, L. C.; Hoffman, B. M.; DeBeer, S. Spectroscopic Description of the  $E_1$  State of Mo Nitrogenase Based on Mo and Fe X-Ray Absorption and Mössbauer Studies. *Inorg. Chem.* **2019**, *58*, 12365–12376.

(152) Van Stappen, C.; Thorhallsson, A. T.; Decamps, L.; Bjornsson, R.; DeBeer, S. Resolving the Structure of the  $E_1$  State of Mo Nitrogenase through Mo and Fe K-Edge EXAFS and QM/MM Calculations. *Chem. Sci.* **2019**, *10*, 9807–9821.

(153) Harris, D. F.; Yang, Z.-Y.; Dean, D. R.; Seefeldt, L. C.; Hoffman, B. M. Kinetic Understanding of  $N_2$  Reduction versus  $H_2$  Evolution at the  $E_4(4H)$  Janus State in the Three Nitrogenases. *Biochemistry* **2018**, *57*, 5706–5714.

(154) Harris, D. F.; Lukyanov, D. A.; Kallas, H.; Trncik, C.; Yang, Z.-Y.; Compton, P.; Kelleher, N.; Einsle, O.; Dean, D. R.; Hoffman, B. M.; et al. Mo-, V-, and Fe-Nitrogenases Use a Universal Eight-Electron Reductive-Elimination Mechanism To Achieve  $N_2$  Reduction. *Biochemistry* **2019**, *58*, 3293–3301.

(155) Benediksson, B.; Thorhallsson, A. Th.; Bjornsson, R. QM/MM Calculations Reveal a Bridging Hydroxo Group in a Vanadium Nitrogenase Crystal Structure. *Chem. Commun.* **2018**, *54*, 7310–7313.

(156) Rohde, M.; Sippel, D.; Trncik, C.; Andrade, S. L. A.; Einsle, O. The Critical  $E_4$  State of Nitrogenase Catalysis. *Biochemistry* **2018**, *57*, 5497–5504.

(157) Peters, J. W.; Stowell, M. H. B.; Soltis, S. M.; Finnegan, M. G.; Johnson, M. K.; Rees, D. C. Redox-Dependent Structural Changes in the Nitrogenase P-Cluster. *Biochemistry* **1997**, *36*, 1181–1187.

(158) Peters, J. W.; Szilagyi, R. K. Exploring New Frontiers of Nitrogenase Structure and Mechanism. *Curr. Opin. Chem. Biol.* **2006**, *10*, 101–108.

(159) Keable, S. M.; Zadvornyy, O. A.; Johnson, L. E.; Ginovska, B.; Rasmussen, A. J.; Danyal, K.; Eilers, B. J.; Prussia, G. A.; LeVan, A. X.; Raugei, S.; et al. Structural Characterization of the  $P^{1+}$  Intermediate State of the P-Cluster of Nitrogenase. *J. Biol. Chem.* **2018**, *293*, 9629–9635.

(160) Seefeldt, L. C.; Peters, J. W.; Beratan, D. N.; Bothner, B.; Minteer, S. D.; Raugei, S.; Hoffman, B. M. Control of Electron Transfer in Nitrogenase. *Curr. Opin. Chem. Biol.* **2018**, *47*, 54–59.

(161) Xiao, Y.; Fisher, K.; Smith, M. C.; Newton, W. E.; Case, D. A.; George, S. J.; Wang, H.; Sturhahn, W.; Alp, E. E.; Zhao, J.; et al. How Nitrogenase Shakes – Initial Information about P-Cluster and

FeMo-cofactor Normal Modes from Nuclear Resonance Vibrational Spectroscopy (NRVS). *J. Am. Chem. Soc.* **2006**, *128*, 7608–7612.

(162) George, S. J.; Barney, B. M.; Mitra, D.; Igarashi, R. Y.; Guo, Y.; Dean, D. R.; Cramer, S. P.; Seefeldt, L. C. EXAFS and NRVS Reveal a Conformational Distortion of the FeMo-cofactor in the MoFe Nitrogenase Propargyl Alcohol Complex. *J. Inorg. Biochem.* **2012**, *112*, 85–92.

(163) Mitra, D.; George, S. J.; Guo, Y.; Kamali, S.; Keable, S.; Peters, J. W.; Pelmenschikov, V.; Case, D. A.; Cramer, S. P. Characterization of [4Fe-4S] Cluster Vibrations and Structure in Nitrogenase Fe Protein at Three Oxidation Levels via Combined NRVS, EXAFS, and DFT Analyses. *J. Am. Chem. Soc.* **2013**, *135*, 2530–2543.

(164) Mao, Z.; Liou, S.-H.; Khadka, N.; Jenney, F. E.; Goodin, D. B.; Seefeldt, L. C.; Adams, M. W. W.; Cramer, S. P.; Larsen, D. S. Cluster-Dependent Charge-Transfer Dynamics in Iron–Sulfur Proteins. *Biochemistry* **2018**, *57*, 978–990.

(165) Gee, L. B.; Leontyev, I.; Stuchebrukhov, A.; Scott, A. D.; Pelmenschikov, V.; Cramer, S. P. Docking and Migration of Carbon Monoxide in Nitrogenase: The Case for Gated Pockets from Infrared Spectroscopy and Molecular Dynamics. *Biochemistry* **2015**, *54*, 3314–3319.

(166) Owens, C. P.; Katz, F. E. H.; Carter, C. H.; Luca, M. A.; Tezcan, F. A. Evidence for Functionally Relevant Encounter Complexes in Nitrogenase Catalysis. *J. Am. Chem. Soc.* **2015**, *137*, 12704–12712.

(167) Owens, C. P.; Katz, F. E. H.; Carter, C. H.; Oswald, V. F.; Tezcan, F. A. Tyrosine-Coordinated P-Cluster in *G. diazotrophicus* Nitrogenase: Evidence for the Importance of O-Based Ligands in Conformationally Gated Electron Transfer. *J. Am. Chem. Soc.* **2016**, *138*, 10124–10127.

(168) Rutledge, H. L.; Rittle, J.; Williamson, L. M.; Xu, W. A.; Gagnon, D. M.; Tezcan, F. A. Redox-Dependent Metastability of the Nitrogenase P-Cluster. *J. Am. Chem. Soc.* **2019**, *141*, 10091–10098.

(169) Hinnemann, B.; Nørskov, J. K. Chemical Activity of the Nitrogenase FeMo Cofactor with a Central Nitrogen Ligand: Density Functional Study. *J. Am. Chem. Soc.* **2004**, *126*, 3920–3927.

(170) Dance, I. The Mechanistically Significant Coordination Chemistry of Dinitrogen at FeMo-Co, the Catalytic Site of Nitrogenase. *J. Am. Chem. Soc.* **2007**, *129*, 1076–1088.

(171) Pelmenschikov, V.; Case, D. A.; Noddleman, L. Ligand-Bound  $S = 1/2$  FeMo-cofactor of Nitrogenase: Hyperfine Interaction Analysis and Implication for the Central Ligand X Identity. *Inorg. Chem.* **2008**, *47*, 6162–6172.

(172) Hallmen, P. P.; Kästner, J. N<sub>2</sub> Binding to the FeMo-cofactor of Nitrogenase. *Z. Anorg. Allg. Chem.* **2015**, *641*, 118–122.

(173) Varley, J. B.; Wang, Y.; Chan, K.; Studt, F.; Nørskov, J. K. Mechanistic Insights into Nitrogen Fixation by Nitrogenase Enzymes. *Phys. Chem. Chem. Phys.* **2015**, *17*, 29541–29547.

(174) Schimpl, J.; Petrilli, H. M.; Blöchl, P. E. Nitrogen Binding to the FeMo-cofactor of Nitrogenase. *J. Am. Chem. Soc.* **2003**, *125*, 15772–15778.

(175) Kästner, J.; Blöchl, P. E. Towards an Understanding of the Workings of Nitrogenase from DFT Calculations. *ChemPhysChem* **2005**, *6*, 1724–1726.

(176) Kästner, J.; Blöchl, P. E. Model for Acetylene Reduction by Nitrogenase Derived from Density Functional Theory. *Inorg. Chem.* **2005**, *44*, 4568–4575.

(177) Kästner, J.; Blöchl, P. E. Ammonia Production at the FeMo Cofactor of Nitrogenase: Results from Density Functional Theory. *J. Am. Chem. Soc.* **2007**, *129*, 2998–3006.

(178) Spatzal, T. The Center of Biological Nitrogen Fixation: FeMo-cofactor. *Z. Anorg. Allg. Chem.* **2015**, *641*, 10–17.

(179) Dance, I. Mechanisms of the S/CO/Se Interchange Reactions at FeMo-co, the Active Site Cluster of Nitrogenase. *Dalton Trans* **2016**, *45*, 14285–14300.

(180) Skubi, K. L.; Holland, P. L. So Close, yet Sulfur Away: Opening the Nitrogenase Cofactor Structure Creates a Binding Site. *Biochemistry* **2018**, *57*, 3540–3541.

(181) Čorić, I.; Holland, P. L. Insight into the FeMoco of Nitrogenase from Synthetic Iron Complexes with Sulfur, Carbon, and Hydride Ligands. *J. Am. Chem. Soc.* **2016**, *138*, 7200–7211.

(182) Rittle, J.; Peters, J. C. An Fe-N<sub>2</sub> Complex That Generates Hydrazine and Ammonia via Fe=NNH<sub>2</sub>: Demonstrating a Hybrid Distal-to-Alternating Pathway for N<sub>2</sub> Reduction. *J. Am. Chem. Soc.* **2016**, *138*, 4243–4248.

(183) Schrock, R. R. Catalytic Reduction of Dinitrogen to Ammonia at a Single Molybdenum Center. *Acc. Chem. Res.* **2005**, *38*, 955–962.

(184) Neese, F. The Yandulov/Schrock Cycle and the Nitrogenase Reaction: Pathways of Nitrogen Fixation Studied by Density Functional Theory. *Angew. Chem., Int. Ed.* **2006**, *45*, 196–199.

(185) MacLeod, K. C.; Holland, P. L. Recent Developments in the Homogeneous Reduction of Dinitrogen by Molybdenum and Iron. *Nat. Chem.* **2013**, *5*, 559–565.

(186) Dance, I. The Chemical Mechanism of Nitrogenase: Calculated Details of the Intramolecular Mechanism for Hydrogenation of  $\eta^2$ -N<sub>2</sub> on FeMo-co to NH<sub>3</sub>. *Dalton Trans* **2008**, No. 43, 5977–5991.

(187) McKenna, C. E.; Simeonov, A. M.; Eran, H.; Bravo-Leerabhandh, M. Reduction of Cyclic and Acyclic Diazene Derivatives by *Azotobacter vinelandii* Nitrogenase: Diazirine and Trans-Dimethylidiazene. *Biochemistry* **1996**, *35*, 4502–4514.

(188) Barney, B. M.; Lukyanov, D.; Yang, T.-C.; Dean, D. R.; Hoffman, B. M.; Seefeldt, L. C. A Methyldiazene (HN=N-CH<sub>3</sub>)-Derived Species Bound to the Nitrogenase Active-Site FeMo Cofactor: Implications for Mechanism. *Proc. Natl. Acad. Sci. U. S. A.* **2006**, *103*, 17113–17118.

(189) Barney, B. M.; McClead, J.; Lukyanov, D.; Laryukhin, M.; Yang, T.-C.; Dean, D. R.; Hoffman, B. M.; Seefeldt, L. C. Diazene (HN=NH) Is a Substrate for Nitrogenase: Insights into the Pathway of N<sub>2</sub> Reduction. *Biochemistry* **2007**, *46*, 6784–6794.

(190) Lukyanov, D.; Yang, Z.-Y.; Barney, B. M.; Dean, D. R.; Seefeldt, L. C.; Hoffman, B. M. Unification of Reaction Pathway and Kinetic Scheme for N<sub>2</sub> Reduction Catalyzed by Nitrogenase. *Proc. Natl. Acad. Sci. U. S. A.* **2012**, *109*, 5583–5587.

(191) Davis, L. C. Hydrazine as a Substrate and Inhibitor of *Azotobacter vinelandii* Nitrogenase. *Arch. Biochem. Biophys.* **1980**, *204*, 270–276.

(192) Barney, B. M.; Laryukhin, M.; Igarashi, R. Y.; Lee, H.-I.; Dos Santos, P. C.; Yang, T.-C.; Hoffman, B. M.; Dean, D. R.; Seefeldt, L. C. Trapping a Hydrazine Reduction Intermediate on the Nitrogenase Active Site. *Biochemistry* **2005**, *44*, 8030–8037.

(193) Shaw, S.; Lukyanov, D.; Danyal, K.; Dean, D. R.; Hoffman, B. M.; Seefeldt, L. C. Nitrite and Hydroxylamine as Nitrogenase Substrates: Mechanistic Implications for the Pathway of N<sub>2</sub> Reduction. *J. Am. Chem. Soc.* **2014**, *136*, 12776–12783.

(194) Barney, B. M.; Yang, T.-C.; Igarashi, R. Y.; Dos Santos, P. C.; Laryukhin, M.; Lee, H.-I.; Hoffman, B. M.; Dean, D. R.; Seefeldt, L. C. Intermediates Trapped during Nitrogenase Reduction of N≡N, CH<sub>3</sub>-N=NH, and H<sub>2</sub>N-NH<sub>2</sub>. *J. Am. Chem. Soc.* **2005**, *127*, 14960–14961.

(195) Dilworth, M. J.; Eady, R. R. Hydrazine Is a Product of Dinitrogen Reduction by the Vanadium-Nitrogenase from *Azotobacter chroococcum*. *Biochem. J.* **1991**, *277*, 465–468.

(196) Maia, L. B.; Moura, J. J. G. How Biology Handles Nitrite. *Chem. Rev.* **2014**, *114*, 5273–5357.

(197) Riplinger, C.; Neese, F. The Reaction Mechanism of Cytochrome P450 NO Reductase: A Detailed Quantum Mechanics/Molecular Mechanics Study. *ChemPhysChem* **2011**, *12*, 3192–3203.

(198) Einsle, O.; Messerschmidt, A.; Huber, R.; Kroneck, P. M. H.; Neese, F. Mechanism of the Six-Electron Reduction of Nitrite to Ammonia by Cytochrome c Nitrite Reductase. *J. Am. Chem. Soc.* **2002**, *124*, 11737–11745.

(199) Bykov, D.; Neese, F. Substrate Binding and Activation in the Active Site of Cytochrome c Nitrite Reductase: A Density Functional Study. *JBIC, J. Biol. Inorg. Chem.* **2011**, *16*, 417–430.

(200) Bykov, D.; Neese, F. Reductive Activation of the Heme Iron–Nitrosyl Intermediate in the Reaction Mechanism of Cytochrome *c* Nitrite Reductase: A Theoretical Study. *JBIC, J. Biol. Inorg. Chem.* **2012**, *17*, 741–760.

(201) Bykov, D.; Plog, M.; Neese, F. Heme-Bound Nitroxyl, Hydroxylamine, and Ammonia Ligands as Intermediates in the Reaction Cycle of Cytochrome *c* Nitrite Reductase: A Theoretical Study. *JBIC, J. Biol. Inorg. Chem.* **2014**, *19*, 97–112.

(202) Lee, H.-I.; Sørlie, M.; Christiansen, J.; Yang, T.-C.; Shao, J.; Dean, D. R.; Hales, B. J.; Hoffman, B. M. Electron Inventory, Kinetic Assignment ( $E_n$ ), Structure, and Bonding of Nitrogenase Turnover Intermediates with  $C_2H_2$  and CO. *J. Am. Chem. Soc.* **2005**, *127*, 15880–15890.

(203) Newton, W. E.; Dilworth, M. J. Assays of Nitrogenase Reaction Products. In *Nitrogen Fixation: Methods and Protocols*; Ribbe, M. W., Ed.; Methods in Molecular Biology; Humana Press: Totowa, NJ, 2011; pp 105–127.

(204) Dilworth, M. J. Acetylene Reduction by Nitrogen-Fixing Preparations from *Clostridium pasteurianum*. *Biochim. Biophys. Acta, Gen. Subj.* **1966**, *127*, 285–294.

(205) Lowe, D. J.; Eady, R. R.; Thorneley, N. F. Electron-Paramagnetic-Resonance Studies on Nitrogenase of *Klebsiella pneumoniae*: Evidence for Acetylene- and Ethylene-Nitrogenase Transient Complexes. *Biochem. J.* **1978**, *173*, 277–290.

(206) Sørlie, M.; Christiansen, J.; Dean, D. R.; Hales, B. J. Detection of a New Radical and FeMo-cofactor EPR Signal during Acetylene Reduction by the  $\alpha$ -H195Q Mutant of Nitrogenase. *J. Am. Chem. Soc.* **1999**, *121*, 9457–9458.

(207) Lee, H. I.; Sørlie, M.; Christiansen, J.; Song, R. T.; Dean, D. R.; Hales, B. J.; Hoffman, B. M. Characterization of an Intermediate in the Reduction of Acetylene by the Nitrogenase  $\alpha$ -Gln<sup>195</sup> MoFe Protein by Q-Band EPR and  $^{13}C$ ,  $^1H$  ENDOR. *J. Am. Chem. Soc.* **2000**, *122*, 5582–5587.

(208) Benton, P. M. C.; Mayer, S. M.; Shao, J.; Hoffman, B. M.; Dean, D. R.; Seefeldt, L. C. Interaction of Acetylene and Cyanide with the Resting State of Nitrogenase  $\alpha$ -96-Substituted MoFe Proteins. *Biochemistry* **2001**, *40*, 13816–13825.

(209) Burgess, B. K. The Iron-Molybdenum Cofactor of Nitrogenase. *Chem. Rev.* **1990**, *90*, 1377–1406.

(210) Hardy, R. W. F.; Jackson, E. K. Reduction of Model Substrates—Nitriles and Acetylenes—by Nitrogenase ( $N_2$ Ase). *Fed. Proc.* **1967**, *28*, 725.

(211) Schöllhorn, R.; Burris, R. H. Acetylene as a Competitive Inhibitor of  $N_2$  Fixation. *Proc. Natl. Acad. Sci. U. S. A.* **1967**, *58*, 213–216.

(212) Hardy, R. W.; Knight, E. J. ATP-Dependent Reduction of Azide and HCN by  $N_2$ -Fixing Enzymes of *Azotobacter vinelandii* and *Clostridium pasteurianum*. *Biochim. Biophys. Acta* **1967**, *139*, 69–90.

(213) Li, J.; Burgess, B. K.; Corbin, J. L. Nitrogenase Reactivity: Cyanide as Substrate and Inhibitor. *Biochemistry* **1982**, *21*, 4393–4402.

(214) Lowe, D. J.; Fisher, K.; Thorneley, R. N. F.; Vaughn, S. A.; Burgess, B. K. Kinetics and Mechanism of the Reaction of Cyanide with Molybdenum Nitrogenase from *Azotobacter vinelandii*. *Biochemistry* **1989**, *28*, 8460–8466.

(215) Keable, S. M.; Vertemara, J.; Zadvornyy, O. A.; Eilers, B. J.; Danyal, K.; Rasmussen, A. J.; De Gioia, L.; Zampella, G.; Seefeldt, L. C.; Peters, J. W. Structural Characterization of the Nitrogenase Molybdenum-Iron Protein with the Substrate Acetylene Trapped near the Active Site. *J. Inorg. Biochem.* **2018**, *180*, 129–134.

(216) McLean, P. A.; True, A.; Nelson, M. J.; Lee, H. I.; Hoffman, B. M.; Orme-Johnson, W. H. Effects of Substrates (Methyl Isocyanide,  $C_2H_2$ ) and Inhibitor (CO) on Resting-State Wild-Type and NifV<sup>+</sup> *Klebsiella pneumoniae* MoFe Proteins. *J. Inorg. Biochem.* **2003**, *93*, 18–32.

(217) Benton, P. M. C.; Laryukhin, M.; Mayer, S. M.; Hoffman, B. M.; Dean, D. R.; Seefeldt, L. C. Localization of a Substrate Binding Site on the FeMo-cofactor in Nitrogenase: Trapping Propargyl Alcohol with an  $\alpha$ -70-Substituted MoFe Protein. *Biochemistry* **2003**, *42*, 9102–9109.

(218) Igarashi, R. Y.; Dos Santos, P. C.; Niehaus, W. G.; Dance, I. G.; Dean, D. R.; Seefeldt, L. C. Localization of a Catalytic Intermediate Bound to the FeMo-cofactor of Nitrogenase. *J. Biol. Chem.* **2004**, *279*, 34770–34775.

(219) Mayer, S. M.; Niehaus, W. G.; Dean, D. R. Reduction of Short Chain Alkenes by a Nitrogenase  $\alpha$ -70<sup>Ala</sup>-Substituted MoFe Protein. *J. Chem. Soc., Dalton Trans.* **2002**, No. 5, 802–807.

(220) Dos Santos, P. C.; Mayer, S. M.; Barney, B. M.; Seefeldt, L. C.; Dean, D. R. Alkyne Substrate Interaction within the Nitrogenase MoFe Protein. *J. Inorg. Biochem.* **2007**, *101*, 1642–1648.

(221) Lockshin, A.; Burris, R. H. Inhibitors of Nitrogen Fixation in Extracts from *Clostridium pasteurianum*. *Biochim. Biophys. Acta, Gen. Subj.* **1965**, *111*, 1–10.

(222) Maskos, Z.; Fisher, K.; Sørlie, M.; Newton, W. E.; Hales, B. J. Variant MoFe Proteins of *Azotobacter vinelandii*: Effects of Carbon Monoxide on Electron Paramagnetic Resonance Spectra Generated during Enzyme Turnover. *JBIC, J. Biol. Inorg. Chem.* **2005**, *10*, 394–406.

(223) Liang, J.; Madden, M.; Shah, V. K.; Burris, R. H. Citrate Substitutes for Homocitrate in Nitrogenase of a *nifV* Mutant of *Klebsiella pneumoniae*. *Biochemistry* **1990**, *29*, 8577–8581.

(224) Scott, D. J.; Dean, D. R.; Newton, W. E. Nitrogenase-catalyzed Ethane Production and CO-sensitive Hydrogen Evolution from MoFe Proteins Having Amino Acid Substitutions in an  $\alpha$ -Subunit FeMo Cofactor-Binding Domain. *J. Biol. Chem.* **1992**, *267*, 20002–20010.

(225) Yang, Z.-Y. *Substrate Binding and Reduction Mechanism of Molybdenum Nitrogenase*; Utah State University: Logan, UT, 2013.

(226) Pham, D. N.; Burgess, B. K. Nitrogenase Reactivity: Effects of pH on Substrate Reduction and Carbon Monoxide Inhibition. *Biochemistry* **1993**, *32*, 13725–13731.

(227) Lee, C. C.; Hu, Y.; Ribbe, M. W. Vanadium Nitrogenase Reduces CO. *Science* **2010**, *329*, 642.

(228) Hu, Y.; Lee, C. C.; Ribbe, M. W. Extending the Carbon Chain: Hydrocarbon Formation Catalyzed by Vanadium/Molybdenum Nitrogenases. *Science* **2011**, *333*, 753–755.

(229) Fisher, K.; Hare, N. D.; Newton, W. E. Another Role for CO with Nitrogenase? CO Stimulates Hydrogen Evolution Catalyzed by Variant *Azotobacter vinelandii* Mo-Nitrogenases. *Biochemistry* **2014**, *53*, 6151–6160.

(230) Pollock, R. C.; Lee, H.-In.; Cameron, L. M.; DeRose, V. J.; Hales, B. J.; Orme-Johnson, W. H.; Hoffman, B. M. Investigation of CO Bound to Inhibited Forms of Nitrogenase MoFe Protein by  $^{13}C$  ENDOR. *J. Am. Chem. Soc.* **1995**, *117*, 8686–8687.

(231) Yates, M. G. Nitrogenase of *Azotobacter chroococcum*: A New Electronparamagnetic-Resonance Signal Associated with a Transient Species of the MoFe Protein during Catalysis. *FEBS Lett.* **1976**, *72*, 127.

(232) Davis, L. C.; Henzl, M. T.; Burris, R. H.; Orme-Johnson, W. H. Iron-Sulfur Clusters in the Molybdenum-Iron Protein Component of Nitrogenase. Electron Paramagnetic Resonance of the Carbon Monoxide Inhibited State. *Biochemistry* **1979**, *18*, 4860–4869.

(233) Cameron, L. M.; Hales, B. J. Investigation of CO Binding and Release from Mo-Nitrogenase during Catalytic Turnover. *Biochemistry* **1998**, *37*, 9449–9456.

(234) Sørlie, M.; Christiansen, J.; Lemon, B. J.; Peters, J. W.; Dean, D. R.; Hales, B. J. Mechanistic Features and Structure of the Nitrogenase  $\alpha$ -Gln<sup>195</sup> MoFe Protein. *Biochemistry* **2001**, *40*, 1540–1549.

(235) Christie, P. D.; Lee, H.-In.; Cameron, L. M.; Hales, B. J.; Orme-Johnson, W. H.; Hoffman, B. M. Identification of the CO-Binding Cluster in Nitrogenase MoFe Protein by ENDOR of  $^{57}Fe$  Isotopomers. *J. Am. Chem. Soc.* **1996**, *118*, 8707–8709.

(236) Lee, H.-I.; Cameron, L. M.; Hales, B. J.; Hoffman, B. M. CO Binding to the FeMo Cofactor of CO-Inhibited Nitrogenase:  $^{13}CO$  and  $^1H$  Q-Band ENDOR Investigation. *J. Am. Chem. Soc.* **1997**, *119*, 10121–10126.

(237) Lee, H.-I.; Hales, B. J.; Hoffman, B. M. Metal-Ion Valencies of the FeMo Cofactor in CO-Inhibited and Resting State Nitrogenase by  $^{57}\text{Fe}$  Q-Band ENDOR. *J. Am. Chem. Soc.* **1997**, *119*, 11395–11400.

(238) Lee, H. I.; Cameron, L. M.; Sorlie, M.; Pollock, R. C.; Christie, P. D.; Christiansen, J.; Ryle, M. J.; Peters, J. W.; DeRose, V. J.; Seefeldt, L. C.; et al. Study of Substrate Inhibitor Interactions in Nitrogenase MoFe Protein by Advanced Paramagnetic Resonance. *J. Inorg. Biochem.* **1999**, *74*, 202–202.

(239) Maskos, Z.; Hales, B. J. Photo-Lability of CO Bound to Mo-Nitrogenase from *Azotobacter vinelandii*. *J. Inorg. Biochem.* **2003**, *93*, 11–17.

(240) Yan, L.; Dapper, C. H.; George, S. J.; Wang, H.; Mitra, D.; Dong, W.; Newton, W. E.; Cramer, S. P. Photolysis of Hi-CO Nitrogenase – Observation of a Plethora of Distinct CO Species Using Infrared Spectroscopy. *Eur. J. Inorg. Chem.* **2011**, 2064–2074.

(241) Yan, L.; Pelmenschikov, V.; Dapper, C. H.; Scott, A. D.; Newton, W. E.; Cramer, S. P. IR-Monitored Photolysis of CO-Inhibited Nitrogenase: A Major EPR-Silent Species with Coupled Terminal CO Ligands. *Chem. - Eur. J.* **2012**, *18*, 16349–16357.

(242) Scott, A. D.; Pelmenschikov, V.; Guo, Y.; Yan, L.; Wang, H.; George, S. J.; Dapper, C. H.; Newton, W. E.; Yoda, Y.; Tanaka, Y.; et al. Structural Characterization of CO-Inhibited Mo-Nitrogenase by Combined Application of Nuclear Resonance Vibrational Spectroscopy, Extended X-Ray Absorption Fine Structure, and Density Functional Theory: New Insights into the Effects of CO Binding and the Role of the Interstitial Atom. *J. Am. Chem. Soc.* **2014**, *136*, 15942–15954.

(243) Lee, C. C.; Fay, A. W.; Weng, T.-C.; Krest, C. M.; Hedman, B.; Hodgson, K. O.; Hu, Y.; Ribbe, M. W. Uncoupling Binding of Substrate CO from Turnover by Vanadium Nitrogenase. *Proc. Natl. Acad. Sci. U. S. A.* **2015**, *112*, 13845–13849.

(244) George, S. J.; Ashby, G. A.; Wharton, C. W.; Thorneley, R. N. F. Time-Resolved Binding of Carbon Monoxide to Nitrogenase Monitored by Stopped-Flow Infrared Spectroscopy. *J. Am. Chem. Soc.* **1997**, *119*, 6450–6451.

(245) Tolland, J. D.; Thorneley, R. N. F. Stopped-Flow Fourier Transform Infrared Spectroscopy Allows Continuous Monitoring of Azide Reduction, Carbon Monoxide Inhibition, and ATP Hydrolysis by Nitrogenase. *Biochemistry* **2005**, *44*, 9520–9527.

(246) Yang, Z.-Y.; Seefeldt, L. C.; Dean, D. R.; Cramer, S. P.; George, S. J. Steric Control of the Hi-CO MoFe Nitrogenase Complex Revealed by Stopped-Flow Infrared Spectroscopy. *Angew. Chem., Int. Ed.* **2011**, *50*, 272–275.

(247) Yang, Z.-Y.; Dean, D. R.; Seefeldt, L. C. Molybdenum Nitrogenase Catalyzes the Reduction and Coupling of CO to Form Hydrocarbons. *J. Biol. Chem.* **2011**, *286*, 19417–19421.

(248) Lee, C. C.; Tanifugi, K.; Newcomb, M.; Liedtke, J.; Hu, Y.; Ribbe, M. W. A Comparative Analysis of the CO-Reducing Activities of MoFe Proteins Containing Mo- and V-Nitrogenase Cofactors. *ChemBioChem* **2018**, *19*, 649–653.

(249) Rebelein, J. G.; Lee, C. C.; Newcomb, M.; Hu, Y.; Ribbe, M. W. Characterization of an M-Cluster-Substituted Nitrogenase VFe Protein. *mBio* **2018**, *9*, E00310-18.

(250) Paengnakorn, P.; Ash, P. A.; Shaw, S.; Danyal, K.; Chen, T.; Dean, D. R.; Seefeldt, L. C.; Vincent, K. A. Infrared Spectroscopy of the Nitrogenase MoFe Protein under Electrochemical Control: Potential-Triggered CO Binding. *Chem. Sci.* **2017**, *8*, 1500–1505.

(251) Wiig, J. A.; Lee, C. C.; Hu, Y.; Ribbe, M. W. Tracing the Interstitial Carbide of the Nitrogenase Cofactor during Substrate Turnover. *J. Am. Chem. Soc.* **2013**, *135*, 4982–4983.

(252) Seefeldt, L. C.; Rasche, M. E.; Ensign, S. A. Carbonyl Sulfide and Carbon Dioxide as New Substrates, and Carbon Disulfide as a New Inhibitor, of Nitrogenase. *Biochemistry* **1995**, *34*, 5382–5389.

(253) Khadka, N.; Dean, D. R.; Smith, D.; Hoffman, B. M.; Raugei, S.; Seefeldt, L. C. CO<sub>2</sub> Reduction Catalyzed by Nitrogenase: Pathways to Formate, Carbon Monoxide, and Methane. *Inorg. Chem.* **2016**, *55*, 8321–8330.

(254) Yang, Z.-Y.; Moure, V. R.; Dean, D. R.; Seefeldt, L. C. Carbon Dioxide Reduction to Methane and Coupling with Acetylene to Form Propylene Catalyzed by Remodeled Nitrogenase. *Proc. Natl. Acad. Sci. U. S. A.* **2012**, *109*, 19644–19648.

(255) Fixen, K. R.; Zheng, Y.; Harris, D. F.; Shaw, S.; Yang, Z.-Y.; Dean, D. R.; Seefeldt, L. C.; Harwood, C. S. Light-Driven Carbon Dioxide Reduction to Methane by Nitrogenase in a Photosynthetic Bacterium. *Proc. Natl. Acad. Sci. U. S. A.* **2016**, *113*, 10163–10167.

(256) Rey, F. E.; Heiniger, E. K.; Harwood, C. S. Redirection of Metabolism for Biological Hydrogen Production. *Appl. Environ. Microbiol.* **2007**, *73*, 1665–1671.

(257) McKinlay, J. B.; Harwood, C. S. Carbon Dioxide Fixation as a Central Redox Cofactor Recycling Mechanism in Bacteria. *Proc. Natl. Acad. Sci. U. S. A.* **2010**, *107*, 11669–11675.

(258) Heiniger, E. K.; Oda, Y.; Samanta, S. K.; Harwood, C. S. How Posttranslational Modification of Nitrogenase Is Circumvented in *Rhodopseudomonas palustris* Strains That Produce Hydrogen Gas Constitutively. *Appl. Environ. Microbiol.* **2012**, *78*, 1023–1032.

(259) Demtröder, L.; Pfänder, Y.; Schäkermann, S.; Bandow, J. E.; Masepohl, B. NifA Is the Master Regulator of Both Nitrogenase Systems in *Rhodobacter capsulatus*. *MicrobiologyOpen* **2019**, *8*, No. e921.

(260) Zheng, Y.; Harris, D. F.; Yu, Z.; Fu, Y.; Poudel, S.; Ledbetter, R. N.; Fixen, K. R.; Yang, Z.-Y.; Boyd, E. S.; Lidstrom, M. E.; et al. A Pathway for Biological Methane Production Using Bacterial Iron-only Nitrogenase. *Nat. Microbiol.* **2018**, *3*, 281–286.

(261) Hu, B.; Harris, D. F.; Dean, D. R.; Liu, T. L.; Yang, Z.-Y.; Seefeldt, L. C. Electrocatalytic CO<sub>2</sub> Reduction Catalyzed by Nitrogenase MoFe and FeFe Proteins. *Bioelectrochemistry* **2018**, *120*, 104–109.

(262) Connelly, S. J.; Wiedner, E. S.; Appel, A. M. Predicting the Reactivity of Hydride Donors in Water: Thermodynamic Constants for Hydrogen. *Dalton Trans.* **2015**, *44*, 5933–5938.

(263) Rebelein, J. G.; Hu, Y.; Ribbe, M. W. Differential Reduction of CO<sub>2</sub> by Molybdenum and Vanadium Nitrogenases. *Angew. Chem., Int. Ed.* **2014**, *53*, 11543–11546.

(264) Sickerman, N. S.; Hu, Y.; Ribbe, M. W. Activation of CO<sub>2</sub> by Vanadium Nitrogenase. *Chem. - Asian J.* **2017**, *12*, 1985–1996.

(265) Rebelein, J. G.; Hu, Y.; Ribbe, M. W. Widening the Product Profile of Carbon Dioxide Reduction by Vanadium Nitrogenase. *ChemBioChem* **2015**, *16*, 1993–1996.

(266) Rasche, M. E.; Seefeldt, L. C. Reduction of Thiocyanate, Cyanate, and Carbon Disulfide by Nitrogenase: Kinetic Characterization and EPR Spectroscopic Analysis. *Biochemistry* **1997**, *36*, 8574–8585.

(267) Ryle, M. J.; Lee, H. I.; Seefeldt, L. C.; Hoffman, B. M. Nitrogenase Reduction of Carbon Disulfide: Freeze-Quench EPR and ENDOR Evidence for Three Sequential Intermediates with Cluster-Bound Carbon Moieties. *Biochemistry* **2000**, *39*, 1114–1119.

(268) Henthorn, J. T.; Arias, R. J.; Koroidov, S.; Kroll, T.; Sokaras, D.; Bergmann, U.; Rees, D. C.; DeBeer, S. Localized Electronic Structure of Nitrogenase FeMoco Revealed by Selenium K-Edge High Resolution X-Ray Absorption Spectroscopy. *J. Am. Chem. Soc.* **2019**, *141*, 13676–13688.

(269) Chen, P. Y.-T.; Wittenborn, E. C.; Drennan, C. L. Waltzing around Cofactors. *eLife* **2016**, *5*, No. e13977.

(270) Kennedy, I. R.; Morris, J. A.; Mortenson, L. E. N<sub>2</sub> Fixation by Purified Components of the N<sub>2</sub>-Fixing System of *Clostridium pasteurianum*. *Biochim. Biophys. Acta, Bioenerg.* **1968**, *153*, 777–786.